UNIVERSITAT POLITÈCNICA DE CATALUNYA
BARCELONATECH
Departament de Teoria del Senyal
i Comunicacions

Sea Surface Height retrieval using GNSS Reflected Signals

Author
Héctor Esteban Cabezos

Thesis Advisors
Prof. Adriano José Camps Carmona
PhD Alberto Alonso Arroyo

A Thesis submitted to the Universitat Politècnica de Catalunya (UPC) in partial fulfillment of the requirements for the degree of TELECOMMUNICATIONS SYSTEMS

Undergraduate program on Signal Theory and Communications
Remote Sensing Laboratory (RSLAB) Group
Barcelona, June 2017

To my parents, Nuria and Jaime.

Abstract

This work is the result of 6 months of work devoted to the analysis of GNSS scattered signals over coastal Sea.
It starts introducing different ways of monitoring Sea surface level focusing on the use of GNSS reflected signals (GNSS-R) with a GNSS antenna looking to the zenith. This method had been partially studied in other universities such as CU in Boulder and in Chalmers University in Sweden, but not covered before in Spain. Apart from that, as a novelty, the already installed European GNSS reference Network (EUREF) is used instead of proprietary hardware.
This thesis is a continuation of the research done by Dr. Nereida Rodriguez and Dr. Alberto Alonso Arroyo at UPC, although their analysis was focused on linear polarized antennas looking to the horizon and custom-made hardware. The benefit of using zenith looking antennas is that no specific equipment is needed, since GNSS stations already available can be used for this purpose.
The main method analyzed in this thesis, which is based on spectral analysis, is explained theoretically and demonstrated practically using data from two different GNSS reference stations located in Mallorca and Tarifa. The methodologies analyzed use the Lomb Scargle Periodogram and the Lomb Scargle Spectrogram to infer the Sea Surface Height from the interaction between the direct and reflected signals acquired at each GNSS Station. A geophysical retrieval algorithm allows to measure the distance between the Sea Surface and the antenna receiver phase center from the oscillation frequency observed in the interference pattern.
Apart from that, a state of the art method is also presented and tested, called Inverse modeling using B-Splines. This method consists of the use of B-Splines and non-linear least squares methods to obtain the Sea Surface Height information using the same data.
The results obtained encourage the use of GNSS-R technology to monitor Sea Surface Height as an alternative to current methods (altimeters, tide gauges and buoys), although the accuracy and the coverage need to be improved. Therefore, they could be used together or even combined to increase the amount of available observations.

Resum

Aquest Treball de Fi de Grau és el resultat de 6 mesos fent recerca en l'estudi de la senyal reflectida de sistemes GNSS a la costa.
El treball comença introduint els principals mètodes per a monitoritzar el nivell del mar, prestant especial atenció al us de les senyals reflectides de sistemes GNSS (GNSS-R) captades per una antena GNSS mirant cap al zenit. Aquest mètode ha estat parcialment estudiat en altres universitats com la CU en Boulder o la Universitat Chalmers en Suècia, però no pas en cap institució espanyola. A més a més, com a novetat, es farà us de les instal·lacions proporcionades per la Xarxa de GNSS de Referencia Europea (EUREF) i, d'aquesta manera, s'evita la necessitat de desenvolupar hardware específic per aquesta tasca.
Aquesta Tesi és una continuació natural del treball desenvolupat pels Drs. Nereida Rodriguez i Alberto Alonso en la UPC, tot i que el seu anàlisis va anar focalitzat en antenes polaritzades linealment i mirant cap a l'horitzó, dissenyades específicament per a rebre senyals GNSS. El benefici d'utilitzar antenes mirant cap al zenit és que no requereix del desenvolupament de hardware específic, ja que les estacions de GNSS porten incorporades una antena GNSS mirant cap al zenit per a proveir posicionament i localització en qualsevol indret del mon.
El principal mètode utilitzat per a determinar el nivell del mar és aplicant anàlisi espectral. El desenvolupament analític del mètode, així com també l'avaluació de resultats, són analitzats en dos estacions GNSS situades en Mallorca i Tarifa respectivament. El mètode desenvolupat fa us del Periodograma Lomb Scargle i del Espectograma Lomb Scargle per a determinar l'alçada del nivell del mar a partir de la interacció entre dos tipus de senyals rebudes en la estació de GNSS, la senyal directa i la reflectida en el mar. Mitjançant fórmules de la física, es pot determinar la distancia entre la superfície del mar i el centre de fase de la antena receptora simplement observant la freqüència de les oscil·lacions que es produeixen en el patró d'interferència del senyal emmagatzemat.
El segon mètode estudiat, anomenat Modelatge Invers a partir de B-Splines, fa us de B-Splines i d'un algoritme de minimització no lineal per a modelar el comportament del mar, i es analitzat en les mateixes dos estacions que el primer mètode i amb les mateixes dades.
Després d'analitzar els resultats per a diferents sistemes i diferents freqüències, els resultats són força encoratjadors i podria ser un primer pas per a monitoritzar el nivell del mar sense necessitat d'utilitzar eines específiques per aquesta tasca, com podrien ser altímetres o boies. Per a que sigui viable utilitzar aquest mètode a escala global es necessita encara una reducció en l'error comès i també una major freqüència en les dades obtingudes.

Resumen

Este Trabajo de Fin de Grado es el resultado de 6 meses haciendo investigación en el estudio de las señales reflejadas de sistemas de GNSS en la costa.
La Tesis empieza introduciendo los principales métodos de monitorización del nivel del mar, prestando especial atención al uso de las señales reflejadas de sistemas GNSS (GNSS-R) captadas por una antena GNSS mirando al zenit. Este método ha sido parcialmente estudiado en otras universidades como la CU en Boulder o la Universidad de Chalmers en Suecia, pero aún no en ninguna institución española. Además, como novedad, se hace uso de las instalaciones proporcionadas por la Red de GNSS de Referencia (EUREF) y, de esta manera, se evita la necesidad de desarrollar hardware específico.
Esta Tesis es una continuación natural del trabajo desarrollado por los Drs. Nereida Rodriguez y Alberto Alonso en la UPC, aunque su análisis se focalizaba en el uso de antenas polarizadas linealmente y orientadas hacia el horizonte, diseñadas específicamente para recibir la señal reflejada de GNSS. El beneficio de utilizar antenas orientadas hacia el zenit es que no se requiere del desarrollo específico de hardware, ya que las estaciones de GNSS llevan incorporadas antenas de GNSS orientadas hacia el zenit para proveer de posicionamiento y localización en cualquier parte del mundo.
El principal método utilizado para determinar el nivel del mar es aplicando análisis espectral. El desarrollo teórico, así como la evaluación de los resultados, serán analizados para dos estaciones GNSS situadas en Mallorca y Tarifa respectivamente. El método desarrollado hace uso del Periodograma Lomb Scargle y del Espectrograma Lomb Scargle para determinar la altura del nivel del mar a partir de la interacción entre dos tipos de señales recibidas en la estación GNSS, la señal directa y la reflejada en el mar. Mediante fórmulas de la física, se puede determinar la distancia entre la superficie del mar y el centro de fase de la antena receptora simplemente observando la frecuencia de las oscilaciones que se producen en el patrón de interferencia del señal obtenido.
El segundo método estudiado, llamado Modelado Inverso a partir de B-Splines, hace uso de B-Splines y de un algoritmo de minimización no lineal para modelar el comportamiento del mar, y es analizado para las mismas dos estaciones y los mismos datos que el primer método.
Después de analizar los resultados para diferentes sistemas y frecuencias, las conclusiones son bastante esperanzadores y podría ser un primer paso para monitorizar el nivel del mar sin la necesidad de utilizar herramientas específicas para esta misión, como podrían ser altímetros o boyas. Para implementar este método a escala global, aún es necesario reducir el error en los resultados y aumentar la frecuencia de obtención de los datos.

Acknowledgements

This section is devoted to express my gratitude to all those who helped me during this 6 months of hard work.
First and above all, I would like to express my gratitude to Dr. Alberto Alonso and Professor Adriano Camps. My Thesis continues the line of Research that Alberto developed in his PhD Thesis and he has provided me uncountable amount of help during this period. Although he presented his PhD dissertation and started working for Tryo Aerospace in February, he has been always ready to help me in my Thesis, as well as providing me help in some difficult moments I experienced back in Boulder. Professor Adriano Camps, who is my Undergraduate Thesis advisor, introduced me to the Remote Sensing world in PAE (Projecte Avançat d'Enginyeria) as well as in the Remote Sensing class. He contacted people in Boulder in order for me to do Research in their facilities and provided help in my Project, which taking into consideration his experience in Remote Sensing, was highly valuable.
I would also like to thank Professor William Emery, from CU Boulder, for letting me working in his Laboratory and providing me help for my Research, as well as giving me tips to survive in the USA.
To conclude, I am very grateful for the help that Professor Jose Miguel Juan and Dr. Adrià Rovira García provided me in translating the Galileo files to a format that could be used for further analysis.

Revision history and approval record

Revision	Date	Purpose
0	05/03/2017	Document creation
1	10/04/2017	Document revision
3	25/05/2017	Document revision
4	20/06/2017	Document revision

Document distribution list

Name	E-mail
Héctor Esteban	hect.esteban@gmail.com
Adriano José Camps Carmona	camps@tsc.upc.edu
Alberto Alonso Arroyo	alberto.alonso.arroyo@gmail.com

WRITTEN BY:		REVIEWED AND APPROVED BY:	
Date	20/06/17	Date	22/06/17
Name	Héctor Esteban	Name	Adriano Camps
Position	Project author	Position	Project Supervisor

Table of Contents

Abstract 3

Resum..... 4

Resumen..... 5

Acknowledgements 6

Revision history and approval record 7

List of Figures 10

List of Tables 13

1. Sea Level Measurements 14
   1.1. Introduction 14
   1.2. Methods for measuring Sea Level 14
   1.3. Remote Sensing overview 15
   1.4. GNSS-R for measuring Sea Surface Level 15

2. GNSS-R Introduction 16
   2.1. Concept 16
   2.2. GNSS and GNSS-R 16
      2.2.1. Introduction GNSS 16
      2.2.2. GNSS-R for Sea Surface Monitoring 18
         2.2.2.1. Introduction 18
         2.2.2.2. SNR Analysis 18
         2.2.2.3. Inverse Modeling 21
      2.2.3. EUREF Network 25
         2.2.3.1. Concept 25
         2.2.3.2. Data structure and standardization 26
      2.2.4. Description of SW used including data packages 27
      2.2.5. Data Processing 27

3. MAL1 Station 28
   3.1. Station Description 28
   3.2. Ground Truth Available 30
   3.3. Lomb Scargle Spectrogram 30
   3.4. Choosing Criterion 34
   3.5. Results against Ground Truth 34
      3.5.1. Introduction 34
      3.5.2. SNR Analysis against Ground Truth 35

4. TARI Station 36
   4.1. Station Description 36
   4.2. Differences between TARI and MAL1 stations 36
   4.3. Ground Truth Available 38
   4.4. Choosing Criterion 38
   4.5. Spectral Analysis results 39
   4.6. Results B-Splines 40

5. Budget 42

6. Conclusions and Future Research Lines 42
   6.1. Conclusions 42
   6.2. Future Research lines 43

7. Appendix 44
7.1. Sea Height retrievement techniques 44
7.2. GNSS History 44
7.3. GNSS Constellations 45
7.3.1. GPS Constellation and Signal 45
7.3.2. GLONASS Constellation and Signal 46
7.3.3. Galileo Constellation 46
7.4. Phase Difference Method 47
7.5. Spectral Analysis Methods 48
7.5.1. Fourier Periodogram 48
7.5.2. Lomb Scargle Periodogram 48
7.5.3. Least Squares Periodogram 49
7.5.4. Capon 50
7.5.5. Examples 50
7.6. Other Methods for filtering 53
7.7. Result figures 56
7.7.1. Mallorca 56
7.7.1.1. GPS L1 56
7.7.1.2. GPS L2 58
7.7.1.3. GLONASS L1 60
7.7.1.4. GLONASS L2 62
7.7.1.5. Table with results 63
7.7.2. Tarifa 64
7.7.2.1. GPS L1 64
7.7.2.2. GPS L2 66
7.7.2.3. GLONASS L1 68
7.7.2.4. GLONASS L2 70
7.7.2.5. Table with results 72
7.7.3. Results B-Splines 72
7.7.3.1. GPS L1 72
7.7.3.2. GPS, GLONASS L1 73
7.7.3.3. GLONASS L1 73
7.7.3.4. Curves representation with B-Splines 74
7.8. Data Provided 75
7.9. Code developed 77
7.9.1. Obtain results from Spectral Analysis method 77
7.9.2. Filter in elevation and azimuth and detrending 81
7.9.3. Spectral Analysis method and choosing right samples 81
7.9.4. Basis B-Splines (Python) 84
7.10. Gantt Diagram and Work Packages 86
8. Bibliography 89

List of Figures

Figure 2.1: Triangulation technique for positioning. 17
Figure 2.2: Representation of the SNR-Analysis for a zenith-looking antenna. 19
Figure 2.3: Vectorial notation of the three contributions [17]. 20
Figure 2.4: GNSS signal acquired at the station. The direct signal defines the 2nd degree shape, the coherent reflected signal is appreciated in [0.1, 0.15] and the incoherent contribution is the random noise along the whole interval. 20
Figure 2.5: The x axis range [0,1] represents one day and the y axis represents the detrended amplitudes in dB. Each satellite has one specific color. 23
Figure 2.6: EUREF Network. Green dots are GNSS stations that provide daily, hourly and real-time data. Orange dots are stations that provide daily and hourly data. Red dots are stations that just provide daily data. 26
Figure 2.7: Bloc diagram of the process to obtain the data. 27
Figure 2.8: The left plot represents the SNR signal for one day (8.1), the middle plot the elevation of a satellite for one day (8.2), and the right plot is the detrended SNR signal for the 2nd segment of the day (8.3). 28
Figure 3.1: Satellite view of the station location. 28
Figure 3.2: Photo of the GNSS Receiver and the geodetic reference level. 29
Figure 3.3: Skymap plot for all the GPS Satellites for Mallorca (8th of January). 29
Figure 3.4: Information about the tide gauge from http://www.puertos.es/es-es/oceanografia/Paginas 30
Figure 3.5: Spectrogram plot for GPS L1. 31
Figure 3.6: Spectrogram plot for L1 and average azimuth of 122° 32
Figure 3.7: Spectrogram for L1 and changing the minimum elevation angle to 2°. 33
Figure 3.8: Spectrogram for L1. 33
Figure 3.9: Spectrogram for L2. 34
Figure 4.1: Localization of the TARI antenna. 36
Figure 4.2: LEICA antenna in Tarifa Station. 36
Figure 4.3: SNR signal for the MAL1 station. It is more difficult to distinguish between the multipath and the direct signal than in Fig. 21. 37
Figure 4.4: Temporal signal for GPS L1 in Tarifa. The y axis shows the C/N0 in dB and the x axis is the epochs for one day. 38
Figure 4.5: Information of the tide gauge station. 38
Figure 4.6: Representation of the Sea Height for one day considering each window from the spectrogram. 39
Figure 4.7: Results for 100 days without windowing the segments. 40
Figure 4.8: Basis splines multiplied by the returned factor by the least squares method. Due to irregularities in the extremes, from 3 days just 2 days are analyzed [0.5, 2.5]. 41
Figure 7.1: Map showing all the floats around the globe. 44
Figure 7.2: Description of this method with the interaction between the Direct and Reflected Signal. The specular point (Appendix 7.6) represents the center of reflection for the first Fresnel Zone. 47
Figure 7.3: Example of a temporal detrended SNR. 51
Figure 7.4: Spectral response for the Fourier Periodogram technique. 51
Figure 7.5: Spectral response for the Lomb Scargle Periodogram technique. 52
Figure 7.6: Spectral response for the Capon technique. The Capon filter was designed with m= 1500. The Capon Filter is much slower than the rest due to the correlation matrix calculation. The Capon height determination differs a little bit with the rest of methods 53
Figure 7.7: Detrended signal (L1) in orange and elevation(azimuth) in blue for the 13th of September 2016. 54

Figure 7.8: Specular point of reflection. 54
Figure 7.9: The biggest circle represents the reflection for 2° elevation and the little one is 5° elevation. 55
Figure 7.10: Red dots are results obtained using the Spectral Analysis method and the black ones are the Ground Truth provided by Puertos del Estado for GPS L1 56
Figure 7.11: Correlation and Linear Regression between Ground Truth (x axis) and Spectral Analysis (y axis). 57
Figure 7.12: Histogram of the error (positive error is when Spectral Analysis is higher than Ground Truth). 57
Figure 7.13: Red dots are results obtained using the Spectral Analysis method and the black ones are the Ground Truth provided by Puertos del Estado for GPS L2 58
Figure 7.14: Correlation and Linear Regression between Ground Truth (x axis) and Spectral Analysis (y axis). 59
Figure 7.15: Histogram of the error (positive error is when Spectral Analysis is higher than Ground Truth). 59
Figure 7.16: Red dots are results obtained using the Spectral Analysis method and the black ones are the Ground Truth provided by Puertos del Estado for GLONASS L1. 60
Figure 7.17: Correlation and Linear Regression between Ground Truth (x axis) and Spectral Analysis (y axis). 60
Figure 7.18: Histogram of the error (positive error is when Spectral Analysis is higher than Ground Truth). 61
Figure 7.19: Spectral Analysis results (red dots) for GLONASS L2 against Ground Truth (black dots). 62
Figure 7.20: Correlation and Linear Regression between Ground Truth (x axis) and Spectral Analysis (y axis). 62
Figure 7.21: Histogram of the error (positive error is when Spectral Analysis is higher than Ground Truth). 63
Figure 7.22: GPS L1 in red dots against Ground Truth in black. 64
Figure 7.23: Correlation between Spectral Analysis and Ground Truth. 65
Figure 7.24: Histogram of the error. 65
Figure 7.25: Spectral Analysis (red dots) against Ground Truth (black dots) for GPS L2. 66
Figure 7.26: Correlation between Spectral Analysis and Ground Truth. 67
Figure 7.27: Histogram of the error. 68
Figure 7.28: Spectral Analysis (red dots) against Ground Truth (black dots) for GLONASS L1. 68
Figure 7.29: Correlation between Spectral Analysis and Ground Truth. 69
Figure 7.30: Histogram of the error. 69
Figure 7.31: Spectral Analysis (red dots) against Ground Truth (black dots) for GLONASS L2. 70
Figure 7.32: Correlation between Spectral Analysis and Ground Truth. 71
Figure 7.33: Histogram of the error. 71
Figure 7.34: The orange line symbolizes Ground Truth and the blue line the B-Splines Method. 72
Figure 7.35: The orange line symbolizes Ground Truth and the blue line the B-Splines Method. 73
Figure 7.36: The orange line symbolizes Ground Truth and the blue line the B-Splines Method. 73
Figure 7.37: B-Splines fitting of a zero degree curve (y=1). 74
Figure 7.38: B-Splines fitting of a first degree curve (y= Days). 74
Figure 7.39: B-Splines fitting of a second degree curve (y= (Days)^2). 75
Figure 7.40: Name format for RINEX 2 format (i.e. tari0310.17o). The observation data provided by the FTPs in Compact Rinex Format ends with d instead of o. 76
Figure 7.41: Name format for RINEX 3 format (i.e. TARI00ESP_R_20170310000_01D_30S_MO.rnx). 76

Figure 7.42: SNR for a Galileo Satellite in Tarifa Station. Observational files for RINEX 3 are only available sampled every 30 seconds. 77
Figure 7.43: Time Plan 88

List of Tables

Table 3.1: Results for GPS and GLONASS in Mallorca. Error, correlation, coverage and Linear Regression results are presented. 35
Table 4.1: Results Spectral Analysis for GPS and GLONASS in Tarifa..... 39
Table 4.2: Results B-Splines for GPS and GLONASS in Mallorca. 41
Table 5.1: Summary of the software costs. 42
Table 5.2: Summary of the development costs. 42
Table 7.1: Results Spectral Analysis for GPS and GLONASS different combinations in Mallorca. 63
Table 7.2: Results Spectral Analysis for GPS and GLONASS different combinations in Tarifa.... 72

1. Sea Level Measurements

1.1. Introduction

Measuring Sea level has been a study of interest since long ago [1]. In the past, people linked the regular movements of the sea with the movements of the Sun and the Moon. There were even those who believed in a divine (Gods) reason to explain those changes. However, scientific community now understands that neither the sea nor the land levels are constant, since they are varying due to several contributions. Most of the vertical movements of the land are associated with tectonic processes, such as earthquakes and/or volcano eruptions. Changes in the sea level are also affected by tectonic plaques as well as glacial changes, variations in the ocean currents, and specially climate change.

Sea level instantaneous measurements have three different contributions, as shown in Eqn. (1.1):

$$actual\ sea\ level = observed\ mean\ sea\ level + tides + meteorological\ residuals \tag{1.1}$$

Each of these contributions is controlled by different physical processes. The variation of each contributor is independent from the variations of the other ones. Each sea level contributor is defined below:

- Mean Sea level: It is the average level of the Sea surface. It is based on hourly measurements taken over a period of at least one year.
- Tides: Tides are the periodic movements of the sea that have coherent amplitude and phase relationship with respect to some geophysical forces/processes [1]. The dominant one is the variation of the gravitational field on the Earth's surface due to the regular movements of the Earth-Moon and Earth-Sun systems, causing the so called gravitational tides.
- Meteorological residuals: Are the non-tidal components that remain after removing the tides for analysis [2]. They are irregular, as the variations in the weather, i.e. atmospheric pressure. The clearest example is the effect on sea level of tropical storms.

1.2. Methods for measuring Sea Level

Today, there are two main types of Sea Surface level measurements:

- Relative Sea level (RSL): It is the height of the sea surface relative to land [3]. The most common way of measuring it is using tide gauges. It is critical to know whether the land itself is moving before determining the absolute height of the oceans. Some examples of the main processes that can cause RSL are: tectonic uplift, sediment compaction, volcanic isostasy and extraction of natural resources.
- Satellite altimetry: It measures the distance between an Earth-orbiting satellite and the surface of the ocean using RADAR technologies. It measures the delay in time between the EM wave emitted by the satellite and the back-scattered echo [4]. Since the orbit of the satellite is well defined with a precision up to 2cm, the height of the ocean relative to any coordinate system can be measured.

The most important methods for retrieving Sea height measurements are better detailed in the Appendix 7.1.

1.3. Remote Sensing overview

Remote sensing is based on acquiring information of an object or phenomenon without touching it [5]. It is used in several scientific fields, such as geography [6], oceanography, geology, agriculture [7], and it has also military applications [8].

The term "remote sensing" generally refers to the use of satellite, aircraft-based, or ground-based sensors to perform observations of the Earth, including its surface, atmosphere [9], land [10] and oceans [11]. This dissertation is based on inferring information from EM propagated and scattered signals. It can be split in two different groups depending on the mechanism to acquire the information. “Active” remote sensing occurs when the sensor emits the signal that it will sense later [5] (i.e. when a signal is emitted by a satellite or aircraft and its reflection by the object is detected by the same sensor, also known as RADAR). "Passive" remote sensing occurs when the signal sensed is already available in the media and the sensor only acts as a receiver [5] (i.e. the reflection of sunlight is detected by the sensor since the Sun is the EM emitter).

One clear advantage of remote sensing is that it allows collecting data from dangerous or inaccessible areas, such as the Antarctica [12] or the Amazonas forest [13]. Some remote sensing applications include monitoring deforestation in areas such as the Amazon Basin, glacial features in Arctic and Antarctic regions, and sea state parameters of the oceans [11] (i.e. height, pressure, temperature, current speed and direction …). Remote sensing also replaces costly and slow data collection of direct contact on-ground sensors, ensuring that the process is not disturbed by the measurement. Satellites such as Seasat and T/P [5] use advanced dual-band radar altimeters to measure sea surface level from spaceborne platforms.

1.4. GNSS-R for measuring Sea Surface Level

GNSS-R is a technique that uses the GNSS (Global Navigation Satellite System) transmitted and scattered signals to obtain remote sensing observations of the Earth. In the navigation world, the reflected signal is regarded as an error source that deteriorates the system’s positioning accuracy and many efforts have been made to mitigate it [14]. However, these scattered signals, smartly processed, can be used in many remote sensing applications. They allow retrieving certain information from a system which was not designed for that purpose. If this technology improves its accuracy and sample rate it could become a feasible alternative to satellite altimeters and tide gauges, since no specific equipment for Sea monitoring would be required, which may reduce costs drastically.

2. GNSS-R Introduction

2.1. Concept

GNSS-Reflectometry (GNSS-R) remote sensing is a new category of satellite navigation applications. Essentially, it entails a method of remote sensing that receives and processes microwave GNSS signals reflected from different surfaces in order to extract useful information about them.
In this process, the GNSS L-Band satellites act as the transmitter and the receiver is in another platform (ground-based, airborne, and/or spaceborne). For altimetry applications, a GNSS-R receiver can also be placed on land.
The advantages of GNSS-R remote sensing over satellite scatterometry and radar altimetry are the following ones:
1) No additional transmitter (passive).
2) Plenty of signal sources, including GPS, Galileo, GLONASS, and Beidou/Compass (all GNSS transmitters).
3) 24-hour availability.
4) Geo-referenced and time-reference system.

2.2. GNSS and GNSS-R

2.2.1. Introduction GNSS

A brief description about the most important events in GNSS history is given in Appendix 7.2 and a full description of the two GNSS systems used in this project (GPS and GLONASS) is done in Appendix 7.3, including a short description for the Galileo system. Herein an introductory description is given.
Currently, there are two operational GNSS (GPS and GLONASS) and two more in development (Galileo and Bei-Dou2). It is expected that once the four global constellations are fully operational (2020) there will be around 120 GNSS satellites for global positioning and navigation orbiting around the Earth. As some satellites need to share frequencies, differences between them are needed so no interferences are produced. While GPS uses a CDMA spread-spectrum technique and all its satellites broadcast at the same three frequencies (L1, L2 and L5), each GLONASS satellite transmits in a different frequency using a 15-channel frequency division multiple access (FDMA). The individual features of GPS, GLONASS and Galileo are explained in Appendix 7.3.
GNSS systems make use of Time of Arrival (TOA) measurements [15]. They measure the signal time of reception and compute the time that the signal has been travelling from the satellite to the receiver. GNSS satellites have atomic clocks synchronized among them, a crucial property of a TOA system, and the receivers get locked to those clocks. The travel time is directly converted into a distance measurement called Pseudo-Range (PR) [16] multiplying by the speed of the light. For each of the satellites the locations satisfying the PR will form a sphere centered in the satellite and with PR as the radius. In order to determine the 3-D position, three satellites are required to perform triangulation, since the intersection between the spheres will provide two points. However, one can be discarded since it is far away from the Earth surface. Although it seems feasible to retrieve the exact position with just three satellites, an extra satellite is required in order to compensate for clock errors. Figure 2.1 depicts the triangulation method.

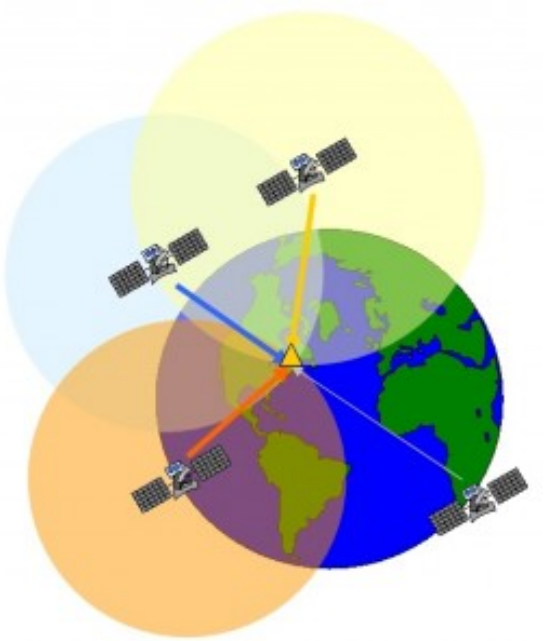

Figure 2.1: Triangulation technique for positioning.

In order to provide reliable measurements, all GNSS signals must accomplish some important properties [17]:

- $ACF_{i,i}(\Delta t) \approx 0$ for $\Delta t \neq 0$; i is equal to the code identifier. This equation means that the Auto-Correlation Function (ACF) must be 0 for any range different than the true one. The problem comes from the fact that the satellites repeat their code, so an inherent ambiguity will be impossible to be removed. For the GPS with C/A codes (period of code of 1ms) the ambiguity is 300 km.
- $ACF_{i,i}(\Delta t) = maximum$ for $\Delta t = 0$ .The ACF must be maximum for the true range.
- $CF_{i,k} \approx 0$ for $i \neq k$ and $\forall \Delta t$ where i and k are code identifiers. This means that the Correlation Function between the signals of different satellites must be always 0.
- $CF_{sys1,sys2} \approx 0$ for $\forall \Delta t$, which means that the CF between different systems (i.e. GPS, GLONASS) must be close to 0 in order to avoid interferences.

The first three of these properties are accomplished by the use of Pseudo-Random Noise (PRN) sequences and Direct Sequence Spread Spectrum (DSSS). The first one provides a very low correlation with other sequences in the set, and also with the same sequence at a different time, as random noise. Although, unlike random noise, it must be easy to generate exactly the same sequence both in the transmitter and receiver in order to get a high correlation (matched filter). The latter consists of spreading the resulting signal in a wider spectrum, resulting in greater resistance to interferences and reaching further distances with the same transmitted total power (reduced PSD).
The last property is accomplished because each system uses different techniques to access the propagating medium. When the systems available work at different frequency bands from each other, a Frequency Division Multiple Access (FDMA) is used to access each individual medium. For some cases, different systems need to share bands (i.e. GPS and Galileo with the L1/E1 Band) so different modulations need to be used by these systems.

2.2.2. GNSS-R for Sea Surface Monitoring

2.2.2.1. Introduction

Since it was demonstrated that reflected GNSS signals can be used to monitor local sea-surface heights [18, 19] several improvements have appeared. The first testing campaign [18] was carried out at the Barcelona Port breaker and dedicated to the development of sea-state retrieval algorithms. An experimental system was designed and manufactured for this purpose which collected and processed GPS data in order to automatically generate a times series of the interferometric complex field (ICF). The ICF was analyzed off line and compared to simple developed models that related the ICF coherence time to the ratio of significant wave height (SWH) and mean wave period (MWP). The results showed good correlation between local buoys data and the analysis.

The concept is attractive since it is relatively inexpensive and easy to deploy and operate. Furthermore, GNSS technology can relate the sea level measurements to a global reference frame, which means that GNSS-R can directly distinguish between relative and absolute sea-surface changes, something traditional tide gauges cannot do without additional equipment.

Apart from the ICF, research related to this topic can be categorized into two groups – phase difference analysis [18] and signal-to-noise ratio (SNR) analysis [20], which also includes Inverse Modeling. The first group is detailed in Appendix 7.4 since it is out of the scope of this work.

2.2.2.2. SNR Analysis

2.2.2.2.1. Theoretical view

The SNR analysis technique or Interference Pattern technique uses a single antenna to acquire direct and reflected GNSS signals, analyzing the SNR pattern created due to coherent addition of both signals at the antenna level.
A benefit of using the SNR method is greater robustness to wind and wave conditions [21], and it has also been demonstrated that the method is useful for determining other important sea-state parameters, such as significant wave height [21]. Fig. 2.2 shows the geometrical configuration of this technique which is similar to the phase difference method but with a single antenna. This method can be divided in two sub-methods based on the direction that the single antenna is pointing to: pointing to the horizon [17] or pointing to the zenith [20]. This dissertation will focus on the analysis of the latter because the antenna pointing to the horizon has already been deeply studied at UPC.

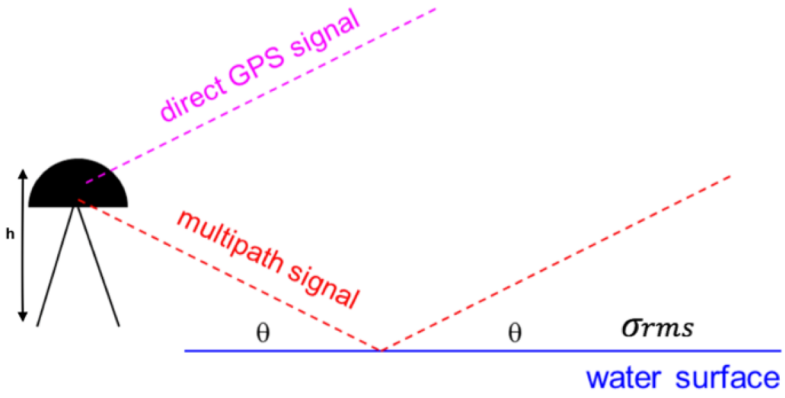

Figure 2.2: Representation of the SNR-Analysis for a zenith-looking antenna.

In Fig. 2.2 h stands for the distance between the water surface and the antenna , θ is the elevation angle which is equal to $90 - \theta_{incident}$; $\theta_{incident,i}$ and $\theta_{elev,i}$ are the incident and elevation angles for the *ith* scatterer respectively, and σ_{rms} is the surface roughness parameter that characterizes the roughness of the reflecting surface.
For this thesis the reflector is assumed constant, i.e., the reflective surface is not moving. In case of a time dependent reflector (moving reflector) the procedure to retrieve the Sea Height would be a little more complex [21] than the one used in this work.

In a real scenario, an infinite number of scatters can be considered. However, since satellites are very far away, some approximations can be applied. The wave front that reaches the antenna directly and the ones that are reflected of the ground are considered parallel, and the rays impinging on the ground can be considered as a plane wave. The contribution of each individual scatter based on its local reference frame is taken into account at the antenna level. Mathematically the IPT can be expressed as:

$$U_{IPT} = U_{dir} + U_{ref,coh} + U_{ref,incoh} \tag{2.1}$$

which is the sum of the direct component and the reflected component (both coherent and incoherent [23]). In order to estimate what a system would measure, the direct and reflected components need to be weighted by the voltage antenna pattern. Since the satellites are constantly moving, these three contributions can be considered vectors that rotate. For the direct signal the rotation is due to the satellite's movement and the Earth's rotation. The coherent reflected signal depends on the same two terms, but when compared to the direct signal, it also depends on the antenna height. For the case of the incoherent reflected signal, the rotation is considered random but there is a rotation speed defined by the correlation among samples. In the case where samples are uncorrelated this speed will be null and the rotation will be completely random. All these contributions will result in a vector rotating (Fig. 2.3) due to the satellite's movement, and a fading in the interference pattern amplitude due to the multi-path contamination (Fig. 2.4). This fading has two mean features:

- The coherent reflected signal creates a slow regular fading, increasing its speed/frequency by increasing the antenna height.
- Fast-time irregular random fading due to the non-coherent component.

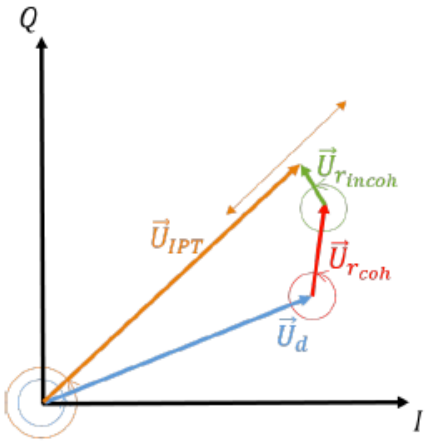

Figure 2.3: Vectorial notation of the three contributions [17].

The received power pattern (P_R) can be inferred from Eqn. (2.1) and can be expressed as [24]:

$$P_R \propto |U_{IPT}|^2 = \left|U_{dir} + U_{ref,coh} + U_{ref,incoh}\right|^2 = |U_{do}|^2 \cdot \left|F_n(\theta_{elev}, \phi_{azim}) + \sum_{m=1}^{M} F_n(\theta_m, \phi_m) A_m e^{j\phi_m} e^{j\frac{4\pi h_m}{\lambda}\sin(\theta_m)}\right|^2 \quad (2.2)$$

where U_{do} is the incident electric field altitude, F_n the antenna radiation pattern, $\theta_{elev}, \phi_{azim}$ the elevation and azimuth of the satellite, λ the wavelength , m the scatter's index, M the total number of scatters, θ_m, ϕ_m local elevation and azimuths for the mth scatterer. The term $F_n(\theta_{elev}, \phi_{azim})$ is related to the direct signal whereas the term $\sum_{m=1}^{M} F_n(\theta_m, \phi_m) A_m e^{j\phi_m} e^{j\frac{4\pi h_m}{\lambda}\sin(\theta_m)}$ refers to the reflected signal. When the coherent scattering mechanism dominates, it is simplified to just having one scatterer because all the terms in the summation are in phase. If the incoherent scattering dominates there is no useful information in the IPT.

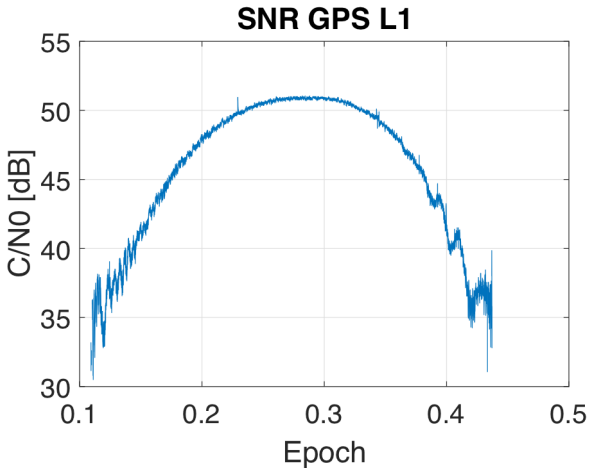

Figure 2.4: GNSS signal acquired at the station. The direct signal defines the 2nd degree shape, the coherent reflected signal is appreciated in [0.1, 0.15] and the incoherent contribution is the random noise along the whole interval.

When the coherent part of the interference pattern dominates, the received power can be defined as:

$$P_R = |E_{0_i}|^2 \cdot \left(|F_n|^2 + |F_{-n} \cdot R|^2 + 2 \cdot F_n F_{-n} R cos\left(\frac{4\pi}{\lambda} h \sin(\theta_{elev}) + \phi_R + \phi_{F_{-n}} - \phi_{F_n} \right) \right) \quad (2.3)$$

where F_n is equal to $F_n(\theta, \phi)$ for $\forall m$ from Eqn. (2.2), F_{-n} is equal to $F_n(-\theta, \phi)$, R (Fresnel reflection coefficient) is $R(\theta, \phi)$, h the vertical distance between the antenna phase center and the reflecting surface. Looking into the phase terms (the ones inside the cosine), $\frac{4\pi}{\lambda} h \sin(\theta_{elev})$ is identified as the fundamental frequency whereas the contribution of the other three elements can be considered negligible as they remain constant along the antenna beamwidth.
The most widely used criterion to determine if a surface is smooth or rough is applying the "Rayleigh criterion" [25], which determines that a surface is smooth if:

$$\sigma_h < \frac{\lambda}{8 \sin(\theta_{elev})} \quad (2.4)$$

which means that the phase difference for all the scatters is lower than $\frac{\pi}{2}$. As it can be seen from Eqn. (2.4) whether a surface is smooth or rough will depend on the wavelength and elevation angle. The larger the incidence angle, the smoother the surface appears to be and vice versa.

Once it has been determined that the entire phase of the function will be driven by the first term inside the cosine in Eqn. (2.3), h can be isolated from the frequency in the multipath oscillations of the acquired signal.
A clarification about the relationship between the frequency term and the Sea Height is required. The oscillation frequency of the SNR signal acquired is not constant in terms of θ_{elev}, but it is terms of $sin(\theta_{elev})$. As stated by the first order Taylor Series of the sine ($\sin(x) \approx x$ for $x \ll 1$), for low elevation angles the sinusoidal function could be approximated by its argument, but for higher elevation angles this approximation would be no longer valid. Therefore, a change of variables is necessary so when Spectral Analysis is defined as a function of $sin(\theta_{elev})$, the angular speed (w) will become constant as $\frac{4\pi}{\lambda}$ and the frequency (f) will be $\frac{2h}{\lambda}$.
One big problem arises from this change of variables, the x axis will no longer be evenly sampled because of the sine function. In order to perform the spectral analysis of the signal, only the methods that accept unevenly sampling can be used, and for example methods such as FFT will no longer be valid.
Unevenly sampling analysis has been studied before in different observational sciences, like astronomy, where the observer cannot completely control the time of the observations, but must simply accept a certain dictated set of $t_i's$. Among the most important methods used are: Fourier Periodogram, Least Squares Periodogram, Lomb Scargle Periodogram [10] and CAPON. These methods are completely analyzed in Appendix 7.5.

2.2.2.3. Inverse Modeling

2.2.2.3.1. Introduction

This method was first introduced by [26] and consists on retrieving sea-surface heights from GNSS-R data by inverse modeling of SNR observations from a single geodetic receiver. This method relies on a B-Spline [27] representation of the temporal sea level variations in order to account for its continuity (periodicity). The corresponding B-Spline coefficients are determined

through a non-linear least-squares fit to the SNR data, and a consistent choice of model parameters enables the combination of multiple GNSS in a single inversion process. This fact leads to an increase in precision as better spatial and temporal sampling is accomplished. The method will be tested in the same two stations as the SNR-analysis.
When analyzing the Spectral Analysis method it has been defined the detrended SNR in Eqn. (2.3):

$$\delta SNR = A \cdot \cos\left(\frac{4\pi h}{\lambda} x + \varphi\right) \tag{2.5}$$

where A is a constant factor depending on the direct power received from the satellite, the relative interferometric power from the reflections, the incoherent power and noise power, and $x = \sin(\theta_{elev})$. An assumption made when detecting the peak of the spectral amplitude (or the reflector height peak) is that the LSP spectrum, or at least the peak of the LSP spectrum, only consists of one single frequency. Obviously, this does not have to be true. First of all, the sea surface is usually not perfectly flat. Second, the observed SNR data are affected by multipath from multiple reflectors located in the surroundings of the GPS antenna. With a satellite azimuth and elevation mask it is possible to select observations from directions where the sea surface is expected to be the only reflector, but there can be additional sources of reflection from, e.g., the ground next to the antenna or the antenna installation. If these additional reflections are close in multipath frequency to the reflection from the sea surface, they will overlap in the LSP spectrum, which could distort the peak and introduce an error in the retrieved sea level. In [28] they propose a correction derived from using a time dependent reflector height for the stations where the tidal variations are considerably high. The correction was the following one:

$$\frac{d\ phase\{dSNR\}}{d\ sin(\theta_{elev})} = \frac{4\pi h}{\lambda} + \frac{4\pi \hat{h}}{\lambda} \frac{\tan(\theta_{elev})}{\hat{\theta}_{elev}} \tag{2.6}$$

where $\hat{h}$ and $\hat{\theta}_{elev}$ are the time derivative of the reflector height and the satellite elevation angle, respectively. The second term of the equation can therefore be seen as a correction term.

This method only considers a correction term for linear temporal changes of the reflector height. In contrast to this, the inverse modelling directly accounts for temporal changes in sea-surface heights, by modeling height as a smooth function.
The inverse modelling consists on fitting an analytic function to measured δSNR oscillations. Thus, the result does not rely on spectral methods, but use a physical model for the data analysis. A similar method was used in [28] for snow depth determination. The oscillations of the δSNR will be modelled based on Eqn. (2.5) and an attenuation factor in order to account for the decrease of the multipath oscillation amplitude with increasing elevation. The attenuation factor is:

$$S^2 = e^{-4k^2 s^2 sin^2(\theta_{elev})} \tag{2.7}$$

where k is the wave number and s is the standard deviation of the reflector surface height. The s term accounts for loss of coherence in the reflected signal due to surface random roughness [23]. The oscillation part of the δSNR will then be modelled as:

$$\widehat{\delta SNR} = (C_1 \cdot \sin\left(\frac{4\pi h}{\lambda}x\right) + C_2 \cdot \cos\left(\frac{4\pi h}{\lambda}x\right))e^{-4k^2\Lambda x^2} \tag{2.8}$$

where the sine and cosine term replace the amplitude and phase from Eqn. (2.5) in order to have more stability during the inversion process. The term $\Lambda = s^2$ is introduced for clearer notation and $x = \sin(\theta_{elev})$.
The conversion back to amplitude and phase is straightforward:

$$A = \sqrt{{C_1}^2 + {C_2}^2} \tag{2.9}$$

$$\varphi = tan^{-1}(\frac{C_2}{C_1}) \tag{2.10}$$

As it can be seen, Eqn. (2.8) combines geometric and radiometric information and represents a well suited model function to retrieve the heights from inverse modeling.
For instance, Fig. 2.5 shows all the segments that fulfill the requirements for one day for GPS and GLONASS L1.

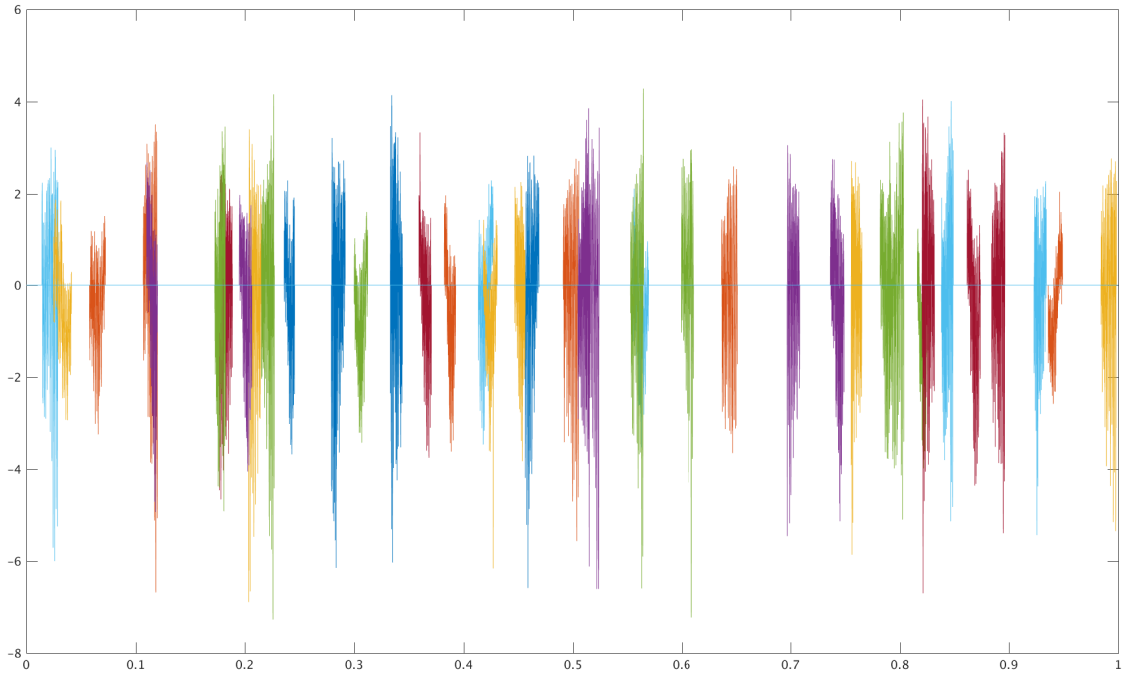

Figure 2.5: The x axis range [0,1] represents one day and the y axis represents the detrended amplitudes in dB. Each satellite has one specific color.

According to [29] the amplitude is mainly influenced by satellite signal strength, receiver characteristics, and electromagnetic properties of the reflecting surface. These factors can be considered to be constant over a few days for each satellite. The surface random roughness, which is driven by average local wind speed and directions, will be also considered constant, but in this case for all the satellites. A lot of trouble was caused by this value as it was the reason why the system did not converge to a minimum at the beginning. As the values in the exponential are negative, the bigger the values the less amplitude that the detrended model will have so if Λ is too big, the variables obtained from LS will be wrong as there will be no way to reduce the LS. At the end Λ was set to 0.02, future study needs to be done in order to find a more accurate way to decide this variable.
The process followed in this project for the pre-processing was the following one:

1. Obtain the C_1 and C_2 parameters for each individual satellite. This was accomplished doing the least squares between the detrended model and all the segments for the same satellite.
2. Normalize the amplitude of all transects by $A_{max} = \sqrt{{C_{1,nmax}}^2 + {C_{2,nmax}}^2}$

In order to handle the temporal variations of the sea-surface height the B-Spline representation will be used to model the sea-surface height.

2.2.2.3.2. Modeling SSH using B-Spline functions

The larger difference between inverse modeling and Spectral analysis is that the first one uses a function that considers tidal and long term variations to determine h. In other words, a smooth function considers previous results to determine the actual results as well as considers the daily sinusoidal behavior of tides. In principle, any analytic function that considers tidal and long-term variations is sufficient to be implemented in an inversion algorithm, although some of them lead to discontinuities at the nodes when computing first-order derivatives. In [27] B-Splines functions were proposed to overcome these deficits while still providing enough variability to consider the most dominant sub-daily and long-term level variations.
B-Splines functions are constructed from zero-degree basis functions which are defined as:

$$ {N_j}^0(t) = \begin{cases} 1 \; if \; t_j \le t < t_{j+1} \\ 0 \; otherwise \end{cases} \tag{2.11} $$

and B-Splines of higher order "r" are recursively calculated based on Eqn. (2.11):

$$ {N_j}^r(t) = \frac{t - t_j}{t_{j+r} - t_j} {N_j}^{r-1}(t) + \frac{t_{j+r+1} - t}{t_{j+r+1} - t_{j+1}} {N_{j+1}}^{r-1}(t) \tag{2.12} $$

where ${N_j}^r(t)$ is the basis B-Spline function for knot j. Once all the basis functions have been created, the sea-surface height variations can be approximated as:

$$ h(t) = \sum_{j=0}^{N} h_j {N_j}^r(t) \tag{2.13} $$

where $h_0, \dots, h_N$ are the coefficients of the knots for the N+1 basis splines. These coefficients are obtained in the least squares fitting process. For this application quadratic B-Splines were chosen as bigger order B-Splines needed a lot more time to compute and also because the SSH is assumed to be smooth enough. The capability of resolving certain spectral features depends only on the temporal spacing of the nodes, which means that one can place more nodes when expecting higher frequency components or increase the temporal node spacing when dealing with rather low-frequent signals.

2.2.2.3.3. Non-linear least-squares parameter estimation

Considering Λ as a constant variable, the parameters that need to be estimated from a consistent inverse modelling are: $C_1, C_2, h_0, \dots, h_N$. Although C_1, C_2 are estimated, their value does not give any meaningful result.

It is obvious that the number of observations (1 Hz) is much larger than the unknowns that need to be estimated (nodes every one hour at most). Therefore, one faces an over-determined parameter estimation problem which will be solved by minimizing the following cost function:

$$min \sum_N (y_i - f(C_1, C_2, h_0, \dots, h_N))^2 \tag{2.14}$$

where y_i are the SNR values depicted in Fig. 2.5. Due to the high non-linearity of Eqn. (2.8) a non-linear least-squares method needs to be applied. The Python environment was used along the MINPACK [30] from SciPy package because the minimization problem did not converge with the *lsqcurvefit* function in MATLAB.

The choice of initial parameters in the non-linear least-squares estimation process is crucial, especially the initial distance between the antenna and the sea surface is of importance, since it determines whether the solver converges to the global or a local minimum. Therefore, the initial height should be chosen site-specific, using a representative value for the average antenna height above the sea level, setting all a priori B-spline node values to this initial estimate. The other parameters, C_1 and C_2 are less sensitive to their a priori values, and do not need to be initialized for each site.
Another point of interest is the number of nodes used for the B-spline implementation, as it determines the maximum temporal resolution of the solution. For a high temporal resolution, a large number of nodes is desirable, however this will increase the computational load of the non-linear least-squares estimation and may eventually degrade the final solution due to overfitting. Furthermore, the SNR data are not continuous, and there are data gaps when no satellites are within the azimuth/elevation sectors considered in the analysis process. These periods without data impose a limit on the temporal resolution of the inversion process, since all B-spline intervals must cover a time span with sufficient data. Thus the B-spline intervals must be larger than the longest gaps in the data set, in this Thesis the interval chosen was three hours.

2.2.3. EUREF Network

2.2.3.1. Concept

The Regional Reference Frame Sub-Commission for Europe (EUREF) Permanent GNSS Network is a GNSS network continuously operating GNSS reference stations (GPS, GLONASS, Galileo, Beidou, ...). It includes several data centers that provide access to the stations data and continuously analyze it. Product centers or coordinators generate the EPN products. A Central Bureau is responsible for the daily monitoring and management of the EUREF Permanent Network (EPN).

All contributions to the EPN are provided on a voluntary basis, with more than 100 European agencies/universities involved, Fig. 2.6 depicts the stations that belong to EUREF. The EPN operates under well-defined international standards and guidelines which are subscribed by its contributors. These guidelines guarantee the long-term quality of the products.

The EUREF's website provides the RINEX data for the stations we were interested as well as the site information form for each station (site location, GNSS Receiver Information, GNSS

Antenna Information, Surveyed Local Ties, Meteorological Instrumentation and contact information).

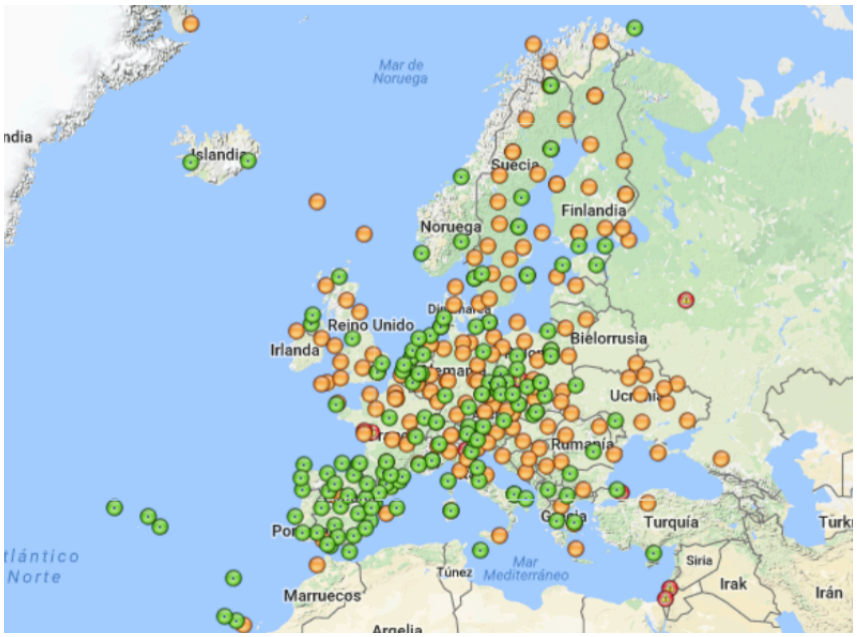

Figure 2.6: EUREF Network. Green dots are GNSS stations that provide daily, hourly and real-time data. Orange dots are stations that provide daily and hourly data. Red dots are stations that just provide daily data.

2.2.3.2. Data structure and standardization

Data from all the stations that are part of the EUREF Network is publicly available in different websites and FTPs for free, including the EUREF website and different local networks (i.e. ERGNSS is the Spanish Network). The FTPs show information about the last 90 days. If any other period different than that one is desired one must contact the responsible people of EUREF or local network. In order to analyze Spanish stations, the following ftp should be consulted: http://ftp.geodesia.ign.es. Therein, information of the station's main parameters is provided, such as the stations sampling frequency (1, 5, 15, 30 seconds). For this work, since the sampling period determines the maximum spectral range available, the higher the better, so 1 second sampled data will be used. Even though it was planned to study the Galileo system, the information files are sampled every 30 seconds, and no results could be obtained from such a low sample frequency. Apart from this information, the FTP also provides geodetic data, tide gauges measurements, and correction information.

In this work we will only focus on the information provided by ERGNSS. Daily data is given in Compact Rinex Format (CRX) (Appendix 7.8) divided in a group of 24 files (one per hour). For each hour, at least three different files are provided (these are RINEX 2 format):

- .N : GPS ephemeris data, which provides the position of every Satellite during the entire day.
- .G : GLONASS ephemeris data, the same as the .N files but with GLONASS satellites positions.
- .d : Data file. Signal data received by all the satellites in the stations antenna FOV.

Those files are zipped so unzipping software will be required to work with those files.
Further information about the different formats of the data used in this thesis is provided in

Appendix 7.8.

2.2.4. Description of SW used including data packages

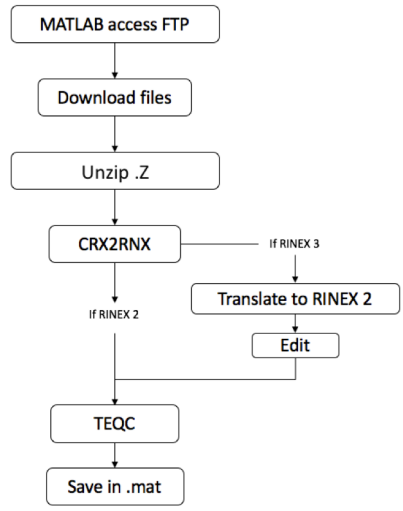

Figure 2.7: Bloc diagram of the process to obtain the data.

In this section all the steps and tools required to move from the data available in the FTP to the data that can be processed in MATLAB or Python are explained (Fig. 2.7), although the use explanation for each program is covered in Appendix 7.8 including the special case when Galileo satellites are to be included in the analysis.

First, all files need to be unzipped and 7-zip file has been used for this purpose [31]. After that, data files need to be translated into RINEX observation files (.o for RINEX 2 and MO.rnx for RINEX 3) from their original format. To do so, the tool *crx2rnx* from RNXCMP software has been used. Once the RINEX files have been obtained TEQC Software provided by UNAVCO has been used in order to get the data of interest (SNR, epochs, elevation, …).

The output files of interest generated by Teqc are:

- .azi , .ele : azimuth and elevation of each SV as seen from the receiver. Azimuth is defined clockwise from North, and elevation is the angle above the horizon.
- .sn1 , .sn2 : signal to noiseratio values. If Galileo files are included, .sn7 and .sn8 are added (Appendix 7.8).

The epoch information as well as the PRN are also available to know precisely the sampling time of each data sample. The last step is to save the data from those files into a Matlab format. For this work, table format has been used.

2.2.5. Data Processing

Before applying the different methods to infer the Sea Surface Height, several steps are required to prepare the data for further analysis:

- Divide the SNR of each Satellite for one day between each ascending path and descending path (Fig. 2.8(b)). The easiest way to achieve this is by looking when there is a change of sign in: $\frac{delevation}{dx}$
  As the data acquired from time to time has individual corrupted samples, these ones need to be filtered in order to divide the desired segments only.
- Afterwards, each segment needs to be detrended. This step is needed to erase the lower period contribution of the direct signal as well as setting the average SNR to 0 (Fig. 2.8(c)). The literature [32] recommends a low degree polynomial so the fast fluctuations of the multipath do not get affected. After testing several degrees, the chosen one was 6.
- If the detrended signal stills has an average different than 0, subtract that value.

- Apply the elevation and azimuth filters to each segment. These filters will depend on the station location. Two different methods can be used: testing with the Lomb Scargle Spectrogram (Section 3.3) the range where results perform better or by looking at the 1st Fresnel zone reflection (Appendix 7.6) on Google Maps.

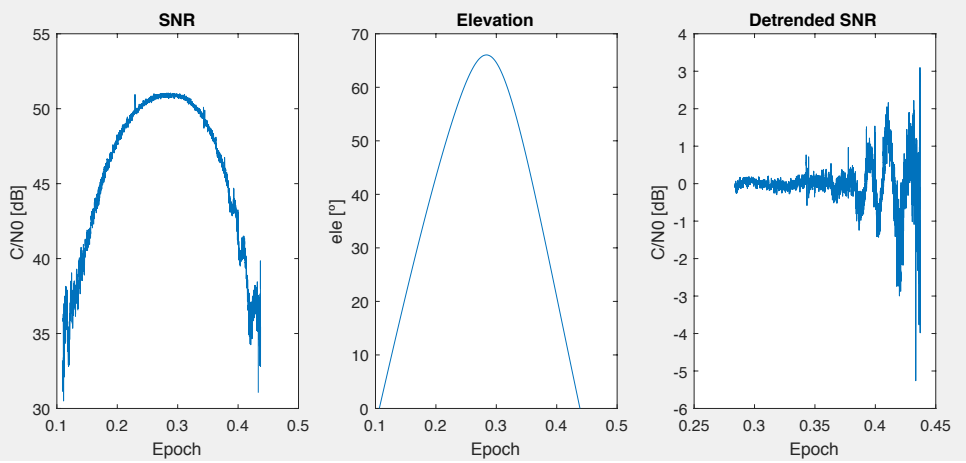

Figure 2.8: The left plot represents the SNR signal for one day (a), the middle plot the elevation of a satellite for one day (b), and the right plot is the detrended SNR signal for the 2nd segment of the day (c).

Once the reflected signal has been isolated from the other contributions and filtered it is time to perform the Spectral Analysis of unevenly samples (Appendix 7.5).

3. MAL1 Station

3.1. Station Description

The first station that has been studied is located in Palma de Mallorca harbor. This station belongs both to ERGNSS (Spanish GNSS Network) and Puertos del Estado. The exact coordinates of the GNSS station are 39° 33' 36,63788'' N, 2° 38' 14,83684'' E whose exact position is shown in Fig. 3.1:

Figure 3.1: Satellite view of the station location.

The station is composed by a LEIAT504GG antenna together with a GRX1200GGPRO GPS Receiver, which stores, processes, and sends GNSS data 24/7. The receiver records data at 1 Hz

sampling rate. The constellations that this station is able to track are GPS (L1, L2 and L5) and GLONASS (L1 and L2). Only RINEX 2 data is provided so Galileo is not included (Appendix 7.8).

Figure 3.2: Photo of the GNSS Receiver and the geodetic reference level.

The Receiver is at the top of a pillar of height 0.5 meters made of concrete block. As it can be seen from Fig. 3.2 the range of azimuth angles looking at the open Sea are limited, so during the processing of the data a filter in azimuth will be needed in order to save only the valuable information. Moreover, as the station is inside a commercial harbor, some data periods could be corrupted due to the presence of big ships close to the station. The Station is power supplied by a horizontal solar panel. Fig. 3.2 depicts the GNSS station along with the geodetic reference level (red circle) on the floor and Fig. 3.3 plots a Skymap for all the GPS Satellites for one day.

The average vertical distance between the Sea surface and the phase center of the antenna is around 4.8 meters.
The results will be compared with a local tide gauge close to the GNSS station. The data of the tide gauge was provided by Puertos del Estado and it is sampled every 5 minutes.

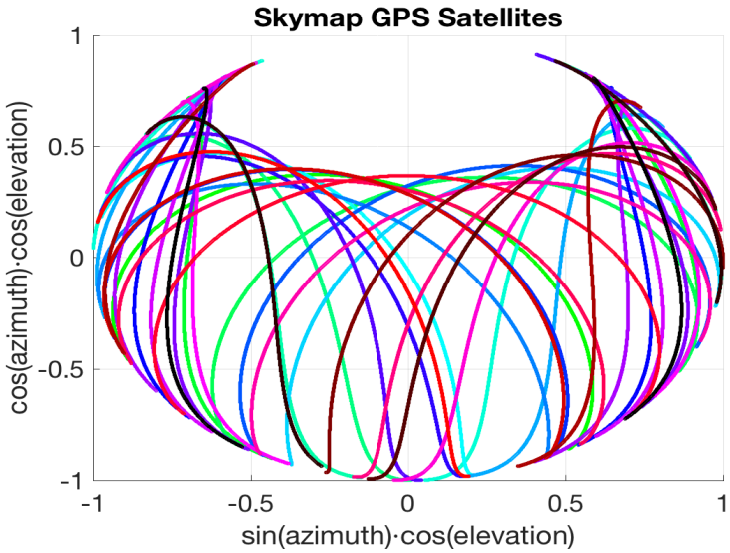

Figure 3.3: Skymap plot for all the GPS Satellites for Mallorca (8th of January).

3.2. Ground Truth Available

Figure 3.4: Information about the tide gauge from http://www.puertos.es/es-es/oceanografia/Paginas

One of the reasons for choosing the station in Palma de Mallorca was because of the closeness of a tide gauge station. The station belongs to REDMAR. This network has the objective of measuring, recording, analyzing and saving continuous flux of data from the Sea level in the harbors. In order to check the quality of the results, these will be compared against the ground truth provided by the tide gauge.
The type of sensor for this station is a Radar manufactured by Miros. Tide gauge measurements for this station have been recorded since September of 2009. The cadence that Puertos del Estado stipulates is one sample every minute, although after asking for the data to them, these was provided for one sample every five minutes.

3.3. Lomb Scargle Spectrogram

Final results will depend on the azimuth and elevation range chosen, so the range of values needs to be chosen carefully. The easiest way for determining the azimuth range is by just looking at satellite images from the location of the station and trying to deduce the range of angles where the station is looking to the open sea. A more scientifically accurate method can be obtained applying the so called Lomb Scargle Spectrogram. This method consists of analyzing all the detrended paths (without filtering in azimuth and for a range of elevations from 5 to 25) in order to determine when the real contribution for the good results is produced. A spectrogram is a visual representation of the spectrum of frequencies most commonly used in Audio Processing. It consists on windowing the whole signal in more little periods to retrieve the true frequencies for each part of the signal.

For the Mallorca scenario the size of the rectangular window was chosen to be 600 and the step size 40. These values were determined after trying different combinations and looking for the best relation between frequency definition (longer periods in time) and remaining conditions in the Sea (the lower period of time the better). The spectral analysis was performed using the Lomb Scargle Periodogram. Fig. 3.5 depicts an example:

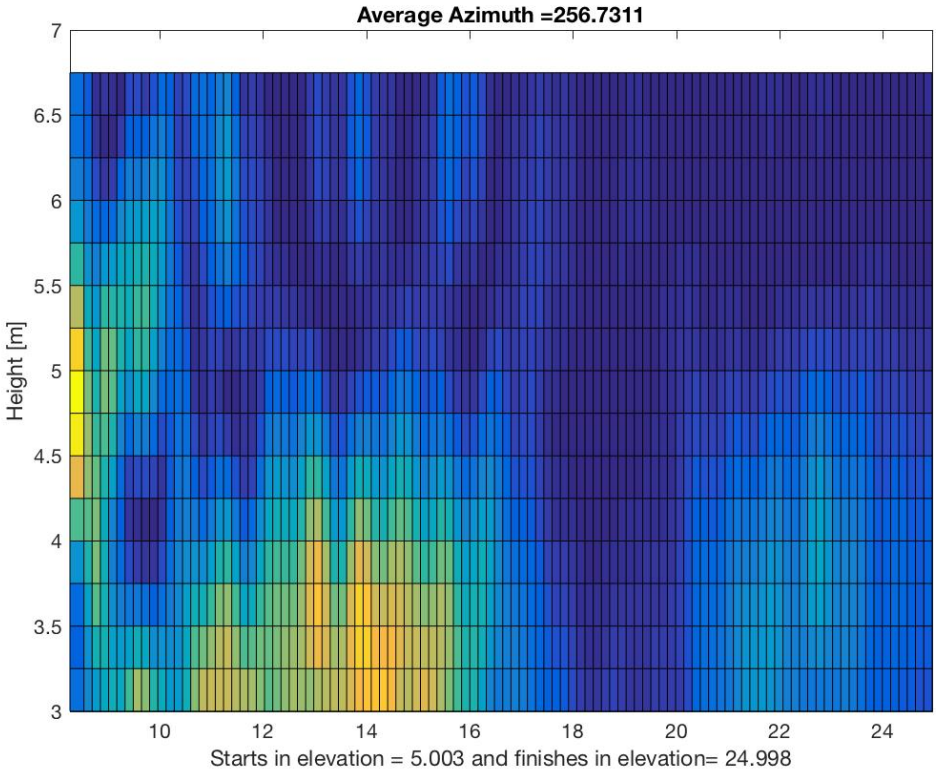

Figure 3.5: Spectrogram plot for GPS L1.

In the spectrogram there is also depicted the average azimuth of the segment and the range of elevations. The objective of adding these information was for better determining the elevation and azimuth range of values. The y axis directly shows the height retrieved (linearly dependent on the frequency, as explained in Section 2.2.2.2.1). The x axis represents the elevation for each windowed segment. After saving the figures by azimuth angles, it was time to analyze one by one to arrive to conclusions.

From Fig. 3.5 it can be seen that for low elevation angles, as the scattering is produced far from the receiving antenna (Appendix 7.6) it is not affected by the surrounding of the station (harbor floor, the station equipment, …). By the other hand, for elevation angles higher than 14° approximately it is common to see a big contribution around 3 meters. This contribution is expected to be from the harbor floor as it is similar than the distance from the floor to the receiving antenna. As the elevation angle increases the scattering is produced closer to the antenna so in order to just getting the contribution from the Sea the maximum elevation angle was set to 12°. The maximum azimuth angle was set to 230° as higher azimuth angles sometimes resulted in just the pick in 3 meters. The minimum azimuth angle was set to 130° because as can be seen from Fig. 3.6 results with lower azimuth angles were not good, the most possible cause is because of the rocks in the pier.

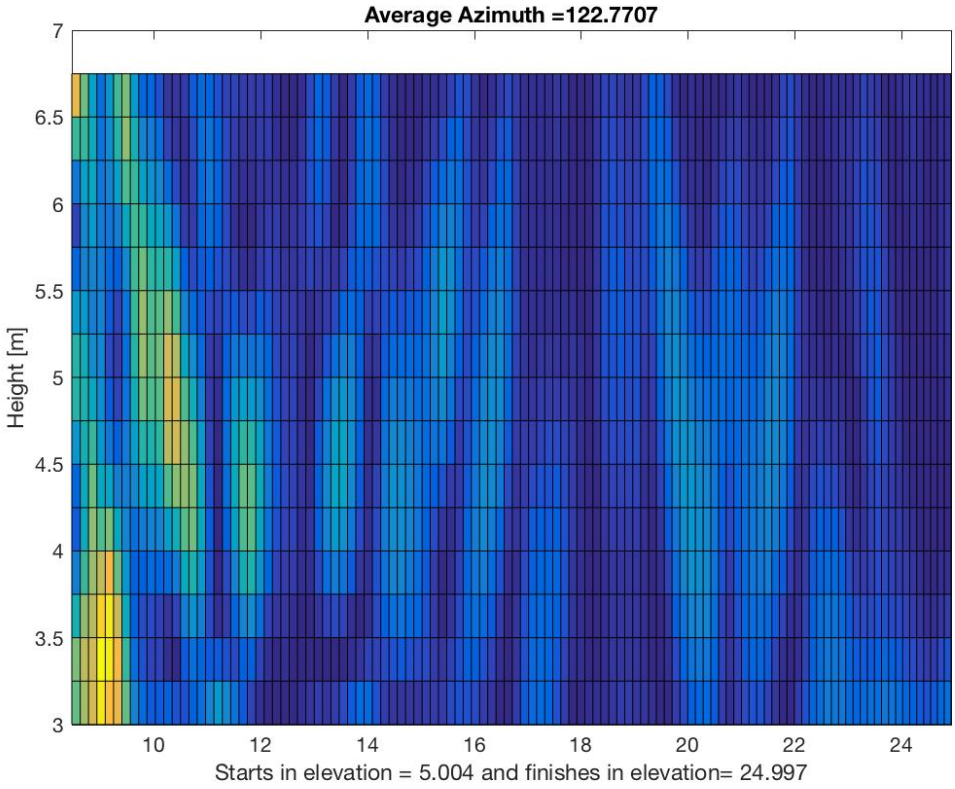

Figure 3.6: Spectrogram plot for L1 and average azimuth of 122°.

The minimum elevation angle value of 5° was set as a standard practice in GNSS-R publications, but due to the lack of enough samples for certain segments it was decided to reduce the minimum to 2° as the cutoff elevation angle for our antenna is 0°. With that change more samples are obtained in order to increase the Spectral resolution. After reducing the minimum elevation angle, the Spectrograms change their frequency picks abruptly for low elevation angles as can be seen in Fig. 3.7. The reason behind this behavior is because as the temporal window reduces the frequency precision, these can alter the main peak from one window to the next one.

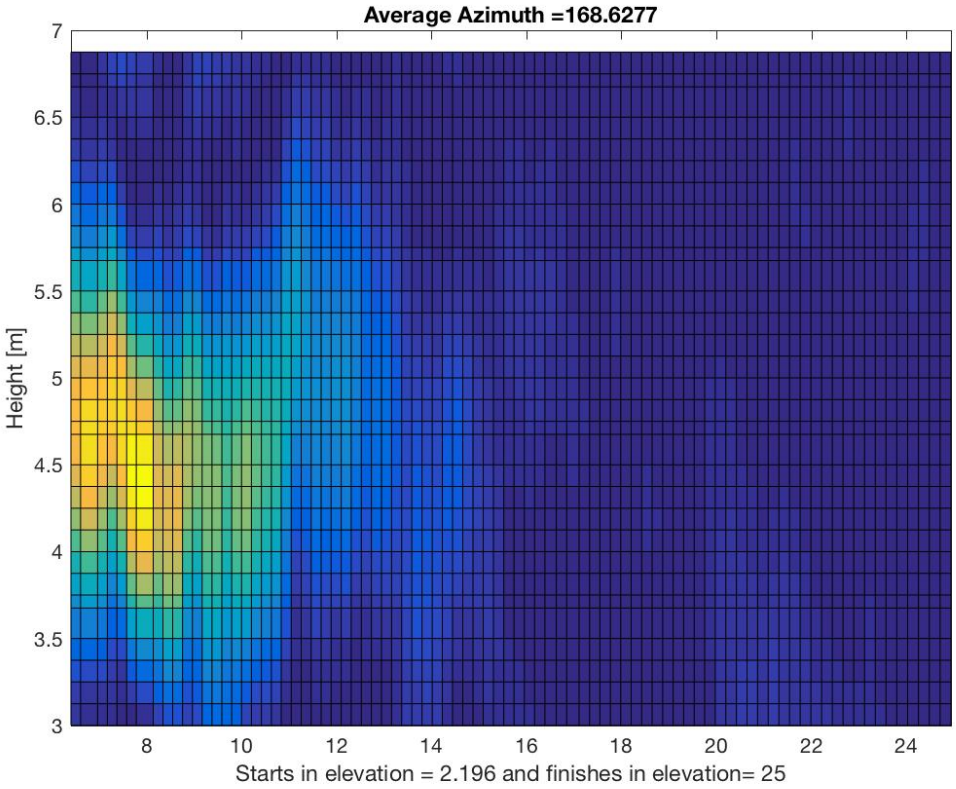

Figure 3.7: Spectrogram for L1 and changing the minimum elevation angle to 2°.

One of the objectives of this project is to asses results for both bands L1 and L2 so Fig. 3.8 and Fig. 3.9 represent both bands to show that results are complementary among both. In these examples L2 still provides accurate information after 12° of elevation whereas L1 just gives valuable results until 7°.

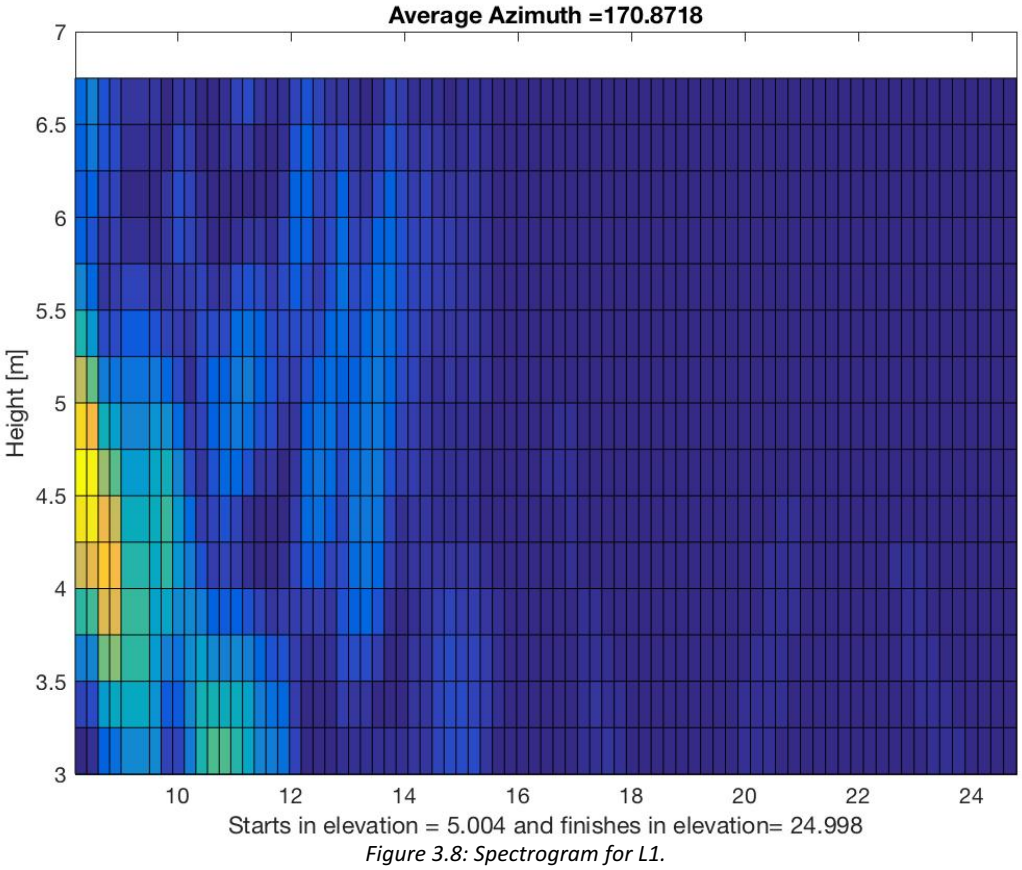

Figure 3.8: Spectrogram for L1.

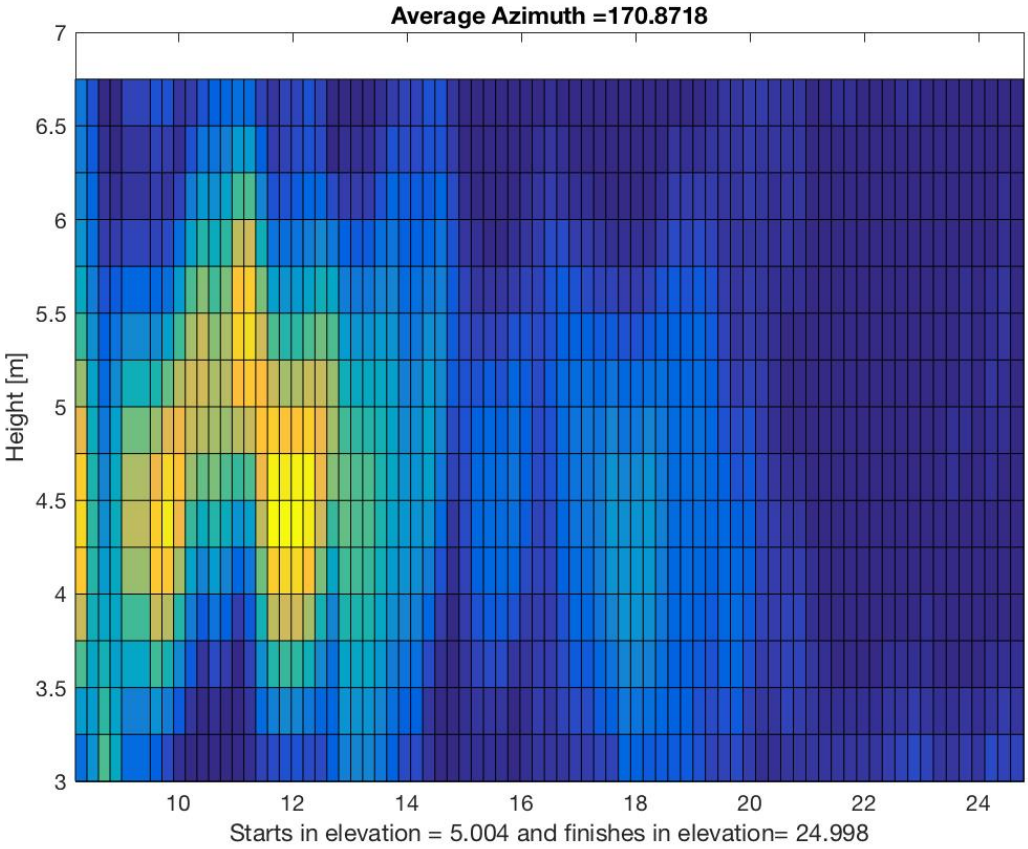

Figure 3.9: Spectrogram for L2.

3.4. Choosing Criterion

Once the Spectral Analysis has been done for a segment, some requirements need to be fulfilled in order to save the pick obtained as a good measure. After several iterations the requirements for the Palma de Mallorca were defined as:

- The maximum peak in the spectral analysis needs to be at least 2.5 times larger than the average of the LSP value.
- The maximum peak needs to be 1.5 times higher than the rest of the picks.
- The maximum peak when converted to heights needs to be more than 3 meters and less than 8 meters.

If all these requirements are fulfilled the result is saved as a good one.

3.5. Results against Ground Truth

3.5.1. Introduction

For the Palma de Mallorca scenario only the SNR analysis method is tested, as B-Splines are more suitable when dealing with large daily tides and also because for Mallorca some data

segments gave a large error which deviates completely the results. For the SNR analysis all the filtered detrended SNR will be analyzed together without windowing in small fragments (this will be done in Tarifa Station). The reason behind that is that for Mallorca after applying the different filters the amount of samples remaining is usually very low so it is not feasible to divide the signal as the frequency resolution would be unacceptable.

3.5.2. SNR Analysis against Ground Truth

The spectral analysis technique was tested for 3 months (8th February to 8th May 2017) in Palma de Mallorca Station. As the ground truth data provided by Puertos del Estado was sampled every 5 minutes an interpolation was required to compare results with our 1Hz data.
The figures presented are after adding a bias term to the GT measures, because in all the stations that have been studied there was a bias error between ground truth and our results. Ground truth sea height is based in a standard reference level set by Puertos del Estado but there can be some divergences or errors in their GT so we only focus in the correlation and error.
The results will be presented for the following combinations: GPS for L1, GPS for L2, GLONASS for L1, GLONASS for L2. The different plots are presented in Appendix 7.7 as well as the results for some combinations between systems.

Table 3.1: Results for GPS and GLONASS in Mallorca. Error, correlation, coverage and Linear Regression results are presented.

	RMSE [cm]	RMSE robust [cm]	Corr.	Corr. robust	Coverage	Linear Regression	Linear Regression robust
GPS L1	43.10	9.61	0.470	0.999	1h 6 min	0.98x + 0.82	1.01x - 0.28
GPS L2	52.73	23.03	0.314	0.996	1h 9 min	0.97x+0.15	0.99x + 0.13
GLO L1	59.23	14.10	0.417	0.998	1h 58 min	0.53x + 2.57	0.90x + 0.46
GLO L2	64.90	17.92	0.240	0.992	2h 11 min	0.12x + 4.62	0.81x + 0.89

The big difference between RMSE and Correlation with respect their robust versions is because the latter omit the samples that differ too much with respect the standard behavior of the Sea Surface Height. In MAL1 several results obtained were around eight meters (Appendix 7.7.1), which considering that historically data from the tide gauge has never reached this value it seems safe to omit them. At first, we were skeptical about the results of robust correlation but several iterations were tested and results did not change. Results for L1 band are better than for L2 band for both systems.

4. TARI Station

4.1. Station Description

The second station that has been studied is located in Tarifa harbor. This station belongs both to ERGNSS (Spanish GNSS Network) and Puertos del Estado, as Palma de Mallorca Station, but also to the EUREF Permanent Network (EPN). The exact coordinates of the GNSS station are 36° 00' 30,62882'' N, 5° 36' 09,43355'' W whose exact position is shown in Fig. 4.1:

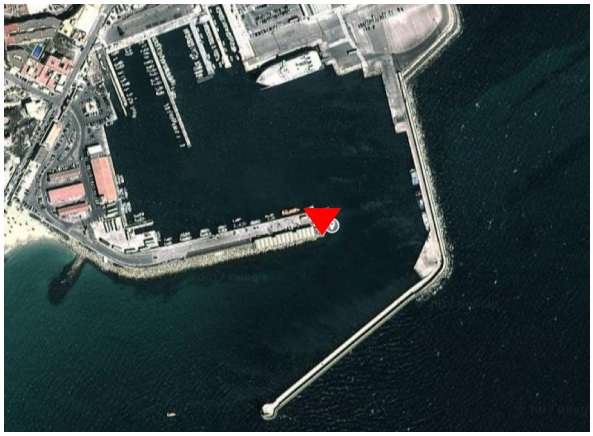

Figure 4.1: Localization of the TARI antenna.

Figure 4.2: LEICA antenna in Tarifa Station.

The station is composed by a LEICA LEIAR20 (Fig. 4.2) antenna together with a GR25 LEIM Receiver, which stores, processes, and sends GNSS data 24/7. The receiver records data at 1 Hz sampling rate. The constellations that this station is able to track are GPS (L1, L2 and L5) and GLONASS (L1 and L2) for RINEX 2 and for RINEX 3 Galileo (L1, L5 and L6) is added.

The Receiver is at the top of a pillar of height 0.4 meters made of concrete block with a foundation of 2 meters. The problem with this station is that it has the pier relatively close to its location so the elevation range will be needed to be assessed as if the elevation is very low it will probably reach the receiving antenna some scatters from the pier. Similar to the MAL1 scenario, being in a commercial harbor can result in some periods with wrong samples due to the interferences of boats.
The average vertical distance between the Sea surface and the phase center of the antenna is around 8.4 meters.

4.2. Differences between TARI and MAL1 stations

The reason behind analyzing this second station was because at first the results obtained in Mallorca were not as good as expected and we wanted to test our method in a different scenario. The biggest difference between this station and MAL1 is that for this scenario the daily tides are considerable and can provoke changes around 80 cm due to the Atlantic Ocean characteristics, while the Mediterranean Sea daily tides can almost be ignored as they have a maximum of 20 cm variation.

The other big difference came when analyzing the temporal data obtained. Although it seems that the MAL1 antenna could have a smoother temporal function due to is looking directly to the open Sea instead of being covered by the pier as in Tarifa, results depicted in Fig. 4.3 and Fig. 4.4 show that it is the opposite.

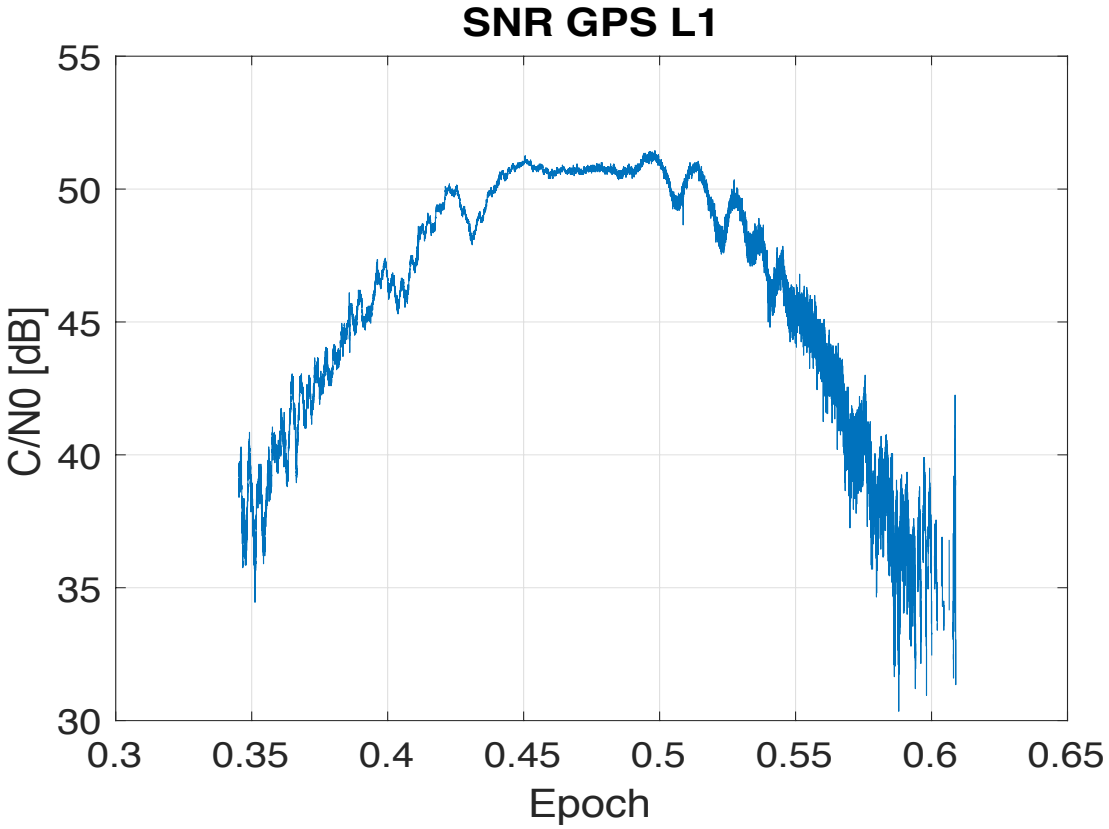

Figure 4.3: SNR signal for the MAL1 station. It is more difficult to distinguish between the multipath and the direct signal than in Fig. 21.

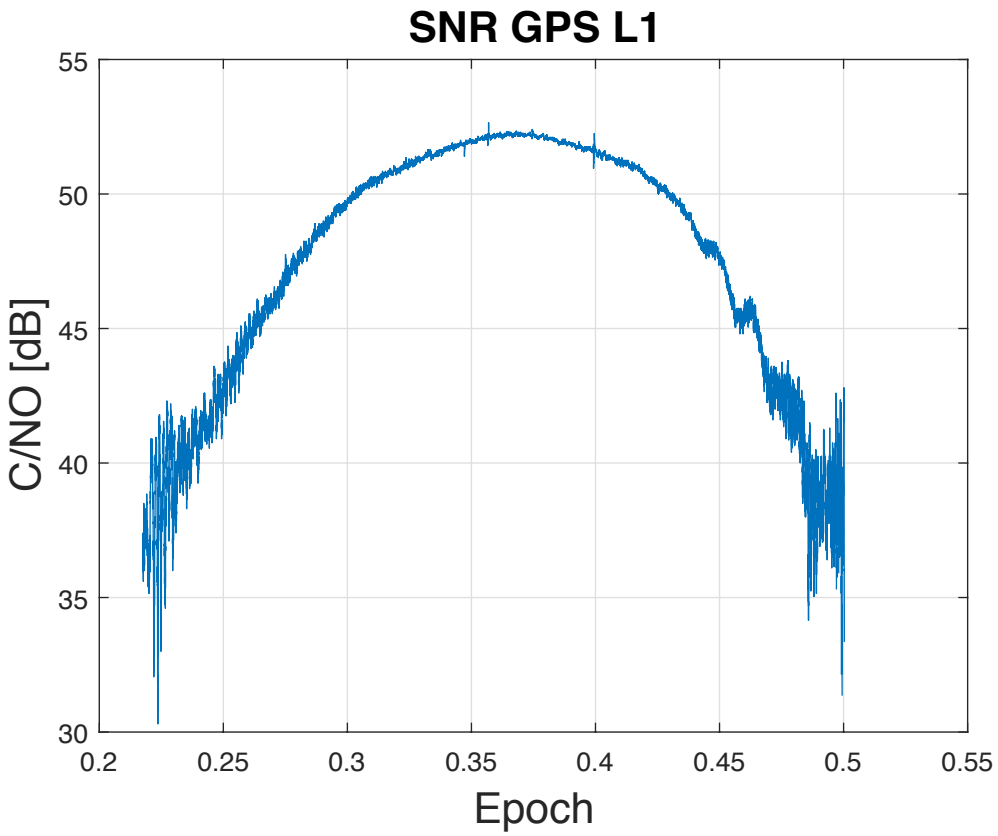

Figure 4.4: Temporal signal for GPS L1 in Tarifa. The y axis shows the C/N0 in dB and the x axis is the epochs for one day.

4.3. Ground Truth Available

Figure 4.5: Information of the tide gauge station.

As in the first scenario, there is a tide gauge with sea level measurement very close to the GNSS station which will be used to compare our results. This station belongs to REDMAR.

4.4. Choosing Criterion

The choosing criteria for the Tarifa Station is the same as the one used in Mallorca (Section 3.4). The only difference is that for this scenario the range of heights considered to be possible

goes from 5 to 11 meters. After using the Lomb Scargle Spectrogram, as in the Mallorca scenario, the azimuth range was set to [145°, 230°] and the elevation range to [5°, 12°]. The minimum elevation angle was chosen to be 5° instead of 2° due to the interference of the pier.

4.5. Spectral Analysis results

For this scenario, as the number of samples was higher for low elevation angles than in the Palma station, it was decided to first determining heights looking at all the windows in one spectrogram individually. The size of the window was set to 750 and a step of 30. What happened was that due to the low frequency resolution there was a big difference in the Sea Height for adjacent windows for the same Satellite (Fig. 4.6) so instead of looking for the median or average of all the results for the same Satellite, it was decided to consider the whole segment without windowing as the frequency resolution would increase and the Sea conditions could be considered static for the whole segment (around 12-15 min), as in the Palma de Mallorca case. Complete plots are shown in Appendix 7.7 as well as the results for different system combinations.

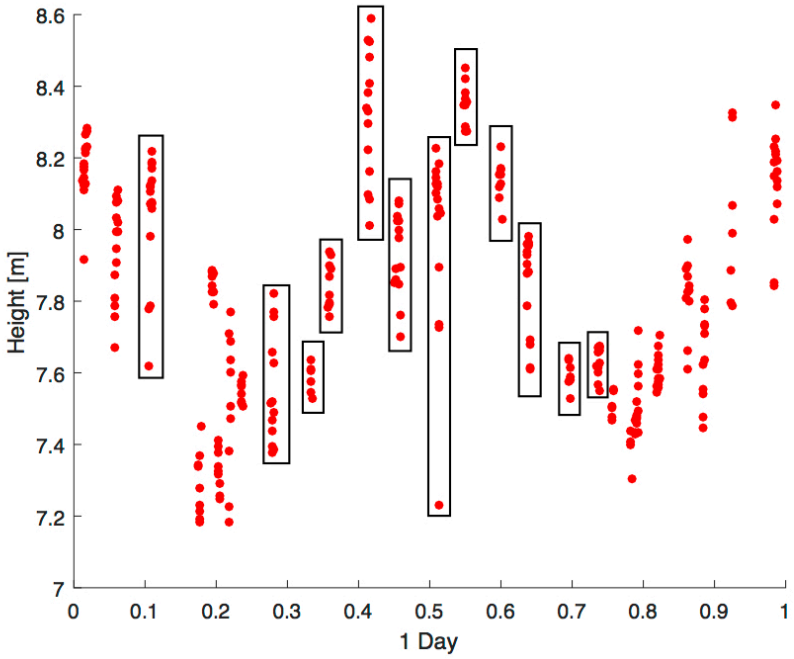

Figure 4.6: Representation of the Sea Height for one day considering each window from the spectrogram.

Table 4.1: Results Spectral Analysis for GPS and GLONASS in Tarifa.

	RMSE [cm]	RMSE robust [cm]	Corr.	Corr. robust	Coverage	Linear Regression	Linear Regression robust
GPS L1	18.68	14.48	0.864	0.999	48 min	0.92x + 0.62	0.98x +0.28
GPS L2	25.93	17.49	0.770	0.989	52 min	0.87x + 0.94	0.94x + 0.61
GLO L1	23.80	15.60	0.847	0.994	2h 35 min	0.93x + 0.56	0.99x + 0.04
GLO L2	25.87	21.49	0.797	0.980	3h 2 min	0.92x + 0.62	0.95x + 0.38

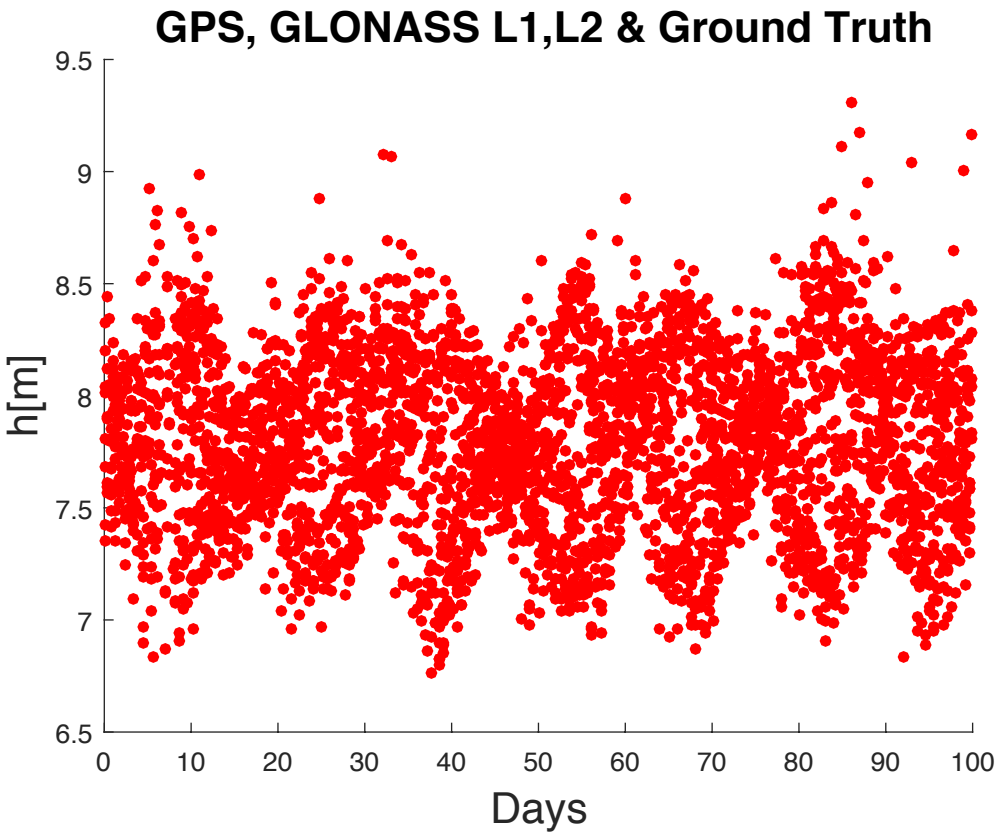

Figure 4.7: Results for 100 days without windowing the segments.

In TARI the difference between original and robust results is little compared with MAL1, so accurate results can be obtained without the need of using the robust function. Moreover, these results were surprising, as the pier is closer to the antenna in this station than in MAL1, so we were expecting more inaccurate results from this station than from the first one.

4.6. Results B-Splines

To test the B-Splines, all the segments inside the range of elevations and azimuths were saved in order to perform the least squares. The objective of the minimization problem is obtaining the factors to multiply to each of the basis splines so that when all of them are added the height of the Sea function is obtained. The results were tested for just two days (12-13th of January 2017). Only two days were tested because of the computational load to obtain B-Splines as well as the memory storage required to save the results (the basis matrix consist on the number of basis splines as rows and the amount of seconds in the days analyzed as columns). B-Splines were fitted to zero, first and second degree curves in order to check if they are suitable to represent Sea Surface Height. These plots as well as plots with results for different systems and frequency bands will be presented in Appendix 7.7:

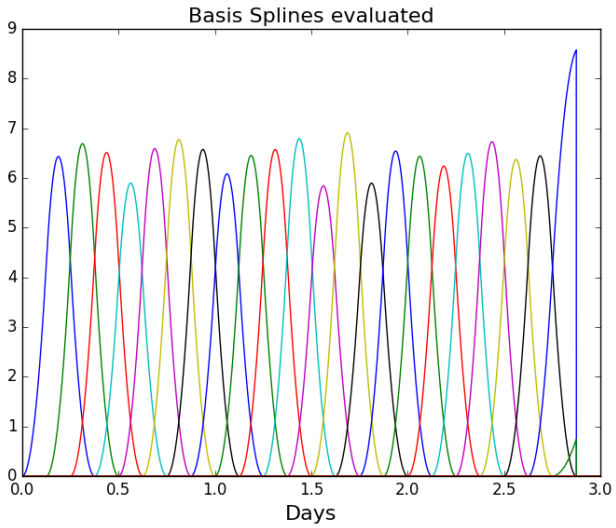

Figure 4.8: Basis splines multiplied by the returned factor by the least squares method. Due to irregularities in the extremes, from 3 days just 2 days are analyzed [0.5, 2.5].

Table 4.2: Results B-Splines for GPS and GLONASS in Mallorca.

	RMSE [cm]	Correlation
GPS L1	15.59	0.8441
GPS, GLO L1	13.25	0.8639
GLO L1	22.10	0.7235
GPS L2	29.43	0.6020
GPS, GLO L2	29.33	0.6087
GLO L2	30.16	0.5704

Results are better for the combination between GPS L1 and GLONASS L1 as stated in [26] than Spectral Analysis, while results for only GPS L1 are a bit worse than Spectral Analysis and for GLONASS L1 alone far worse. The reason behind this behavior, is that B-Splines increase their accuracy when the number of samples acquired increases because the minimization algorithm can iterate throw more samples and find more accurate values. The main problem in using B-Splines in commercial harbors, is that some of the data can be completely corrupted by different interferences (i.e. ships, station repairs, humans) and as no preprocessing is done to choose the right samples (in Spectral Analysis the main pick is compared with the rest of the picks and the average of the Lomb Scargle Periodogram) which can provoke an increase in the global error for both L1 and L2. These results also confirm that L1 band performs better than L2 for SSH. If the location of the GNSS station is isolated from human interferences, B-Splines could be a good alternative to the conventional Spectral Analysis method.

5. Budget

In this chapter the costs of the project are explained:

- Software costs:

Table 5.1: Summary of the software costs.

Tool	Cost (€)
Windows 7 Operating System	40
MATLAB Student Edition	35
TOTAL	**75**

- Development costs:

The assigned development cost of a trainee engineer is 8€/h.

Table 2.2: Summary of the development costs.

Task	Hours	Cost (€)
Theoretical Research in GNSS-R	120	960
Data Extraction from FTPs (RINEX 2)	100	800
Pre-processing	80	640
SNR Analysis	120	960
Test SNR Analysis	30	240
Inverse Modeling with B-Splines	180	1440
Test Inverse Modelling	40	320
Data Extraction from FTPs (RINEX 3) and translation	180	1440
TOTAL	**850**	**6800**

6. Conclusions and Future Research Lines

6.1. Conclusions

This Undergraduate Thesis was a natural continuation of the research done in UPC about GNSS-R, first by Dr. Nereida Rodriguez and after by Dr. Alberto Alonso Arroyo. The main focus of this thesis was introducing the Sea Height analysis by using a GNSS antenna looking at the zenith (a method studied in depth in CU Boulder but not much in UPC) and applying Spectral Analysis to the data gathered for GPS and GLONASS systems and L1 and L2 frequency bands.
Although there is plenty of room for improvement, results are very encouraging and in few years it could be feasible to make a commercial use of this technology instead of common altimeters or tide gauges. Although the height error is around 10 cm, the biggest problem right now is the little amount of satellites for this purpose, which makes that in scenarios where the azimuth and elevation range are reduced, the amount of segments that can be obtained for processing is limited. With the incursion of BeiDou2 and Galileo more segments will be available so the coverage of the data is expected to be reduced.
A new method using B-Splines is also tested, but the main problem faced is that it requires much more computational load than Spectral Analysis as in B-Splines the time required increases exponentially with the degree of the splines. One of the advantages is that it takes

into consideration the daily tides as well as previous results, which it does not happen in the Spectral Analysis method. Results when combining GPS and GLONASS are very promising and when Galileo and Beidou systems are available to work with, results could be even better.

6.2. Future Research lines

After having established the main conclusions of this work, several research lines can be drawn as a continuation of the research developed during this Undergraduate Thesis, which are:

- Analyze the effect of the Electromagnetic Bias [33] in the error of the results obtained. The error in the samples was compared with the wind speed for each time but no conclusions could be made from the results obtained.
- Use the method develop for using the Galileo system in a station where the RINEX 3 observation files are sampled every second. Although the method to retrieve information from RINEX 3 was designed and tested, the two stations studied in this Thesis only included observation files sampled every 30 second for the RINEX 3 format, which made it useless for our purpose. The reason why Galileo observations could not be processed is because the number of samples is reduced by 30 with respect to RINEX 2 and the amount of samples left for each segment (80-90 at most) provide no valuable results.
- Study GNSS stations where no human interference is produced. Both of the stations analyzed in this Thesis are located in commercial harbors, so we can not be sure of the real performance of our algorithm.
- Analyze the effect of combining different frequency bands in Soil Moisture or Snow Depth where different frequency bands can provide different information for different depths.

7. Appendix

7.1. Sea Height retrievement techniques

The most important methods for retrieving Sea height measurements are mainly three:

- Tides: Tide stations are capable of measuring water levels; barometric pressure; wind speed and direction and water temperatures. Over the last decade the precision of these stations has improved to the order of one millimeter in order to be sensitive enough in the measurement of small and gradual changes (i.e. el Niño). Almost 1,500 tide stations are spread around the globe. Public institutions such as NOAA (National Oceanic and Atmospheric Administration, USA) provide pubic data of their stations: https://tidesandcurrents.noaa.gov
- Satellites: Since August 1992 the satellite altimeters have been measuring sea level on a global basis with unprecedented accuracy. The TOPEX/POSEIDON (T/P) satellite mission provided observations of sea level change from 1992 until 2005. Jason-1 and Jason 2 have been the specific satellites for sea level measurement launched after T/P. The newest one, Jason 2, orbits at an altitude of 1,336 km (same orbit as Jason-1) and has a measurement accuracy of 3.3 cm with a goal of achieving 2.5 cm. It also maintains the stability of the global mean sea level measurement with a drift less than 1 mm/year over the life of the mission.
- Drifting Buoys: The network of buoys around the world is called Argo. Argo is a global array of 3,800 free-drifting profiling floats that measures the temperature, salinity, pressure and reference velocity (together with sea surface height from satellite altimetry data) forming a dynamically complete description of the upper ocean. The data is made publicly available within hours after collection. Fig. 7.1 depicts a map with the position of all the floats.

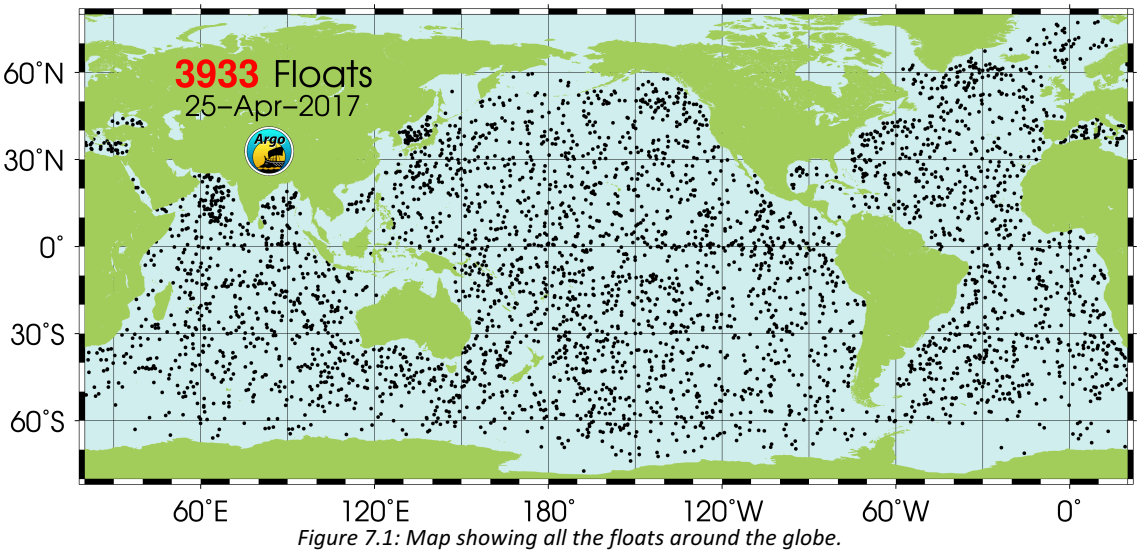

Figure 7.1: Map showing all the floats around the globe.

7.2. GNSS History

The need of positioning and navigation have driven human specie since ancient times. The first traces of position, although very rudimentary, consisted on the use of the stars on the sky in order to determine the position and the navigation route. It was not until the Second World War, when radio waves knowledge and usefulness were massively improved due to its

importance for detecting, tracking or positioning (i.e. Radar [34]), that more sophisticated navigation systems arised, such as Long Range Navigation (LORAN), Decca or OMEGA (the first truly global-navigation system [35]). These predecessors used terrestrial longwave radio transmitters instead of satellites. These systems broadcast a radio pulse from a known "master" location, followed by a pulse repeated from a number of "slave" stations. The delay between the reception of the master signal and the slave signals allowed the receiver to deduce the distance to each of the slaves, providing a fix (position derived from measuring external points). Afterwards, in the 1960s, the first navigation system was deployed by the US military, called Transit. Transit's operation was based on the Doppler effect: the satellites travelled on well-known paths and broadcast their signals on a well-known frequency. The received frequency will differ slightly from the broadcast frequency because of the movement of the satellite with respect to the receiver. By monitoring this frequency shift over a short time interval, the receiver can determine its location to one side or the other of the satellite, and several such measurements combined with a precise knowledge of the satellite's orbit can fix a particular position. However, the true revolution in navigations systems came in 1973, when a constellation of satellites, initially known as NAVigation STAR (NAVSTAR), was proposed to be used for global positioning.

7.3. GNSS Constellations

7.3.1. GPS Constellation and Signal

The GPS Project was launched in the United States in 1973 to provide geolocation and time information to a GPS anywhere on the Earth where there is an unobstructed line of sight to four or more GPS satellites.
The original design was supposed to have 24 SVs in three different circular orbits (eight SVs in each), but was modified to six orbital planes with four satellites each. The orbital planes have approximately 55° inclination (relative to the Earth's equator) and are separated by 60° right ascension of the ascending node (angle along the equator from a reference point to the orbit's intersection). Orbiting at an altitude of approximately 20,200 km, a nearly circular Medium Earth Orbit (MEO), with a period of 11 hours and 58 minutes. This means that the same satellite will be seen the next day at the same position but 4 minutes before.
At the moment of writing this document there are 32 satellites in the constellation, 31 of which are in use. About nine satellites are visible from any point on the ground at any specific time, ensuring considerably redundancy over the minimum four satellites needed for a position.

All GPS satellites broadcast at the same two frequencies, 1.57542 GHz (L1) and 1.22760 GHz (L2). A third band was added in the process of GPS modernization, 1.17645 GHz (L5). The satellite network uses a CDMA spread-spectrum technique where the low-bitrate message data is encoded with a high-rate PRN sequence that is different for each satellite. The receiver must be aware of the PRN codes for each satellite in order to reconstruct the messages. The two main important type of codes are the C/A (civilian use) and P (U.S military use). The C/A code transmits data at 1.023 million chips per second, whereas the P code transmits at 10.23 million chips per second. The L1 carrier is modulated by both the C/A (the one used for this Thesis) and P codes, while the L2 carrier is only modulated by the P code.
Because all of the satellite signals are modulated onto the same carrier frequency, the signals must be separated after demodulation. This is done by using a unique binary sequence known as Gold Code [36]
It also needs to be considered the M codes (military) with a similar bandwidth than P codes and are transmitted in the quadrature component of the GPS signal, together with the C/A

code, whereas the P(Y) code is transmitted in the in-phase component only. To avoid interference between C/A and M codes, the latter is spread along the entire band using a Binary Offset Carrier (BOC) modulation [37].
To summarize, the basic GPS structure for L1 is:

$$s_{L1}(t) = \left(\sqrt{2P_{\frac{C}{A}}} C_{\frac{C}{A}}(t) + \sqrt{2P_M} C_M(t) \right) D(t) \cos(2\pi f_{L1} t) + \sqrt{2P_P} C_P(t) D(t) \sin(2\pi f_{L1} t) \quad \text{(A.1)}$$

Where P_x stands for the power transmitted for the x code, $C_x(t)$ for the code itself, $C(t)$ for the navigation data and f_{L1} is the L1 Band carrier frequency.

7.3.2. GLONASS Constellation and Signal

GLONASS is a space-based satellite navigation systems used by the Russian Aerospace Defense Forces and it provides an alternative to GPS. It provides real time positioning and velocity determination for military and civilian users. The satellites are located in a MEO (Middle Circular Orbit) at 19,100 km altitude with a 64.8° inclination and a period of 11 hours and 15 minutes. GLONASS' orbit makes it especially suited for usage in high latitudes (north or south), where getting a GPS signal can be problematic. The constellation operates in three orbital planes, with eight evenly spaced satellites on each (the full constellation is composed of 24 satellites).
GLONASS satellites transmit two types of signals: open standard-precision signals L1OF/L2OF and obfuscated high-precision signal L1SF/L2SF. The signal uses DSSS encoding and binary phase-shift keying (BPSK) modulation as in GPS signals. The biggest difference with respect to GPS comes from the fact that different frequency bands are used to transmit each of the groups (each one has some satellites and a specific channel number) of GLONASS satellites. The satellites transmit the same code as their standard-precision signal but each one transmits in a different frequency using a 15-channel frequency division multiple access (FDMA) technique with a center frequency of 1602 MHz for L1-Band. The central frequency for each channel will be determined by: $1602\ MHz + n \cdot 0.5625\ MHz$, where n is a satellite's frequency channel number ∈ [-7,6].
The L2 Band uses the same FDMA method but with a different configuration: $1246\ MHz + n \cdot 0.4375\ MHz$.

7.3.3. Galileo Constellation

Galileo is the global navigation satellite system (GNSS) that is currently being created by the European Union (EU) through the European Space Agency (ESA) and the European GNSS Agency (GSA). The 5 billion euros project is named after the Italian astronomer Galileo Galilei. One of the aims of Galileo is to provide an independent high-precision positioning system so European nations do not have to rely on the Russian GLONASS, Chinese BeiDou or US GPS systems, which could be disabled or degraded by their operators at any time. The use of basic (lower-precision) Galileo services will be free and open to everyone. The higher-precision capabilities will be available for paying commercial users. Galileo is intended to provide horizontal and vertical position measurements within 1-metre precision, and better positioning services at high latitudes than other positioning systems.
The system is scheduled to reach full operation in 2020 with the following specifications:

- 30 in-orbit spacecraft (24 in full service and 6 spares)
- Orbital altitude: 23,222 km (MEO)

- 3 orbital planes, 56° inclination, ascending nodes separated by 120° longitude (8 operational satellites and 2 active spares per orbital plane)

The frequency Bands available are: E1 (1575.42 MHz), E5a (1176.45 MHz), E5b (1207.40 MHz), E5 (1191.795 MHz) and E6 (1278.75 MHz).

7.4. Phase Difference Method

Two standard geodetic-type GNSS receivers are used to receive direct GNSS signals through a zenith-looking Right Hand Circular Polarized (RHCP) antenna and GNSS signals reflected from the sea surface through a nadir-looking Left Hand Circular Polarized (LHCP) antenna. The carrier phase delay data from the receivers can be processed using relative positioning and standard geodetic analysis to obtain measurements of local sea level and sea level with respect to the Earth's center of mass, as realized by the GNSS systems [38].

The upward-looking antenna receives the GNSS signals directly and is used the same way as, i.e., an International GNSS Service (IGS) station. By solving for the position of this antenna, the land surface height with respect to the Earth's center of mass is obtained. The downward-looking antenna, on the other hand, receives the GNSS signals that have been reflected off the sea surface (when the GNSS satellites' RHCP signals reflect off the sea surface they change polarization to LHCP). Since the reflected signals travel an additional path, as compared to the directly received signals, the downward-looking antenna will appear to be a virtual RHCP antenna located below the sea surface. This virtual antenna will be at the same distance below the sea surface as the actual LHCP antenna is located above the sea surface (Fig. 7.2). When there is a change in the sea surface, the additional path delay of the reflected signals changes, hence the LHCP antenna appears to change its vertical position. This means that the height of the downward-looking antenna over the sea surface (h) is directly proportional to the sea-surface height (SSH) with respect to the Earth's center of mass. Thus, by combining the RHCP measurement of land surface height with the LHCP measurement of sea surface height, local sea level can be obtained.

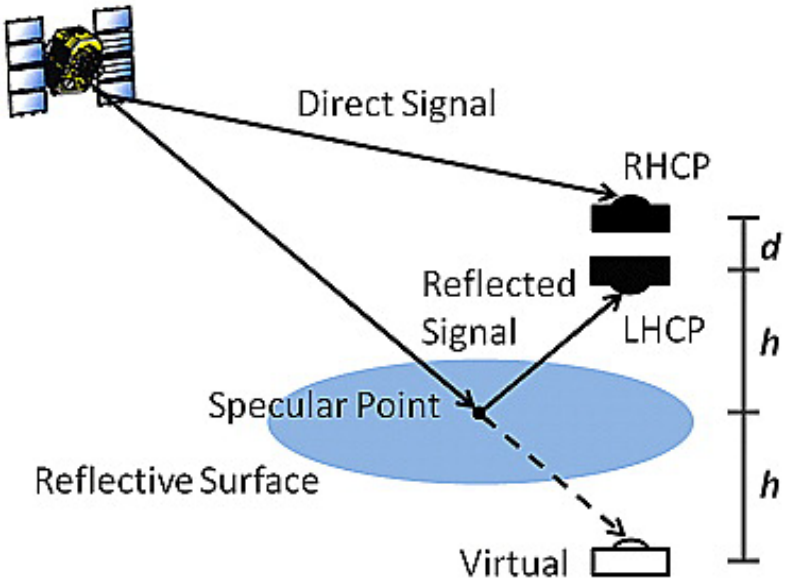

Figure 7.2: Description of this method with the interaction between the Direct and Reflected Signal. The specular point (Appendix 7.6) represents the center of reflection for the first Fresnel Zone.

7.5. Spectral Analysis Methods

7.5.1. Fourier Periodogram

The general formula for the Periodogram spectral analysis method is:

$$P_{Per}(w) = \frac{1}{N^2}\left|\sum_{n=1}^{N} y(t_n)e^{-j\omega t_n}\right|^2$$

(A.2)

where w is the frequency unit ($w = 2\pi f$), N the total number of samples and t_n the specific time for each sample, after the change of variables $t_n = \sin(\theta_{elev_n})$. Depending on the application, the normalization factor might be different from $1/N^2$ (such as $1/N$ [39]). It can be readily verified that $P_{Per}(w)$ can be obtained from the solution to the following least-squares (LS) data fitting problem:

$$P_{Per}(w) = \left|\hat{\beta}(w)\right|^2$$

(A.3)

$$\hat{\beta}(w) = argmin_{\beta(w)} \sum_{n=1}^{N} \left|y(t_n) - \beta(w)e^{j\omega t_n}\right|^2$$

(A.4)

Because $y(t_n) \subset \mathcal{R}$, the S criterion above can be rewritten as (below $\beta(w) \triangleq |\beta(w)|e^{j\phi(\omega)}$):

$$\sum_{n=1}^{N}[y(t_n) - |\beta(w)|\cos(wt_n + \phi(w))]^2 + |\beta(w)|^2 \sum_{n=1}^{N} sin^2(wt_n + \phi(w))$$

(A.5)

As it can be seen, minimization of the first term makes sense, but not with the second term which will act as additive data-independent perturbation.
Although it can be said that this method is suitable for unevenly samples, but for the case of real value data other methods perform better.

7.5.2. Lomb Scargle Periodogram

For real value data the LSP method is more suitable than the FP, and a more satisfactory spectral estimate should be obtained by solving the following LS fitting problem:

$$\min_{\substack{\alpha>0 \\ \phi\in[0,2\pi]}} \sum_{n=1}^{N}[y(t_n) - \alpha \cdot \cos(wt_n + \phi)]^2$$

(A.6)

After following the approach in [40] results in:

$$P_{LSP}(w) = \frac{1}{\widehat{YY}}\left(\frac{\widehat{YC_{\hat{\tau}}}^{\,2}}{\widehat{CC_{\hat{\tau}}}^{\,2}} + \frac{\widehat{YS_{\hat{\tau}}}^{\,2}}{\widehat{SS_{\hat{\tau}}}^{\,2}}\right) \tag{A.7}$$

where:

$$\widehat{YY} = \sum_{n=1}^{N} y(t_n)^2 \tag{A.8}$$

$$\widehat{YC_{\hat{\tau}}} = \sum_{n=1}^{N} y(t_n) \cdot \cos\left(w \cdot (t_n - \hat{\tau})\right) \tag{A.9}$$

$$\widehat{CC_{\hat{\tau}}} = \sum_{n=1}^{N} cos^2(w \cdot (t_n - \hat{\tau})) \tag{A.10}$$

$$\widehat{YS_{\hat{\tau}}} = \sum_{n=1}^{N} y(t_n) \cdot \sin\left(w \cdot (t_n - \hat{\tau})\right) \tag{A.11}$$

$$\widehat{SS_{\hat{\tau}}} = \sum_{n=1}^{N} sin^2(w \cdot (t_n - \hat{\tau})) \tag{A.12}$$

$$\tan(2w\hat{\tau}) = \frac{\sum_{n=1}^{N} \sin(2wt_n)}{\sum_{n=1}^{N} \cos(2wt_n)} \tag{A.13}$$

7.5.3. Least Squares Periodogram

This method is the least squares Fourier Periodogram for real-valued data and it is given by:

$$P_{LS}(w) = \frac{1}{N}\boldsymbol{r}^T(w)\boldsymbol{R}^{-1}(w)\boldsymbol{r}(w) \tag{A.14}$$

where:

$$\boldsymbol{R}(w) = \sum_{n=1}^{N} \begin{bmatrix} \cos(wt_n) \\ \sin(wt_n) \end{bmatrix} \begin{bmatrix} \cos(wt_n) & \sin(wt_n) \end{bmatrix} \tag{A.15}$$

$$\boldsymbol{r}(w) = \sum_{n=1}^{N} \begin{bmatrix} \cos(wt_n) \\ \sin(wt_n) \end{bmatrix} y(t_n) \tag{A.16}$$

7.5.4. Capon

The main idea of the Capon filter is to attenuate the residual term that appears in the Periodogram [41] by filtering the data sequence {y(t)} via a suitable finite-impulse-response filter. The resulting Capon Periodogram is the following:

$$P_{CAP}(w) = \frac{1}{\boldsymbol{a}^H(e^{j\omega\Delta})\widehat{\boldsymbol{R}}^{-1}\boldsymbol{a}(e^{j\omega\Delta})} \tag{A.17}$$

where:

$$a\left(e^{j\omega\Delta}\right) = \left[1 \;\; e^{j\omega\Delta} \;\; \ldots \;\; e^{j\omega\Delta m}\right]^T \tag{A.18}$$

$$\widehat{\boldsymbol{R}} = \frac{1}{\widetilde{N}\Delta}\sum_{p=0}^{\widetilde{N}-1} a(e^{jw_p\Delta})a^H(e^{jw_p\Delta})P_{FP}(w_p) \tag{A.19}$$

which can be related to the standard covariance matrix,

$$\Delta = \frac{1}{N-1}\sum_{k=0}^{N-2}(t_{k+1} - t_k) \tag{A.20}$$

which is the average sampling period, m the length of the Capon filters and $\widetilde{N} \geq N$ is related to the number of spectral components to be estimated, which tends to be larger than the number of samples.

7.5.5. Examples

A graphical comparison for three of this methods applied to a detrended signal are shown in the following images.

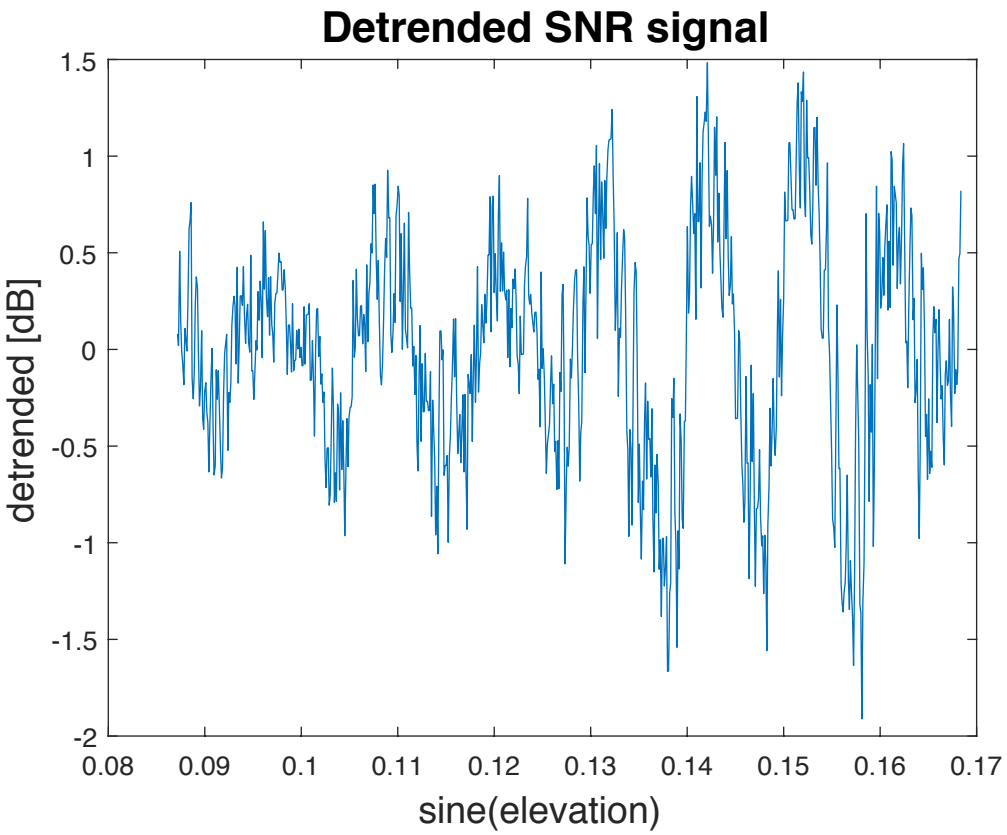

Figure 7.3: Example of a temporal detrended SNR.

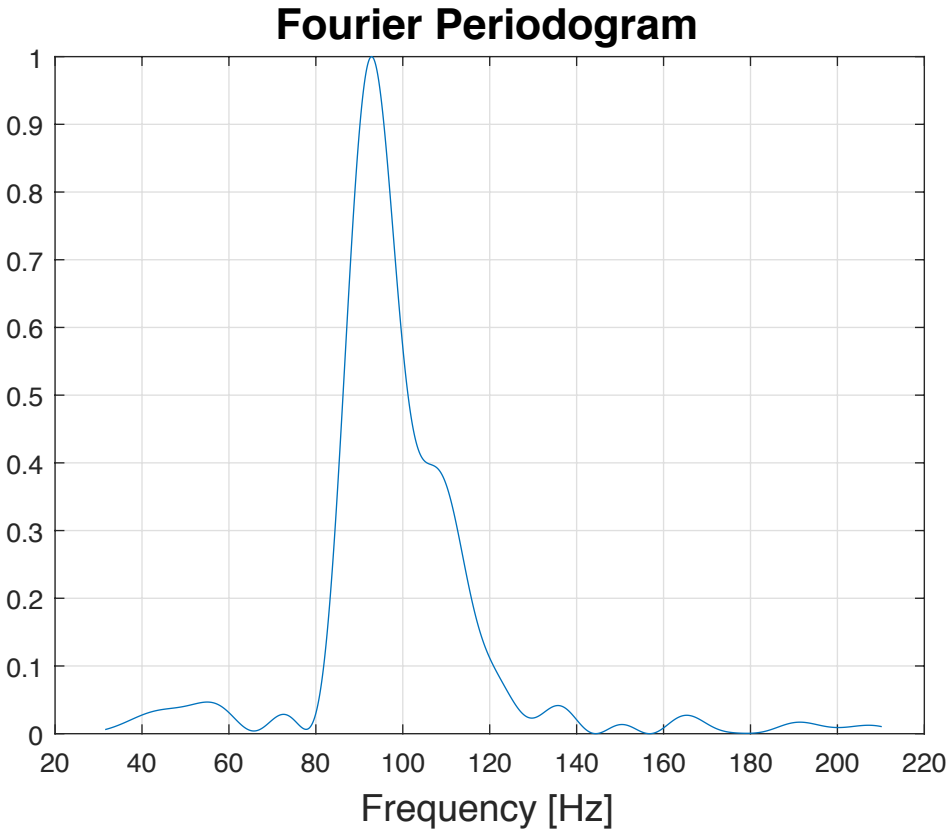

Figure 7.4: Spectral response for the Fourier Periodogram technique.

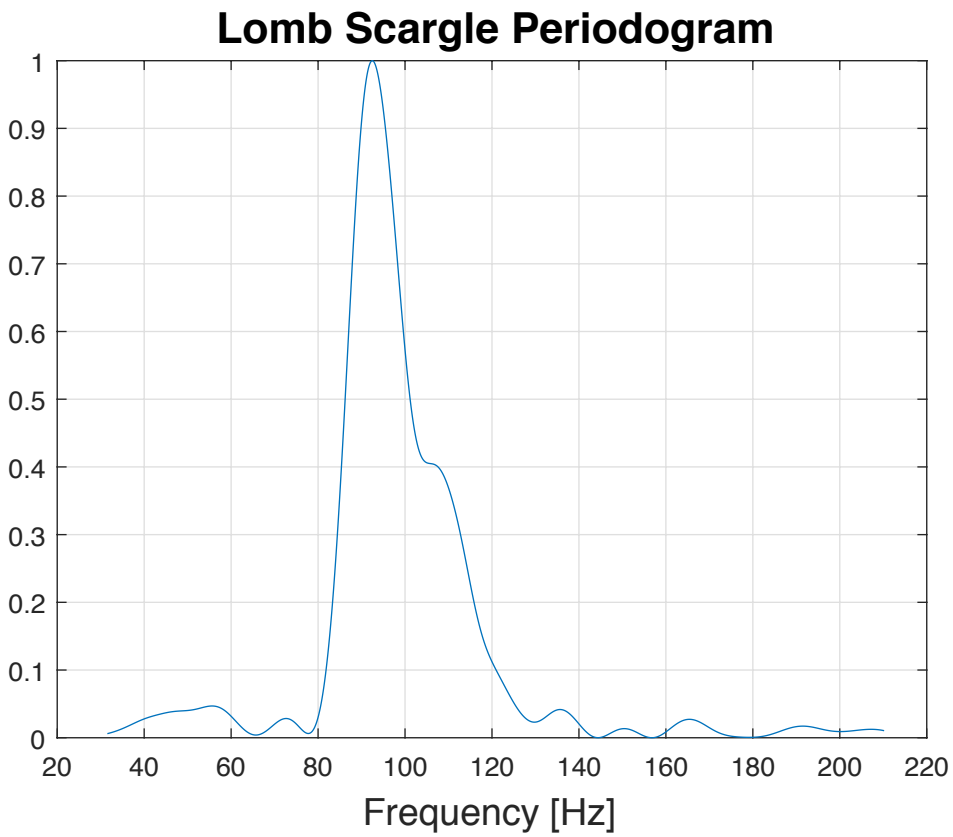

Figure 7.5: Spectral response for the Lomb Scargle Periodogram technique.

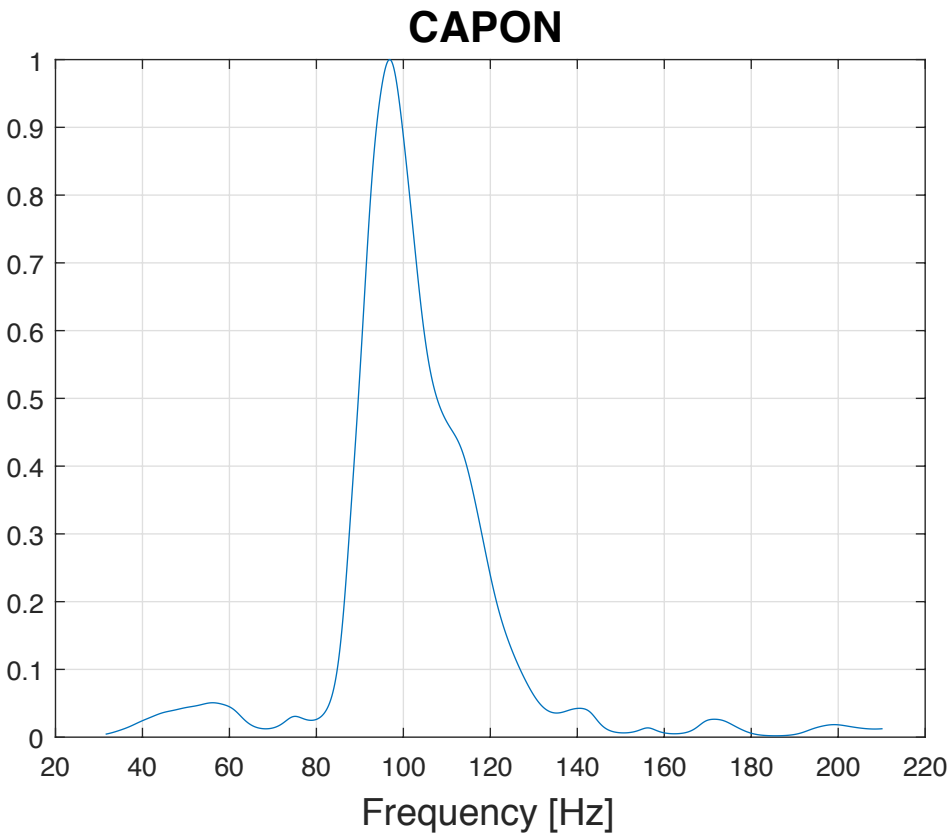

Figure 7.6: Spectral response for the Capon technique. The Capon filter was designed with m= 1500. The Capon Filter is much slower than the rest due to the correlation matrix calculation. The Capon height determination differs a little bit with the rest of methods.

7.6. Other Methods for filtering

Another type of representation that appears in the literature consists on superposing the detrended signal to the elevation(*azimuth*) function in order to see when the incoherent contribution overpasses the coherent one. Fig. 7.7 is included as an example.

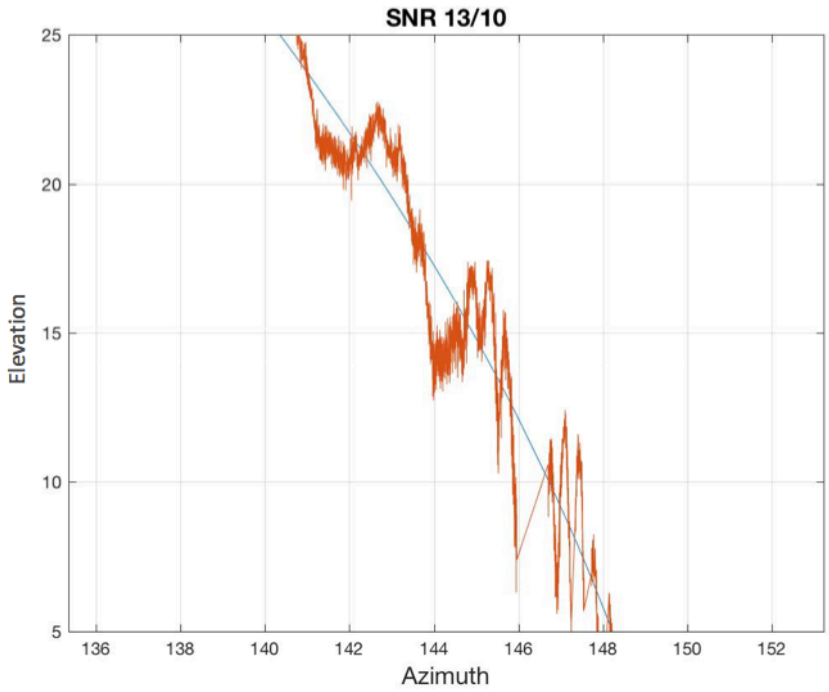

Figure 7.7: Detrended signal (L1) in orange and elevation(azimuth) in blue for the 13th of September 2016.

Since a GNSS satellite signal illuminates a large region of the surface, the reflection off the sea surface can not be considered to originate from only one single geometric point, the specular point. Instead, reflections from the illuminated area surrounding the specular point will contribute to the total reflected signal. In order to approximate this reflection surface, specular reflection is considered, meaning that both the incident and the reflection angles are equal and lie in the receiver-transmitter plane, the reflection surface is perfectly flat, and the reflected signal power is coherent and governed by the Fresnel equations [25]. Based on these assumptions, the reflection area can be described by the first Fresnel zone. The first Fresnel zone, with the specular point in the center, is defined by a phase change of the signal, across the reflective surface, of less than half the signal wavelength. The semi-major axis (a) and the semi-minor axis (b) of the first Fresnel zone (or ellipse) can be calculated as:

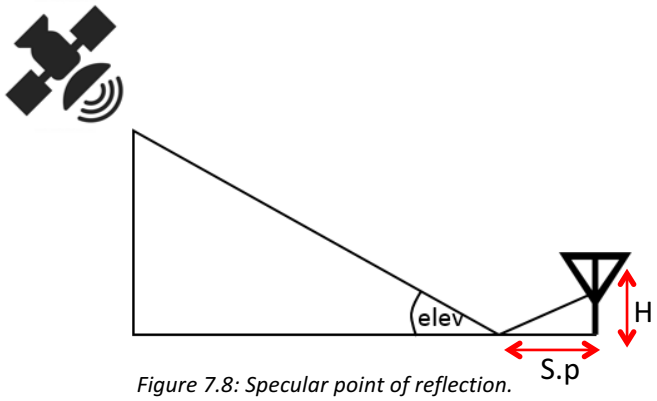

Figure 7.8: Specular point of reflection.

$$specular\ point = \frac{H}{\tan(\theta_{inc})} \tag{A.21}$$

$$a = \frac{\sqrt{2\delta H cos(\theta_{inc})}}{cos^2(\theta_{inc})} \tag{A.22}$$

$$b = \frac{\sqrt{2\delta H cos(\theta_{inc})}}{cos(\theta_{inc})} \tag{A.23}$$

where the specular point is S.p, H the height of the antenna with respect to the reflection surface, $\theta_{inc} = 90 - \theta_{elev}$ and δ the phase change across the surface measured in wavelengths ($\frac{\lambda}{2}$ for the first Fresnel zone).

For the Palma de Mallorca station for L1 (lambda is considered equal for GPS and GLONASS as it does not change results too much) and elevation of 2°: h= 4.8 , $\delta = \frac{\lambda}{2}$, $\theta_{inc} = 88°$; $a = 146.6\ m$, $b = 5.1\ m$ and specular point= 137.5 m.

Figure 7.9: The biggest circle represents the reflection for 2° elevation and the little one is 5° elevation.

Results comparing Spectral Analysis against Ground Truth will be presented in Appendix 7.7.

7.7. Result figures

7.7.1. Mallorca

7.7.1.1. GPS L1

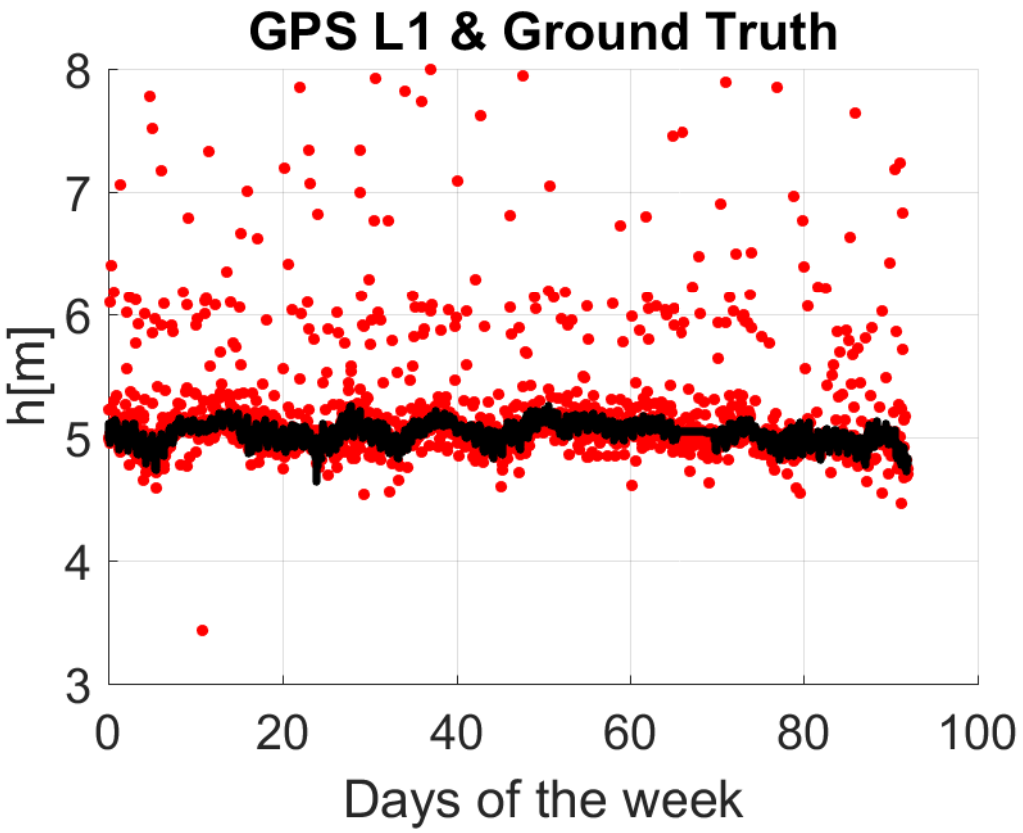

Figure 7.10: Red dots are results obtained using the Spectral Analysis method and the black ones are the Ground Truth provided by Puertos del Estado for GPS L1.

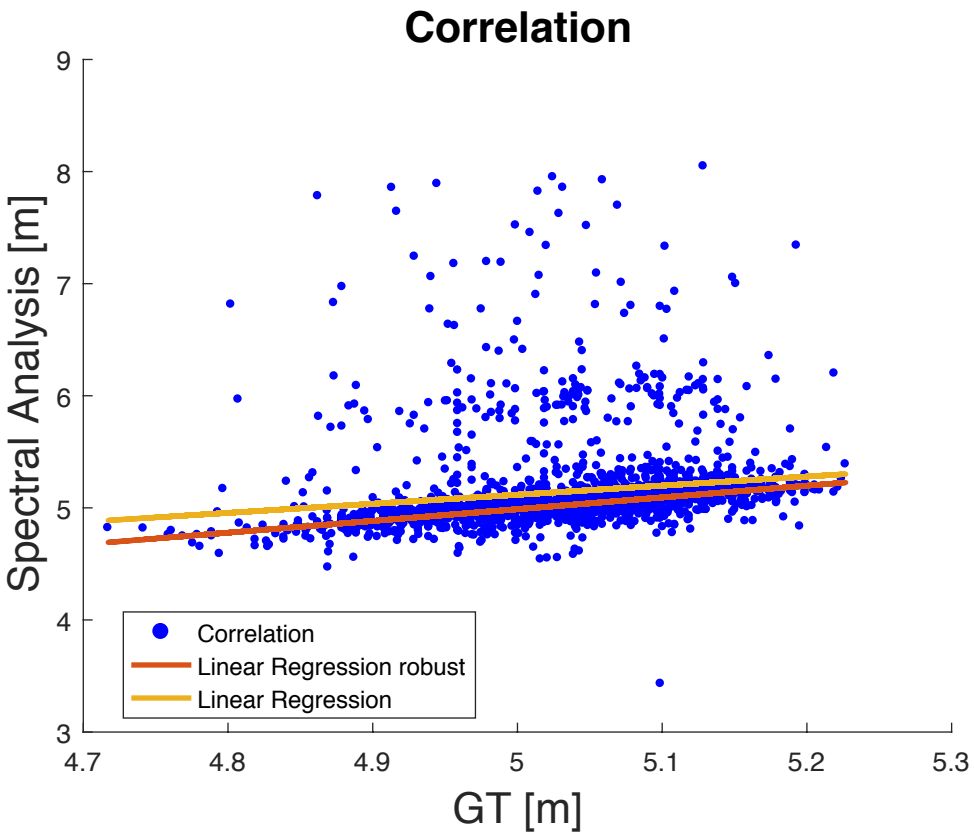

Figure 7.11: Correlation and Linear Regression between Ground Truth (x axis) and Spectral Analysis (y axis).

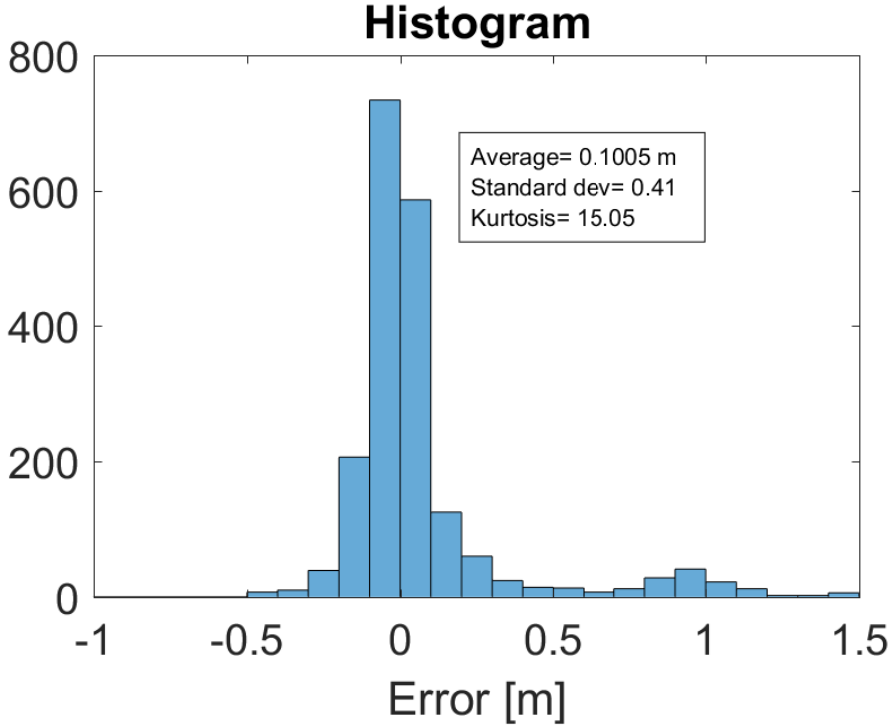

Figure 7.12: Histogram of the error (positive error is when Spectral Analysis is higher than Ground Truth).

7.7.1.2. GPS L2

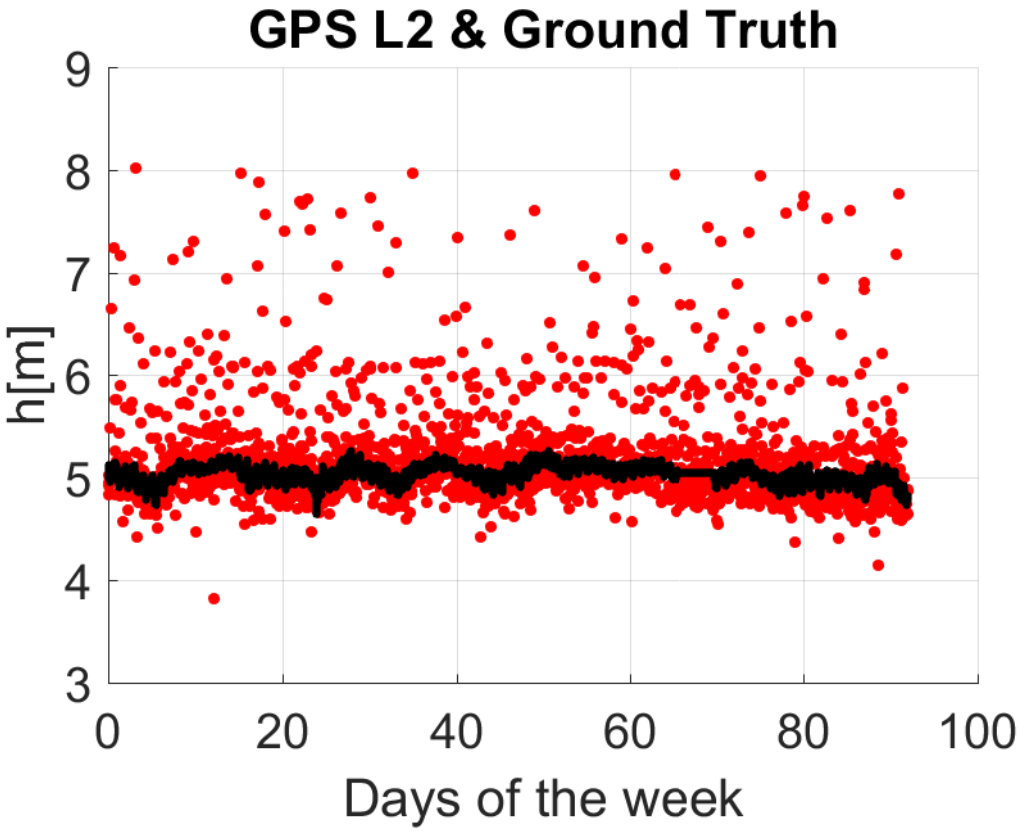

Figure 7.13: Red dots are results obtained using the Spectral Analysis method and the black ones are the Ground Truth provided by Puertos del Estado for GPS L2.

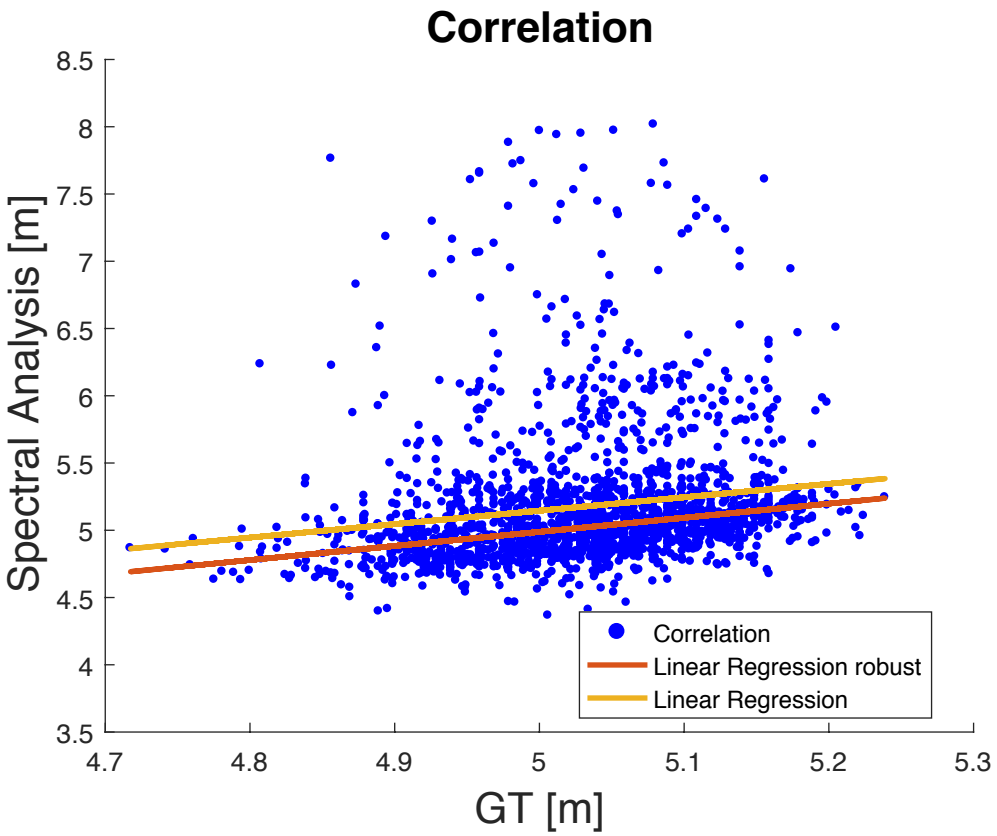

Figure 7.14: Correlation and Linear Regression between Ground Truth (x axis) and Spectral Analysis (y axis).

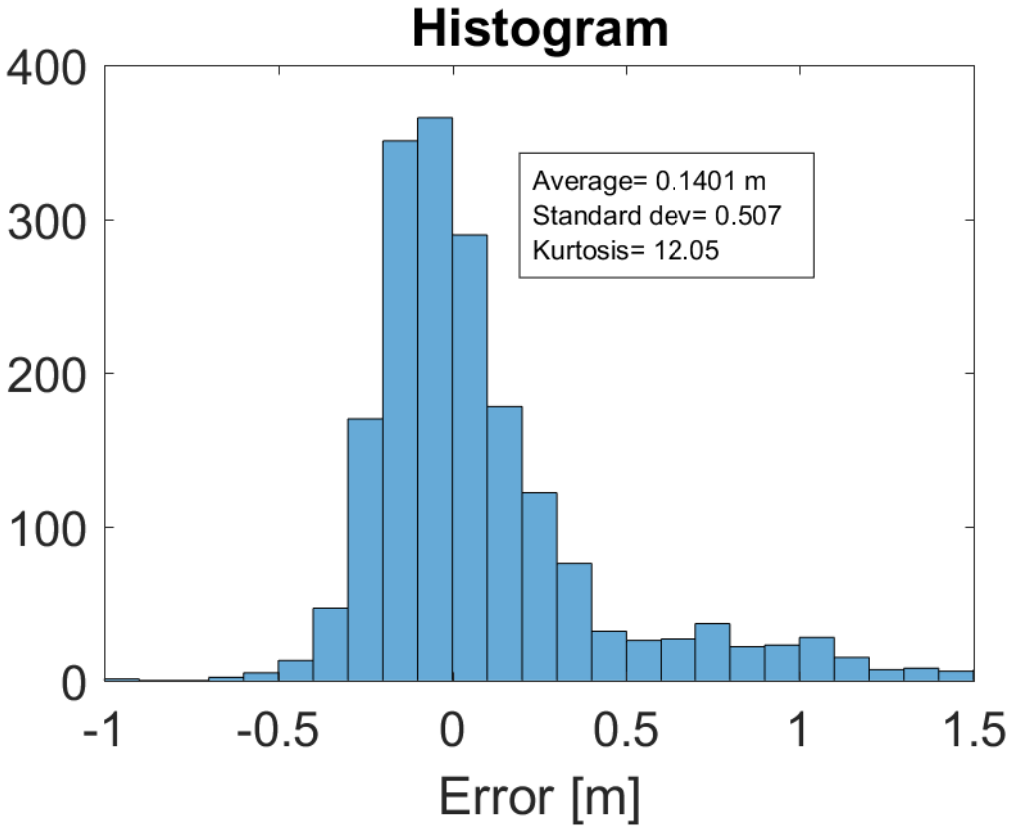

Figure 7.15: Histogram of the error (positive error is when Spectral Analysis is higher than Ground Truth).

7.7.1.3. GLONASS L1

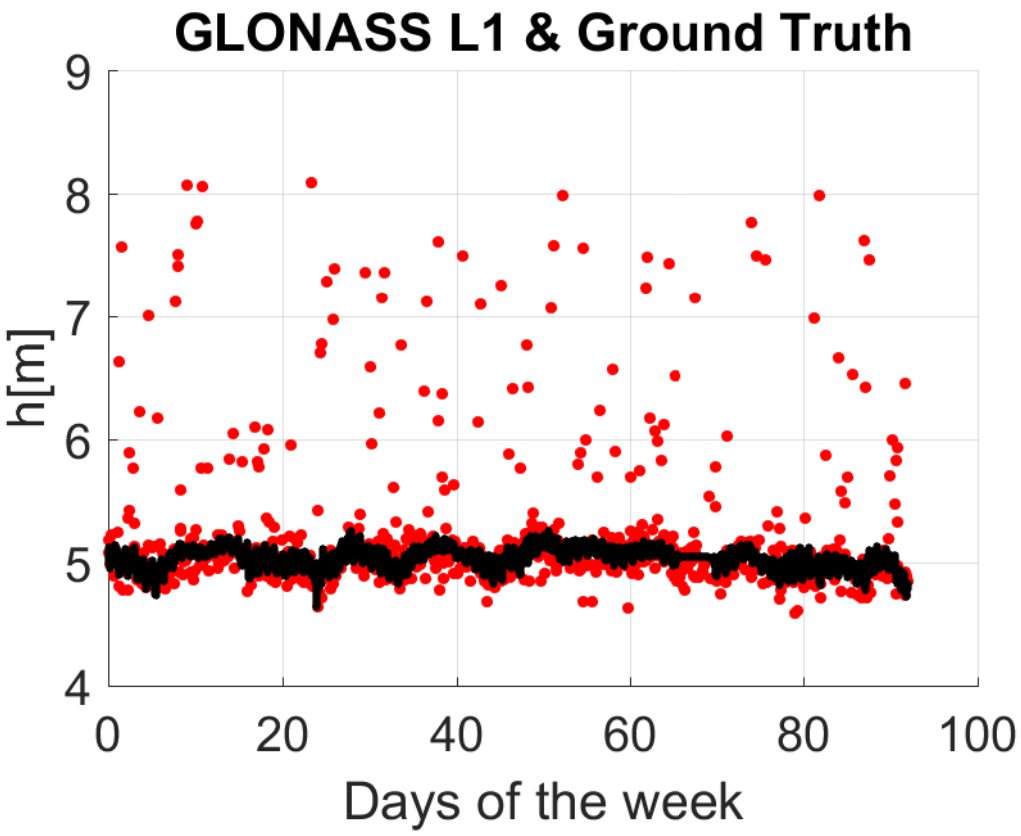

Figure 7.16: Red dots are results obtained using the Spectral Analysis method and the black ones are the Ground Truth provided by Puertos del Estado for GLONASS L1.

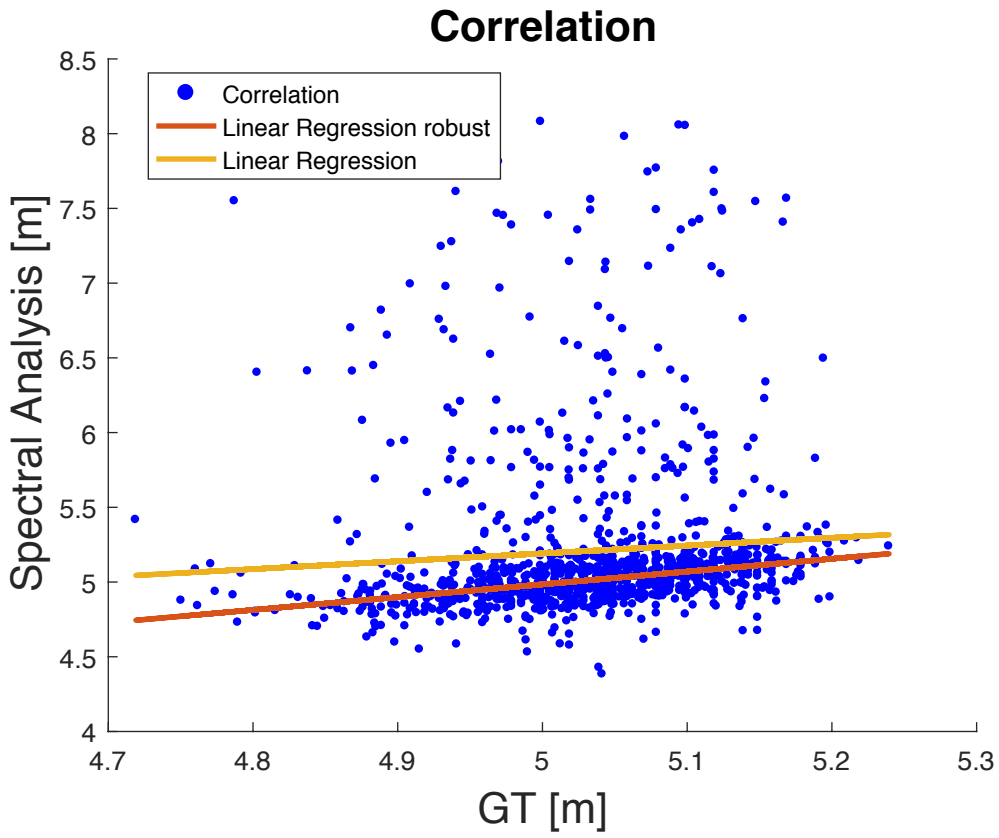

Figure 7.17: Correlation and Linear Regression between Ground Truth (x axis) and Spectral Analysis (y axis).

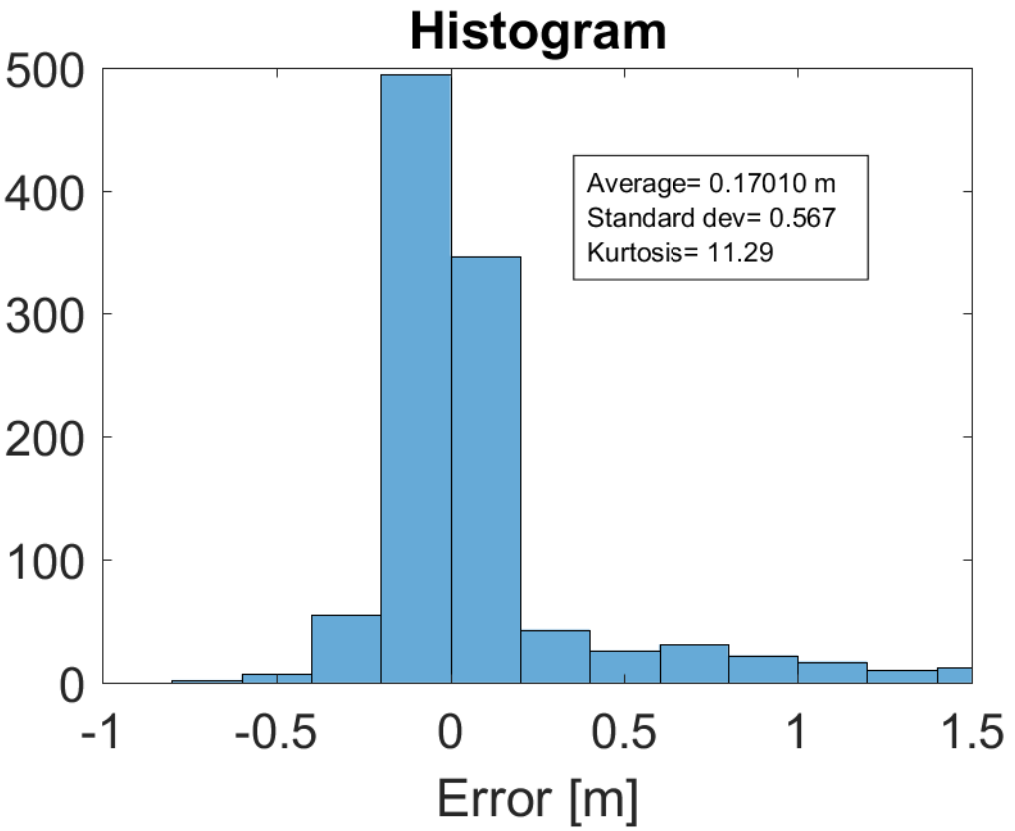

Figure 7.18: Histogram of the error (positive error is when Spectral Analysis is higher than Ground Truth).

7.7.1.4. GLONASS L2

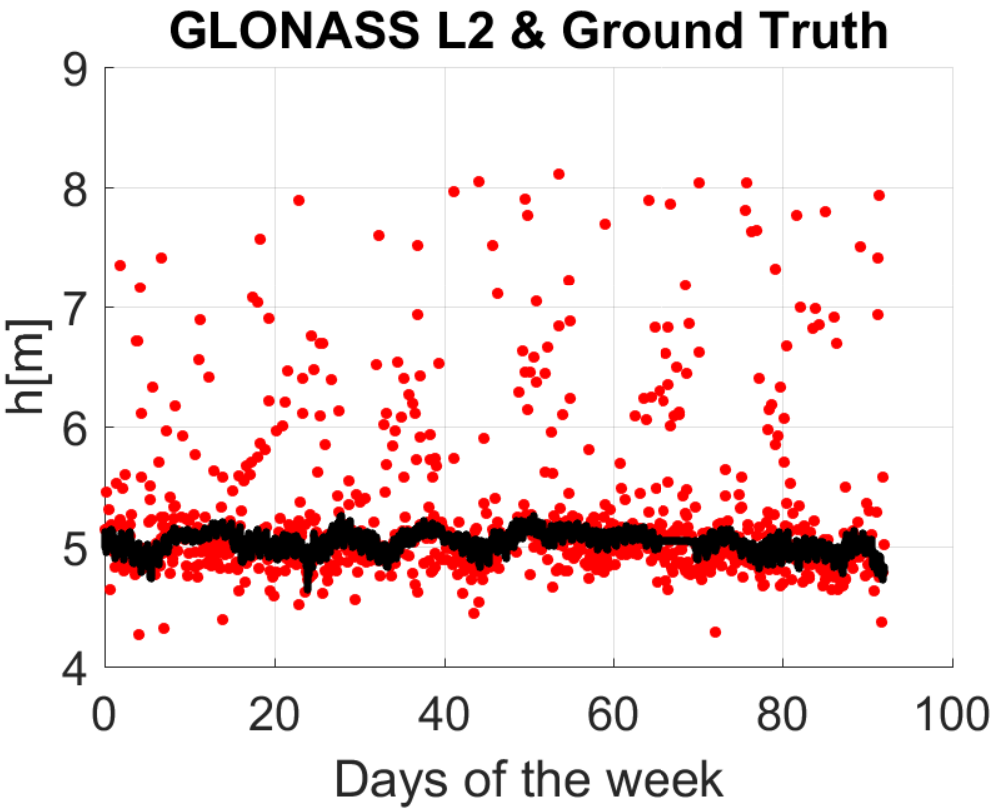

Figure 7.19: Spectral Analysis results (red dots) for GLONASS L2 against Ground Truth (black dots).

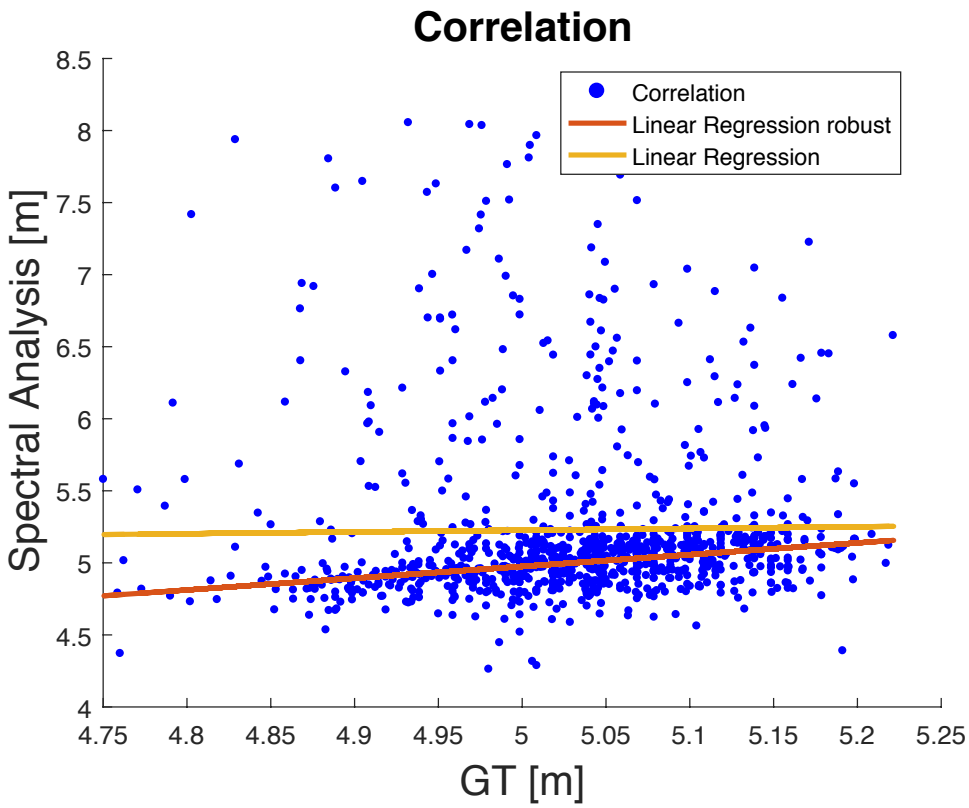

Figure 7.20: Correlation and Linear Regression between Ground Truth (x axis) and Spectral Analysis (y axis).

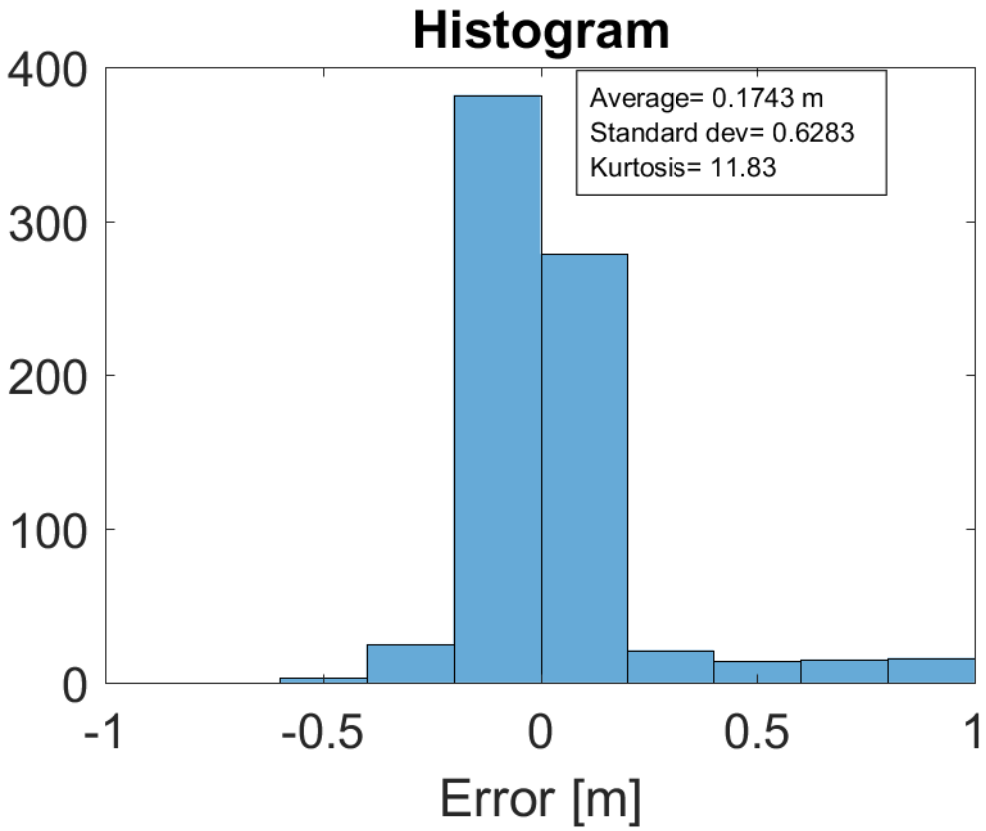

Figure 7.21: Histogram of the error (positive error is when Spectral Analysis is higher than Ground Truth).

7.7.1.5. Table with results

Table 7.1: Results Spectral Analysis for GPS and GLONASS different combinations in Mallorca.

	RMSE [cm]	RMSE robust [cm]	Corr.	Corr. robust	Coverage	Linear Regression	Linear Regression robust
GPS, GLO L1	49.51	11.08	0.4701	0.998	42 min	0.71x + 1.61	0.99x – 0.10
GPS L1 & L2	45.12	14.50	0.4130	0.997	45 min	1.04 + 0.60	1.01x - 0.09
GLO L1 & L2	61.34	15.45	0.3451	0.994	1h 25 min	0.43x + 3.04	0.89x + 0.56
GPS, GLO L2	57.75	21.90	0.2903	0.982	45 min	0.68x + 1.76	0.88x + 0.55

The combination between GPS and GLONASS L1 provides really good results, improving by almost 30 minutes the coverage obtained by GPS L1 alone.

7.7.2. Tarifa

7.7.2.1. GPS L1

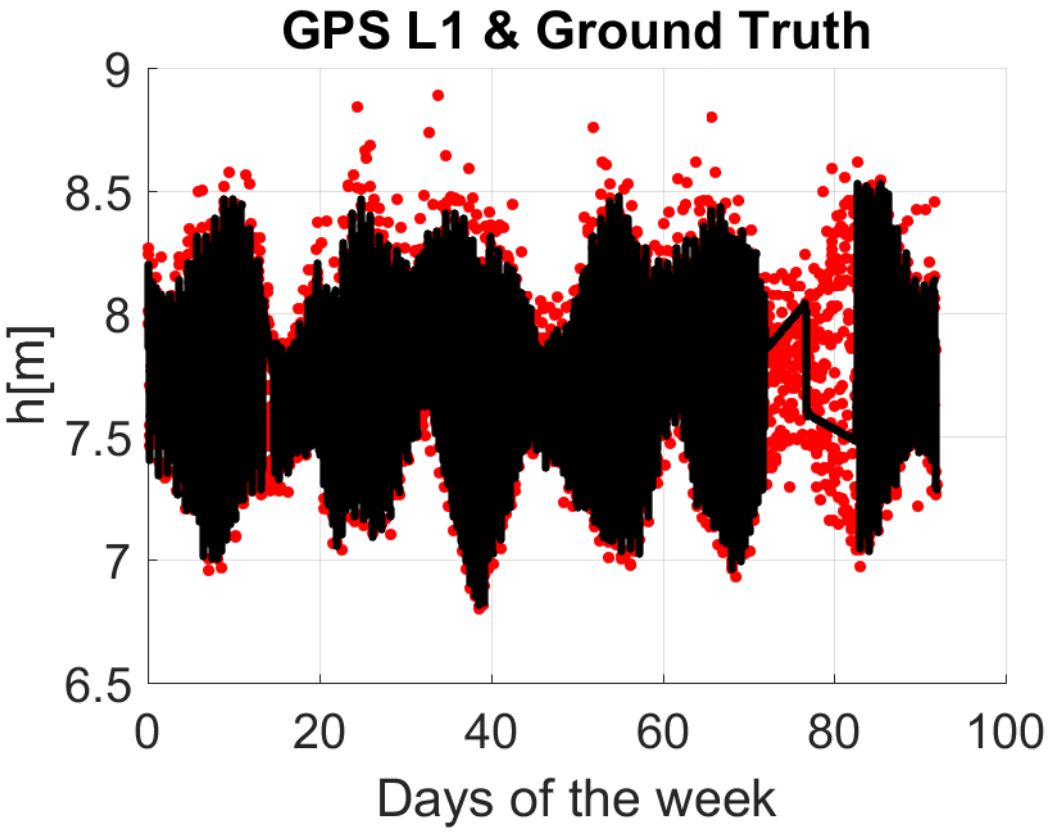

Figure 7.22: GPS L1 in red dots against Ground Truth in black.

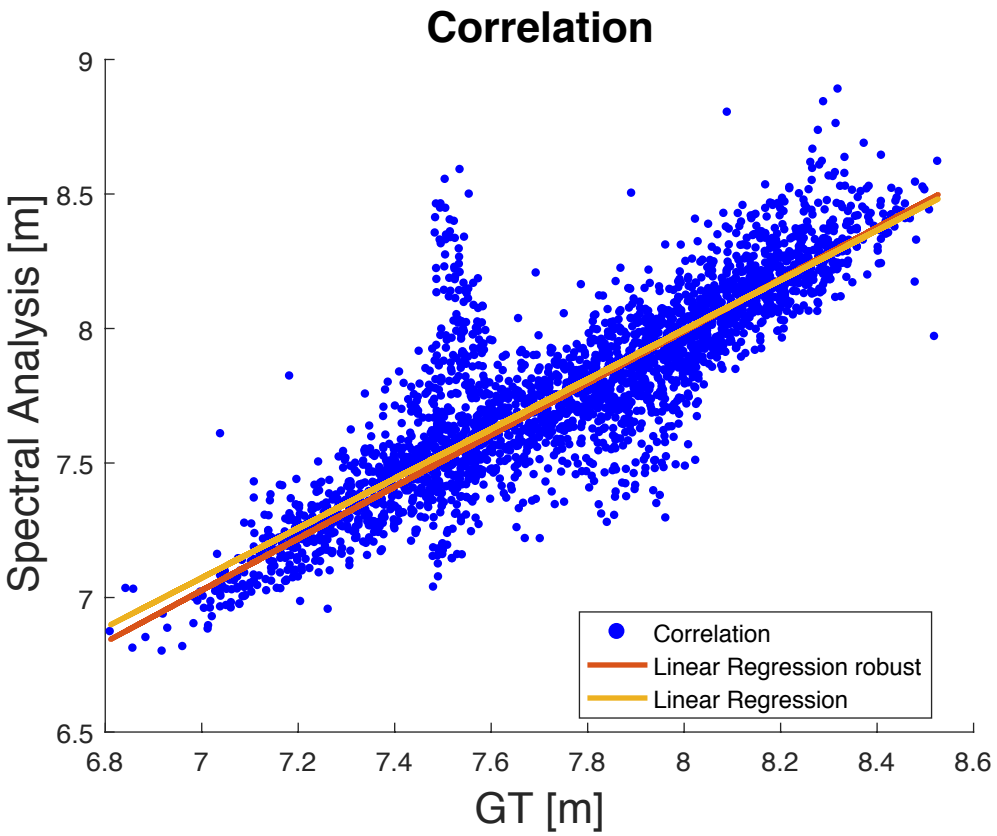

Figure 7.23: Correlation between Spectral Analysis and Ground Truth.

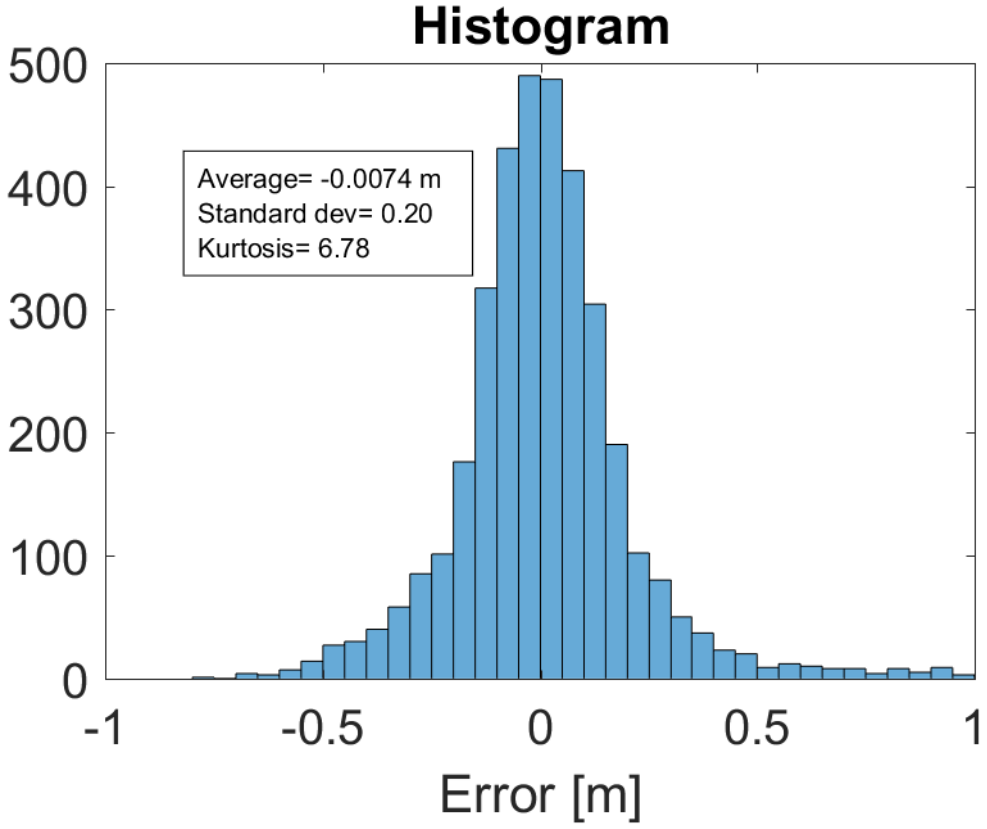

Figure 7.24: Histogram of the error.

7.7.2.2. GPS L2

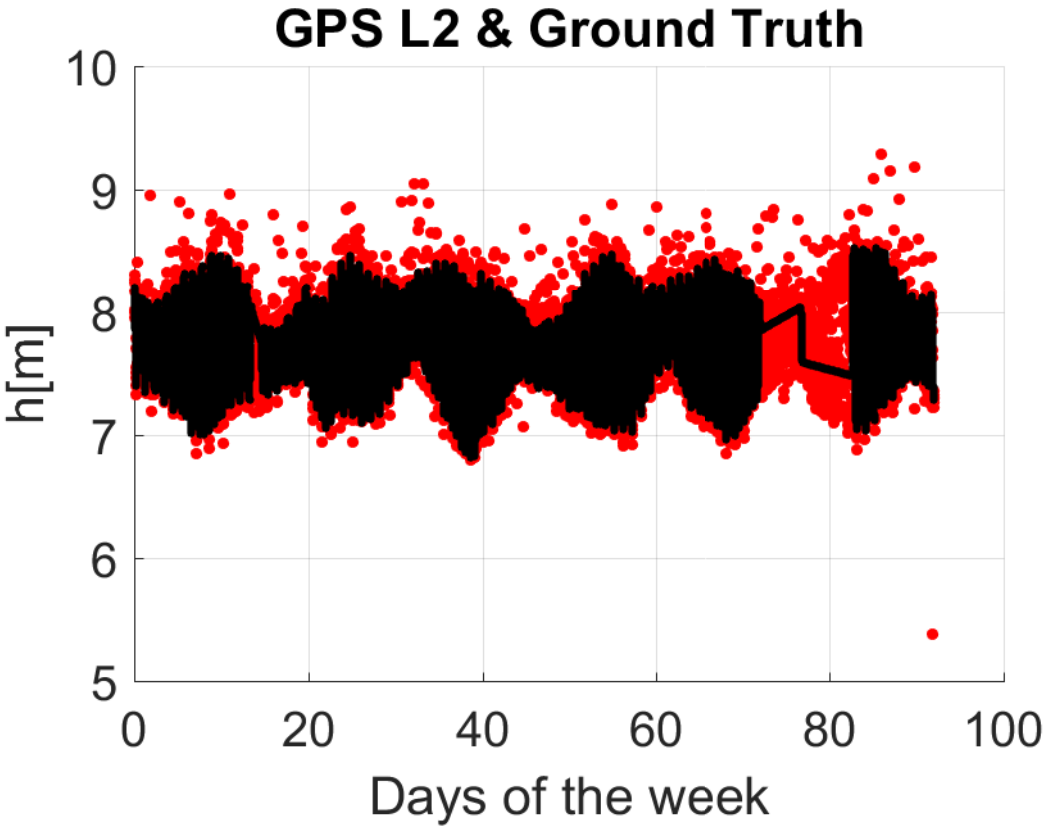

Figure 7.25: Spectral Analysis (red dots) against Ground Truth (black dots) for GPS L2.

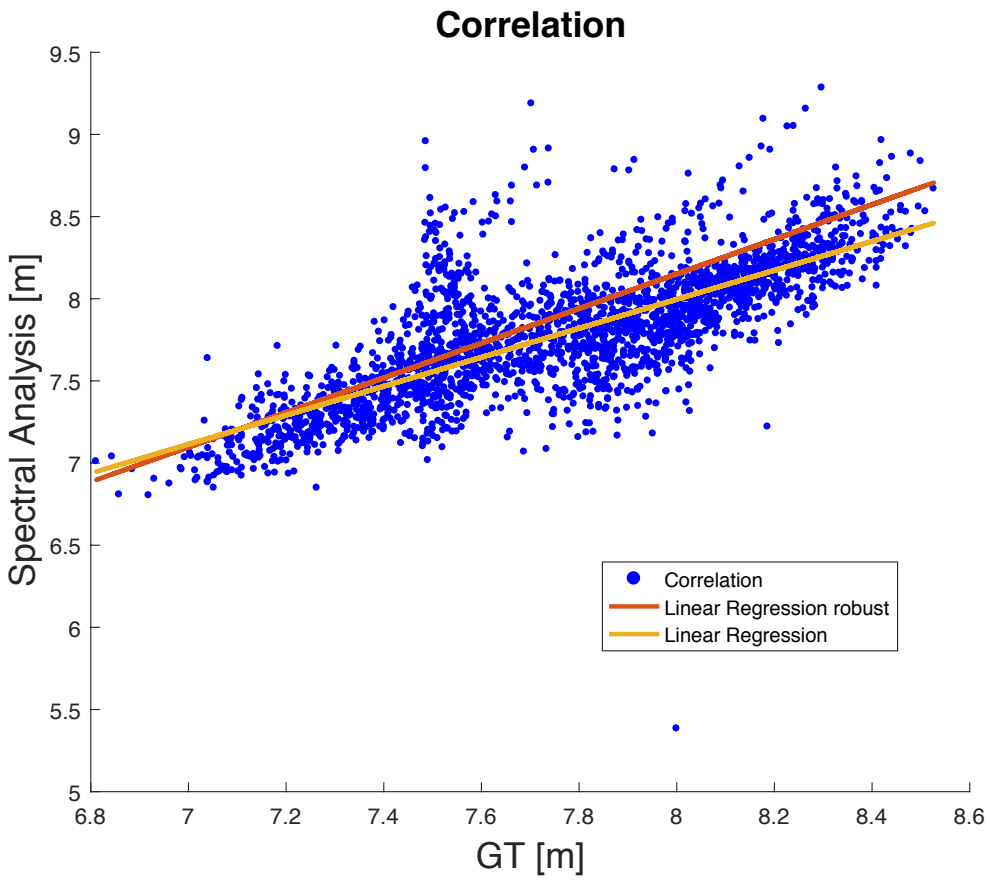

Figure 7.26: Correlation between Spectral Analysis and Ground Truth.

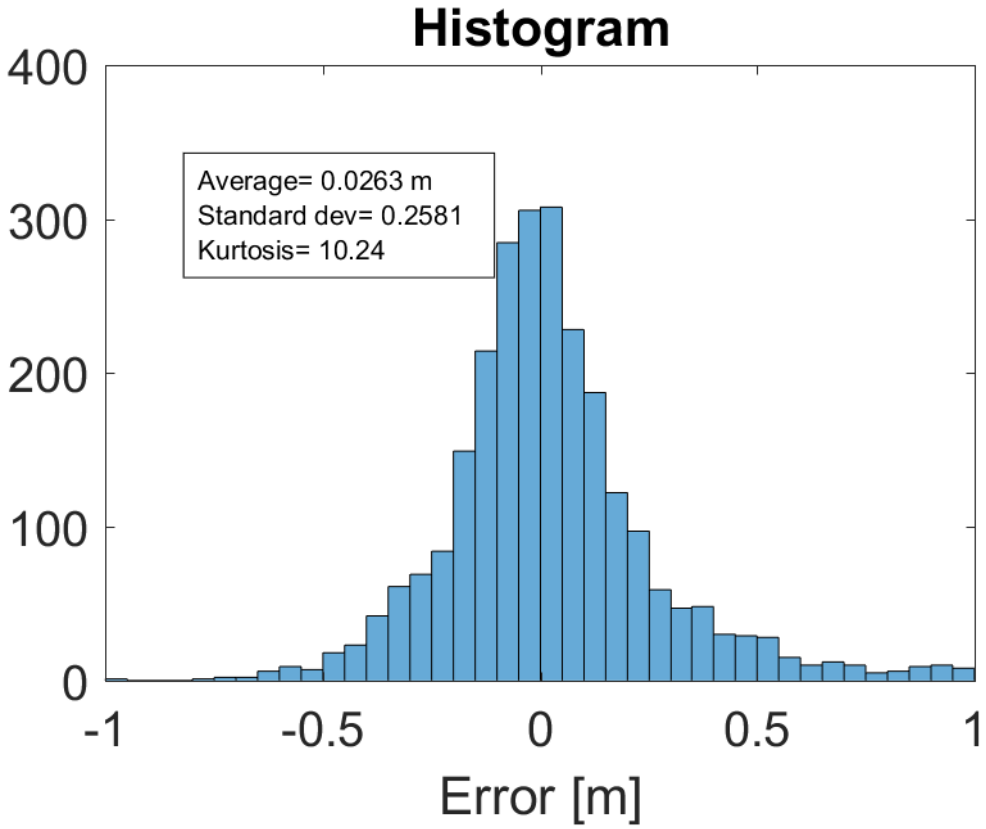

Figure 7.27: Histogram of the error.

7.7.2.3. GLONASS L1

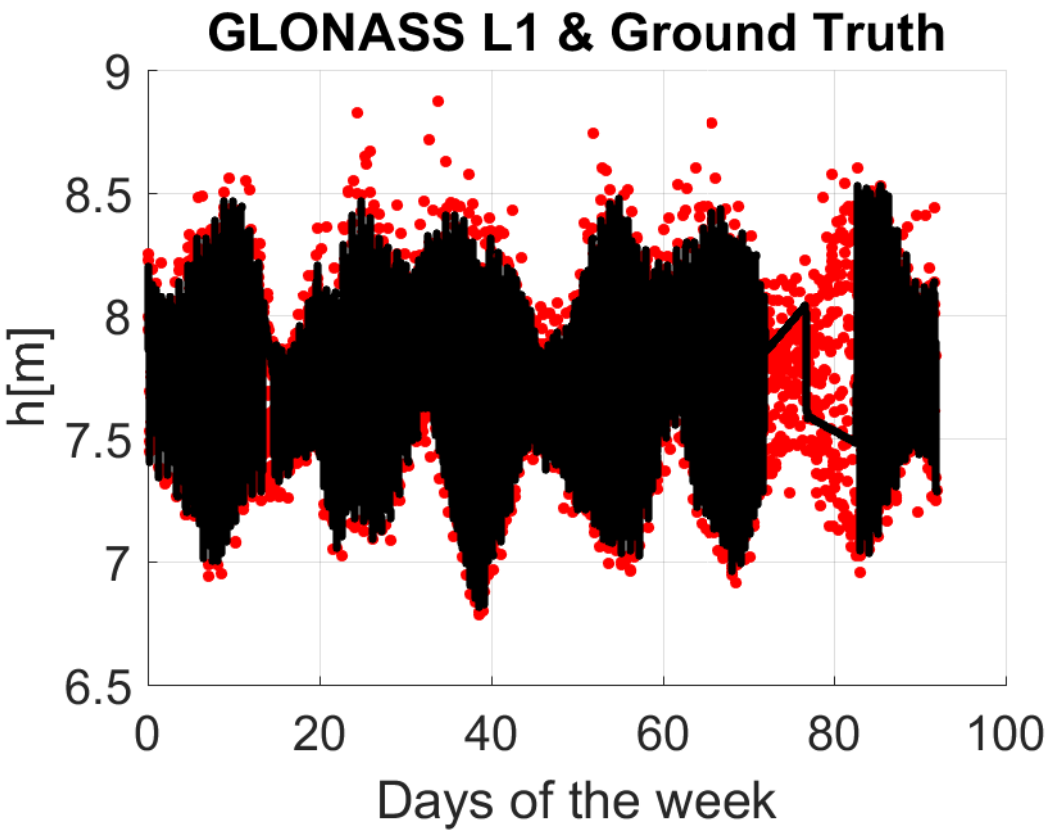

Figure 7.28: Spectral Analysis (red dots) against Ground Truth (black dots) for GLONASS L1.

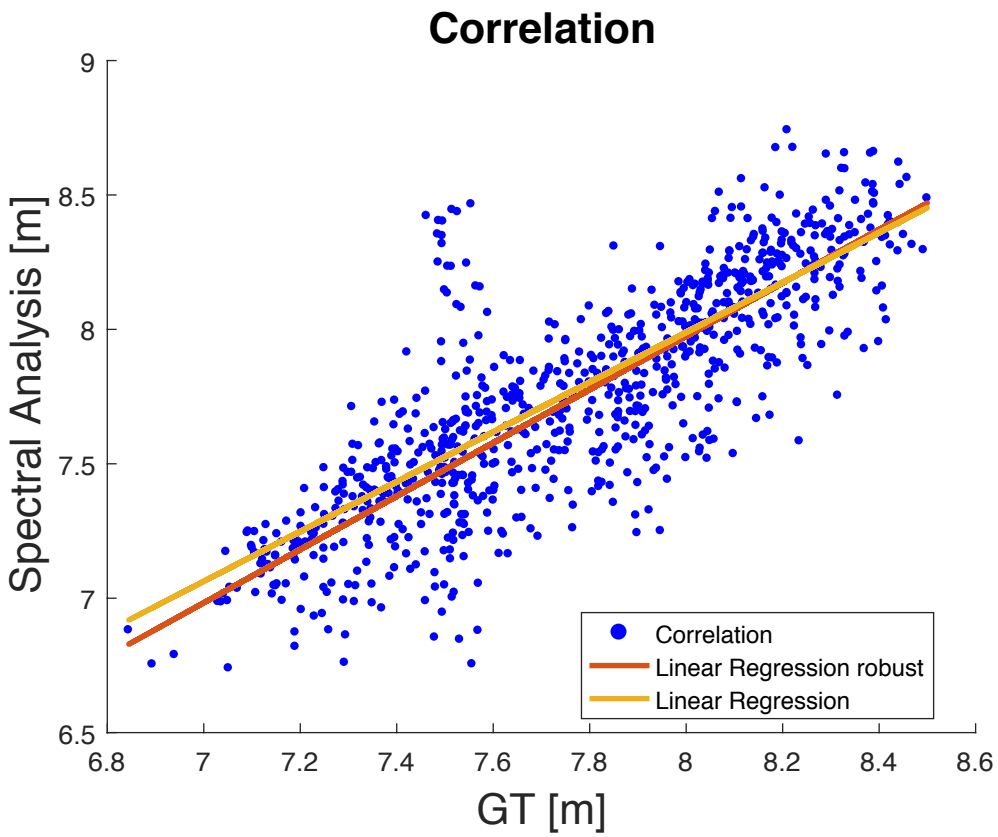

Figure 7.29: Correlation between Spectral Analysis and Ground Truth.

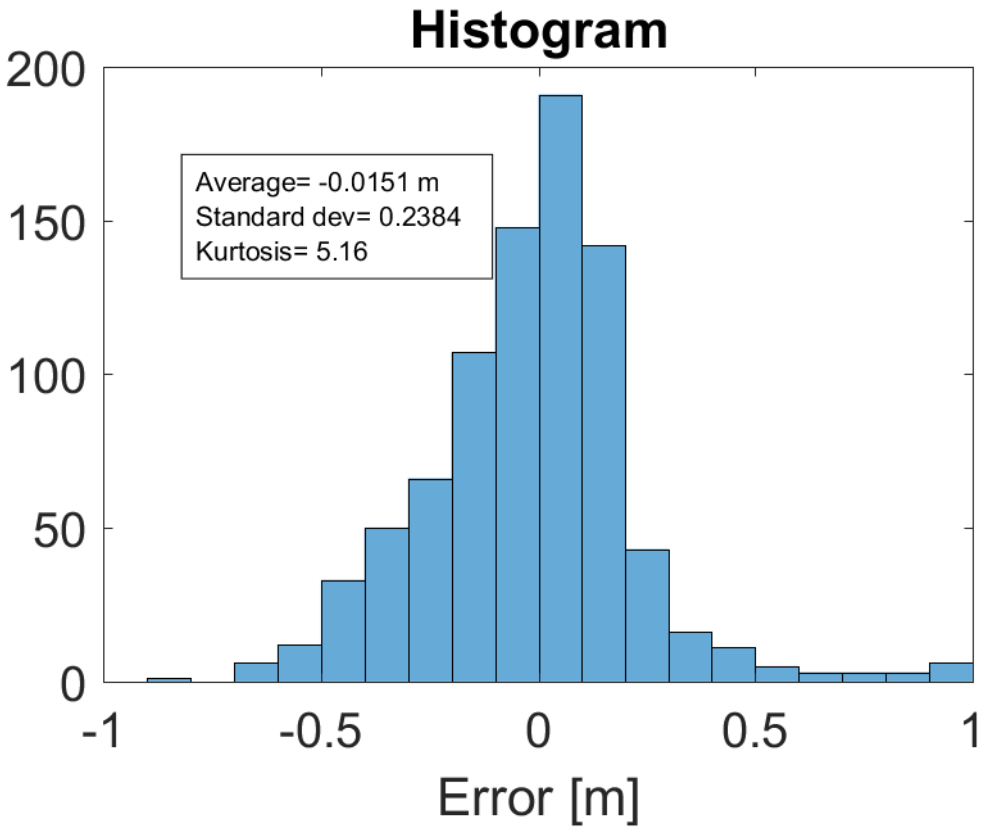

Figure 7.30: Histogram of the error.

7.7.2.4. GLONASS L2

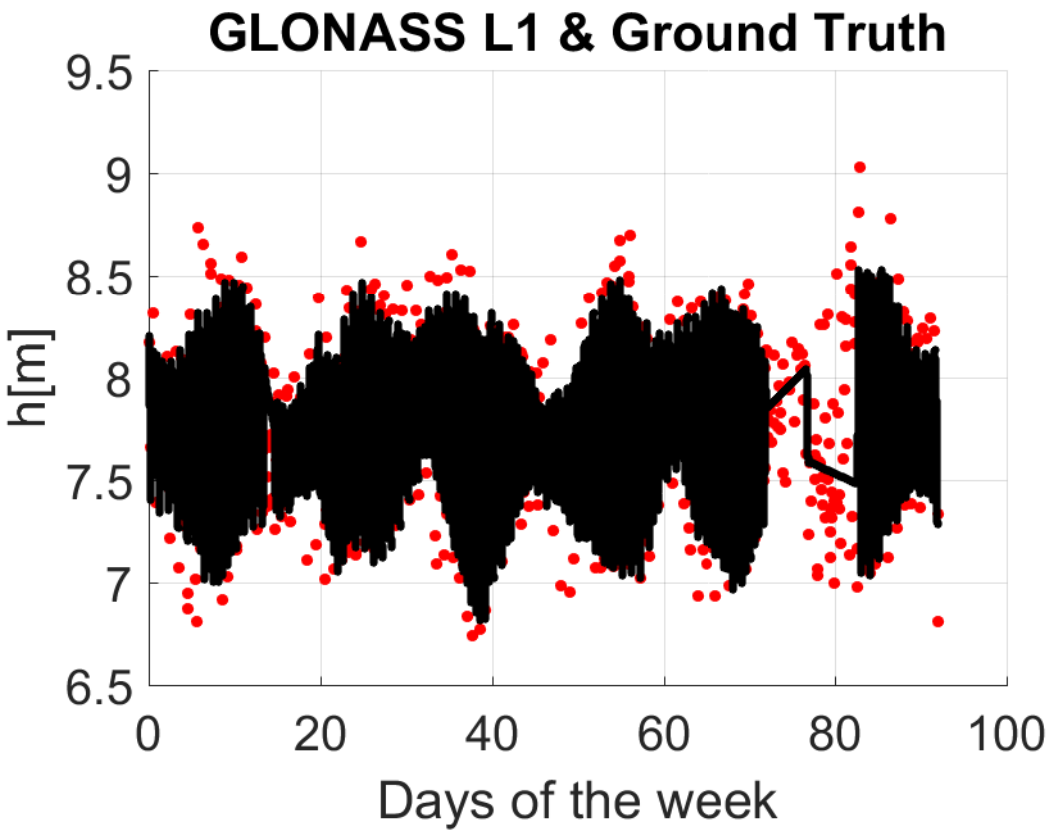

Figure 7.31: Spectral Analysis (red dots) against Ground Truth (black dots) for GLONASS L2.

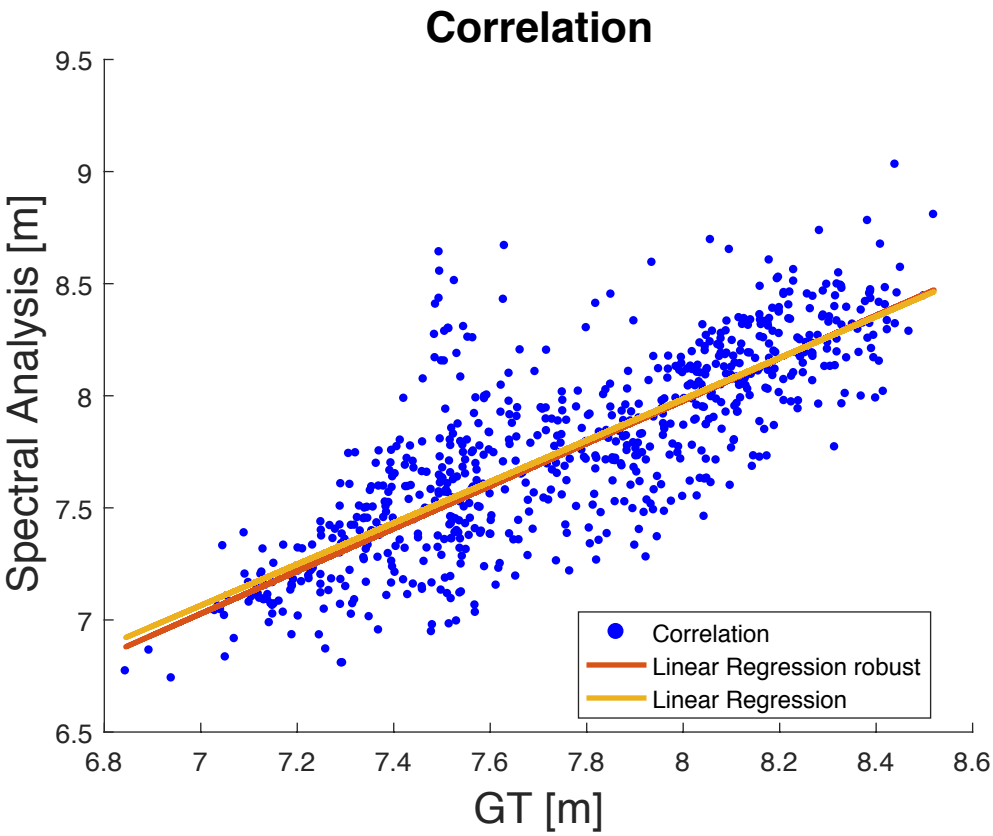

Figure 7.32: Correlation between Spectral Analysis and Ground Truth.

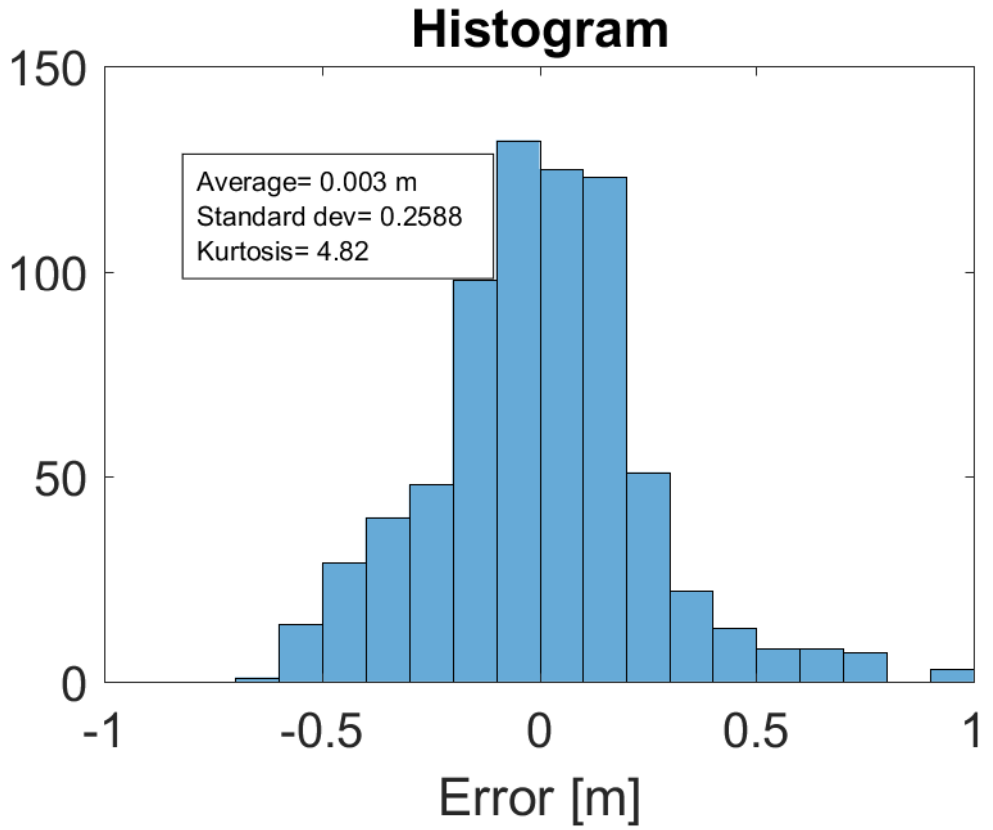

Figure 7.33: Histogram of the error.

7.7.2.5. Table with results

Table 3.2: Results Spectral Analysis for GPS and GLONASS different combinations in Tarifa.

	RMSE [cm]	RMSE robust [cm]	Corr.	Corr. robust	Coverage	Linear Regression	Linear Regression robust
GPS, GLO L1	19.79	14.90	0.851	0.999	40 min	0.93x + 0.60	0.98x +0.19
GPS L1 & L2	21.13	15.99	0.824	0.991	42 min	0.90x + 0.70	0.95x + 0.45
GLO L1 & L2	24.20	18.45	0.812	0.991	2h 19 min	0.92x + 0.57	0.98x + 0.16
GPS, GLO L2	25.90	18.51	0.780	0.988	50 min	0.91x + 0.82	0.93x + 0.55

When combining GPS and GLONASS L1 the coverage is improved a little bit with respect to just GPS L1 and the error increases less than 0.5cm. When combining L1 and L2 for the same system the coverage barely increases as a lot of samples are shared for both bands.

7.7.3. Results B-Splines

7.7.3.1. GPS L1

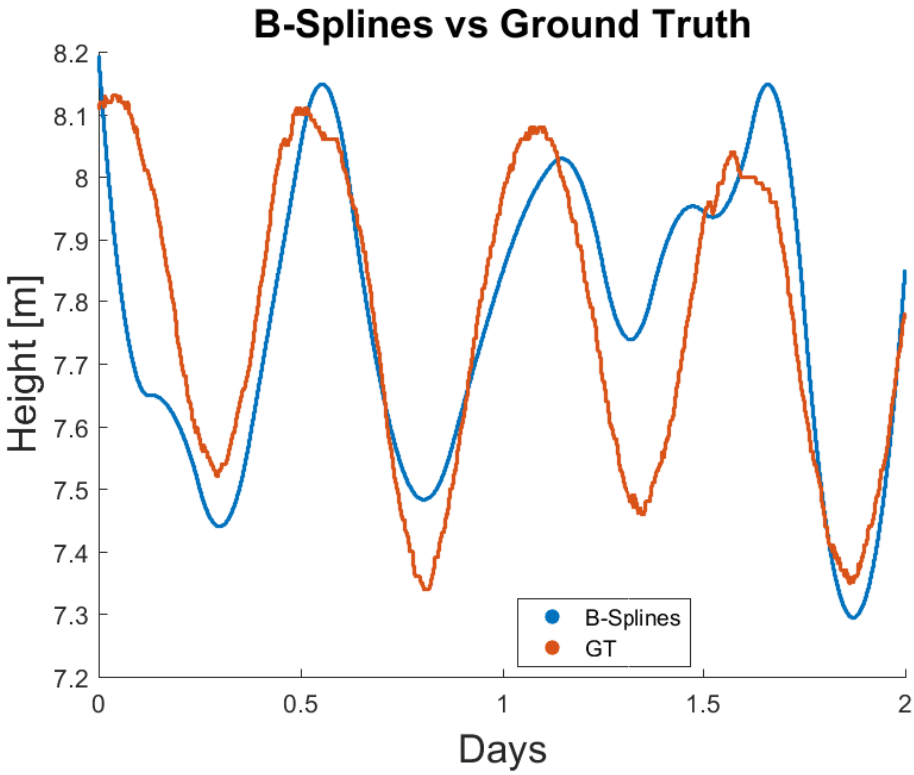

Figure 7.34: The orange line symbolizes Ground Truth and the blue line the B-Splines Method.

7.7.3.2. GPS, GLONASS L1

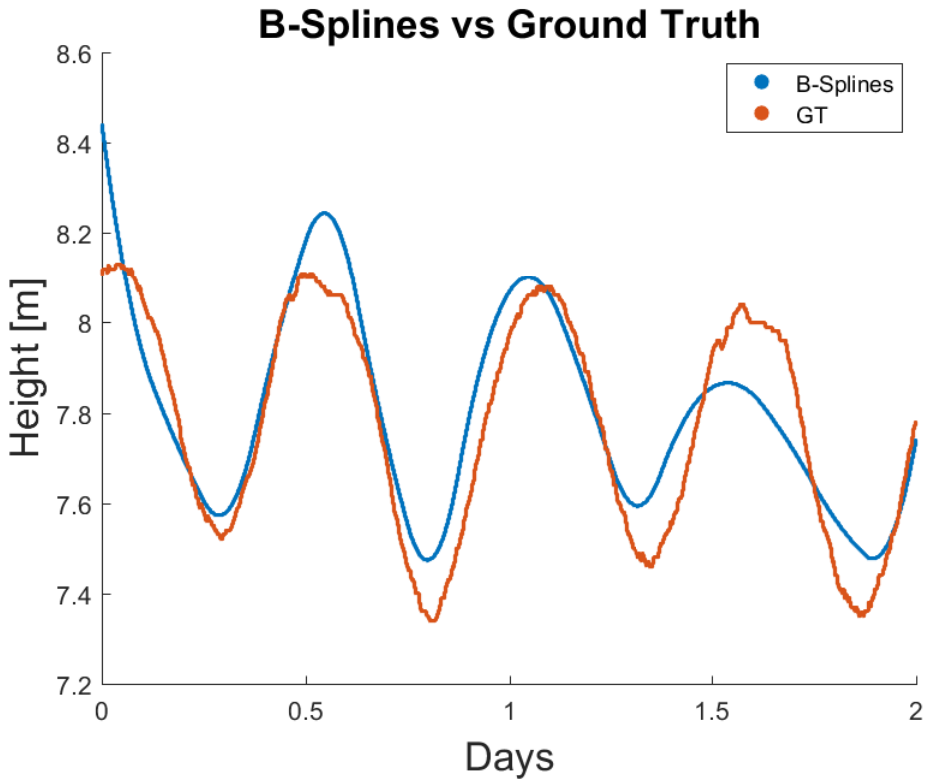

Figure 7.35: The orange line symbolizes Ground Truth and the blue line the B-Splines Method.

7.7.3.3. GLONASS L1

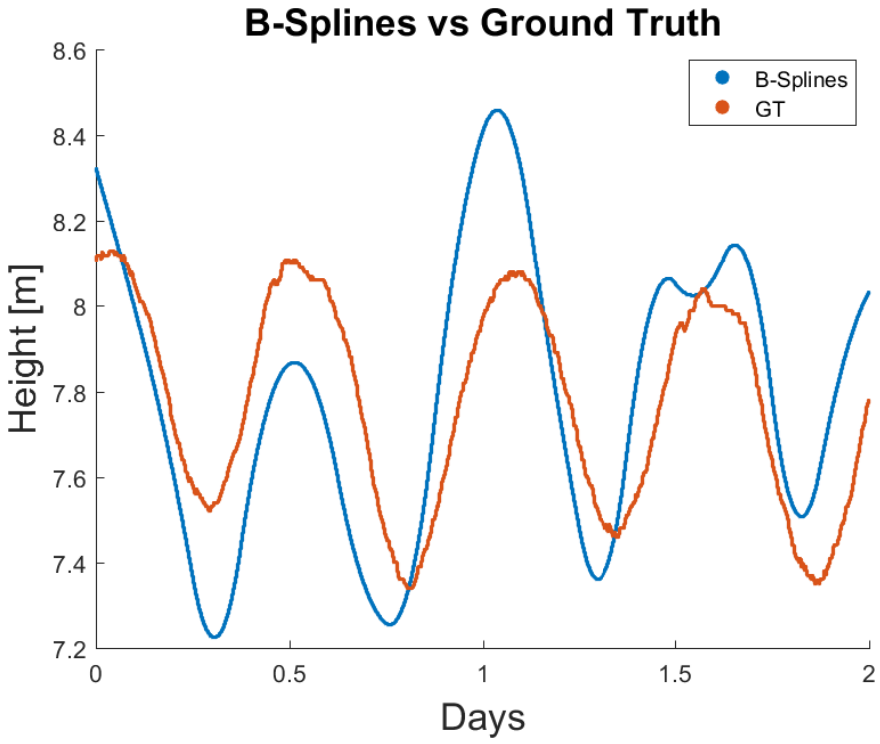

Figure 7.36: The orange line symbolizes Ground Truth and the blue line the B-Splines Method.

7.7.3.4. Curves representation with B-Splines

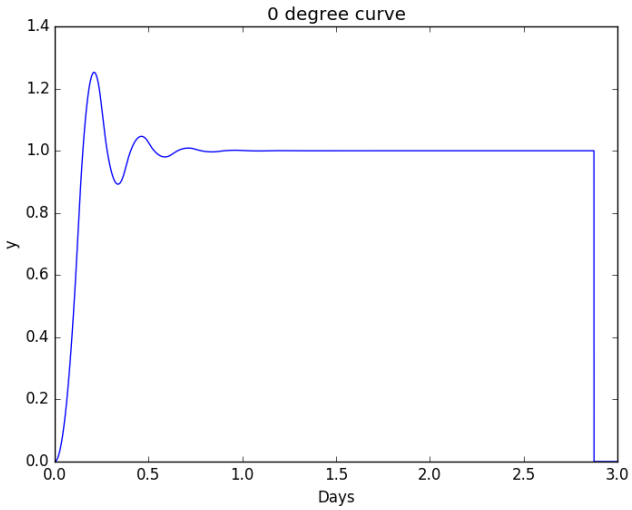

Figure 7.37: B-Splines fitting of a zero degree curve (y=1).

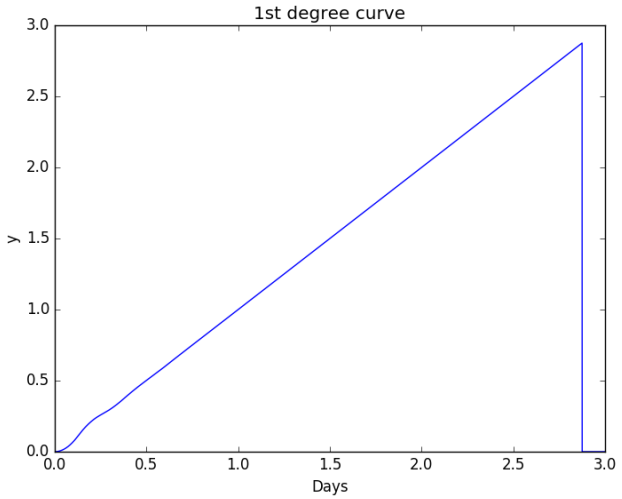

Figure 7.38: B-Splines fitting of a first degree curve (y= Days).

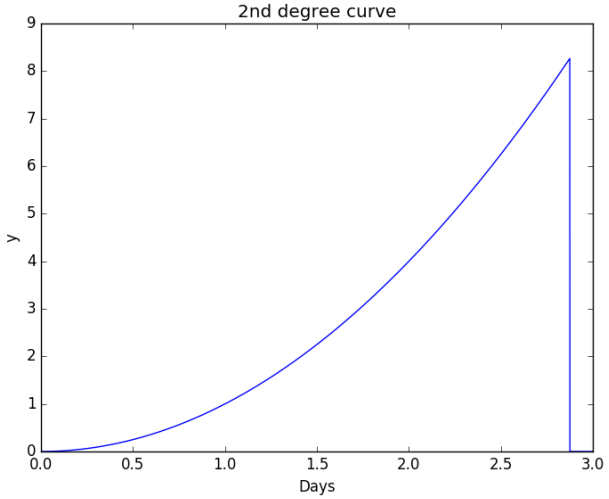

Figure 7.39: B-Splines fitting of a second degree curve (y= (Days)^2).

7.8. Data Provided

Before introducing the file format of the files downloaded, it needs to be explained the method used for accessing the FTPs and downloading the files automatically. The functions *curl()* and *ftp()* were used for this purpose (see the code in Appendix 7.9) from MATLAB.

When accessing the FTPs to download the data, this can be provided in two different formats:

- Compact Rinex Format version 1: It was designed to mitigate the drawback of RINEX format observation files becoming large compared with receiver-specific binary formats. Compact Rinex format version 1.0 is compatible with RINEX version 2 observation file format and was developed by Hatanaka [42], and it has been used to exchange and archive data. Fig. 7.40 depicts the name format of the observation files for RINEX 2 files.
- Compact Rinex Format version 3: The motivation for developing this software [43] was the same as for the first version (reducing size of the observational files) but for RINEX version 3 observational files. RINEX 3 was developed with the mission of including new systems (i.e. Galileo and BeiDou2) that could not be included in the RINEX 2 format. Fig. 7.41 represents the name format for RINEX 3.

Both type of formats need to be translated into RINEX (version 2 and 3 respectively) in order to process the data. The software used is called RNXCMP, and it is devoted to compress from RINEX files to Compact RINEX format and vice versa. This tool deals with the conversion between the new format as well as the older one.
Once the files have been decompressed it is time to use software available to obtain parameters such as SNR, elevation and azimuth from the data. The only tool available right now for this task is TEQC from UNAVCO [44].
Teqc is a comprehensive toolkit for solving many problems when preprocessing GNSS data:

- Translation: read GNSS native receiver files and translate the data to other formats.
- Editing: metadata extraction, editing, and/or correction of RINEX header metadata or BINEX metadata records.
- Quality checking of GPS and/or GLONASS data (native binary, BINEX, or RINEX observation files, with or without navigation files with ephemerides).

Teqc only accepts RINEX version 2, so in case Galileo system wants to be included, translation between RINEX 3 to RINEX 2.11 is required. Versions prior to 2.11 would not accept Galileo ephemeris, as 2.11 was the first version to include a definition of the satellite system code, system type and frequency numbers for Galileo observables.
The tool used for translating from version 3 to 2 is called GFZRNX [45] . To complete the process some terms in the header of the RINEX 2 translated observation file were required to be changed manually . The code developed in this thesis is provided in Apendix 6.9.

```
ssssdddf.yyt

|   |   | | |
|   |   | | +--  t:  file type:
|   |   | |          O: Observation file
|   |   | |          N: GPS Navigation file
|   |   | |          M: Meteorological data file
|   |   | |          G: GLONASS Navigation file
|   |   | |          L: Future Galileo Navigation file
|   |   | |          H: Geostationary GPS payload nav mess file
|   |   | |          B: Geo SBAS broadcast data file
|   |   | |                      (separate documentation)
|   |   | |          C: Clock file (separate documentation)
|   |   | |          S: Summary file (used e.g., by IGS, not a standard!)
|   |   | |
|   |   | +---  yy:  two-digit year
|   |   |
|   |   +-----   f:  file sequence number/character within day
|   |              daily file: f = 0
|   |              hourly files:
|   |              f = a:  1st hour 00h-01h; f = b: 2nd hour 01h-02h; ...
|   |              f = x: 24th hour 23h-24h
|   |
|   +-------  ddd:  day of the year of first record
|
+-----------  ssss:  4-character station name designator
```

Figure 7.40: Name format for RINEX 2 format (i.e. tari0310.17o). The observation data provided by the FTPs in Compact Rinex Format ends with d instead of o.

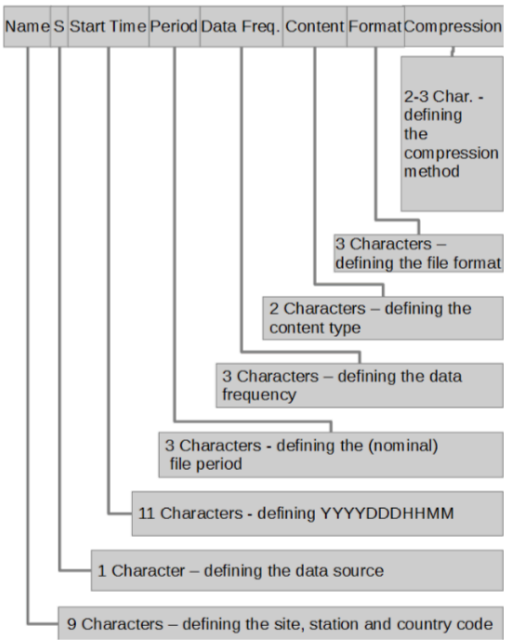

Figure 7.41: Name format for RINEX 3 format (i.e. TARI00ESP_R_20170310000_01D_30S_MO.rnx).

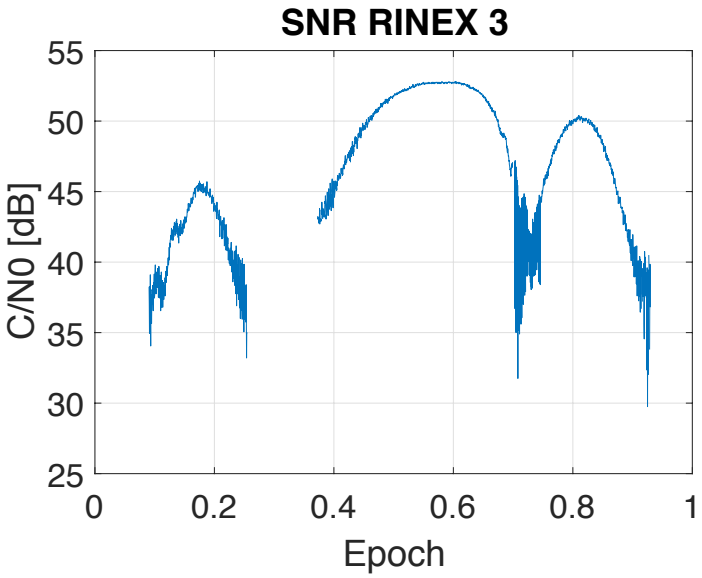

Figure 7.42: SNR for a Galileo Satellite in Tarifa Station. Observational files for RINEX 3 are only available sampled every 30 seconds.

7.9. Code developed

7.9.1. Obtain results from Spectral Analysis method

```
clc;
close all;

freq_glonass= [1 -4 5 6 1 -4 5 6 -2 -7 0 -1 -2 -7 0 -1 4 -3 3 2 4 -3 3
2]; %GLONASS satellite frequency number
fL1_glonass= 1602*1e6 + 562.5*1e3*freq_glonass; %L1 frequency for
GLONASS
fL2_glonass= 1246*1e6 + 437.5*1e3*freq_glonass; %L2 frequency for
GLONASS
fL1= 1575.42*1e6; %frequency of GPS L1
fL2= 1227.60*1e6; %frequency of GPS L2
lambda1= physconst('LightSpeed')/fL1; %GPS L1 wavelength
lambda2= physconst('LightSpeed')/fL2;%GPS L2 wavelength
lambda_l1_glonass= physconst('LightSpeed')./fL1_glonass;
lambda_l2_glonass= physconst('LightSpeed')./fL2_glonass;

inici= XXX; %starting day
final= XXX; %ending day

vector_5_12_complet_finestra750_seguit_tar_l1=
[zeros(2,60*24*60*(final+1-inici));linspace(0,final+1-
inici,60*24*60*(final+1-inici)); zeros(4,60*24*60*(final+1-inici));];
%%(1,:)f (2,:)azimuth (3,:)days (4,:)lambda (5,:) bias terms for L1 or
L2 (6,:) satellite number (7,:) average elevation tram
vector_5_12_complet_finestra750_seguit_tar_l2=
[zeros(2,60*24*60*(final+1-inici));linspace(0,final+1-
inici,60*24*60*(final+1-inici)); zeros(4,60*24*60*(final+1-inici));];
vector_plot_elev_az_snr= zeros(3*200,10000);

fil_az_min = XXX;% minimum filter azimuth
fil_az_max = XXX;% maximum filter azimuth
fil_el_min = XXX;% minimum filter elevation
fil_el_max = XXX;% maximum filter elevation
```

```
inici_glonass= 32; % the 31st previous positions is for GPS
valor_finestra= 800; %windowing value

BD= base_dades('XXXXXXX.txt');% obtain DB from Puertos
BD= BD(:,(BD(end,:)>=inici & BD(end,:)<=final)); %to filter just the
desired days from the data provided by Puertos from tide gauges

for doy=inici:final %iterate through all the days
    integer= doy; %day
    year='2017';
    doy=int2str(doy);
    station='XXX';
    L1_activat=1;
    L2_activat=1;
    if integer < 25 %the data obtained is different after the 25th day
of 2017
        load([station year(3:4) doy 'tablegps.mat']);
    else
        load([station year(3:4) doy 'table.mat']);
    end
    if exist('dataL1L2')==1
        Sats=unique(dataL1L2.prn); %obtain the unique PRN to know all
the Satellites seen
        lambda_escollir= [lambda1 lambda2]; %lambda vector for GPS
L1&L2
        lambda_glonass= [lambda_l1_glonass lambda_l2_glonass]; %lambda
vector for GLO L1&L2
        for aux_lambda= 1:2
            lambda= [
lambda_escollir(aux_lambda)*ones(1,inici_glonass)
lambda_glonass(aux_lambda*24-23:aux_lambda*24)] ; %GPS and GLONASS
lambdas all together
            for i=1:1:length(Sats)
                x= dataL1L2.epoch(dataL1L2.prn==Sats(i));% obtain the
epochs
                if aux_lambda ==1
                    y= dataL1L2.sn1(dataL1L2.prn==Sats(i));% obtain
SNR L1
                else
                    y= dataL1L2.sn2(dataL1L2.prn==Sats(i));% obtain
SNR L2
                end
                elev= dataL1L2.el(dataL1L2.prn==Sats(i));% obtain
elevation
                azimuth= dataL1L2.az(dataL1L2.prn==Sats(i));% obtain
azimuth
                if sum(isnan(y)==0)~=0 % if SNR is not empty
                    %% FIND PICS TO DIVIDE FOR TRAMS
                    [Max,MaxIdx] = findpeaks(elev); %finds all the
maximums pics
                    DataInv = 1.01*max(elev) - elev;
                    [Min,MinIdx] = findpeaks(DataInv); %finds all the
minimums pics
                    vector1= [MaxIdx MinIdx]; %save maximums and
minimums coordinates
                    vector= sort(vector1); %order the vector

                    %% TO ERASE SOME ELEVATION CORRUPTED DATA
                    auxr=length(vector);
                    oo=1;
```

```
                    while oo<auxr
                        if vector(oo+1)==vector(oo)+1
                            vector(oo+1)=[];
                            vector(oo)=[];
                            auxr=auxr-2;
                            oo= oo-1;
                        end
                        oo=oo+1;
                    end
                    %% DEFINEIXO EL VECTOR DE W'S A PARTIR DEL RANG
D'ALTURES
                    altura_probable= linspace(XX,YY,ZZZ); %from XX to
YY meters are considered and ZZZ points for Spectral Analysis
                    f= (2/lambda(Sats(i))).*altura_probable;
%converting from f to Sea Height
                    %% EVALUATION OF EACH TRAM
                    for tram=0:length(vector)
                        if tram==0 %1st tram
                            x_vector= x(1:vector(1)); %only the epochs
for the tram
                            y_vector= y(1:vector(1));% SNRs for the
tram
                            elev_vector= elev(1:vector(1));
                            azim_vector= azimuth(1:vector(1));
                            %% FILTERING IN ELEVATION & AZIMUTH
                            [ SNR_vector, tn_vector, reduit_x_vector,
reduit_azim_vector, reduit_elev_vector ]=
filtre_menys(integer,inici,x_vector,y_vector,elev_vector,azim_vector,f
il_az_min,fil_az_max,fil_el_max,fil_el_min);%afageixo vector_dia_3_10
per a saber els index reals de al cap dun dia on esta el senyal
                            %% SPECTRAL ANALYSIS DECISION
                            if L1_activat==1
                                if length(tn_vector)> valor_finestra
                                    if aux_lambda ==1

vector_5_12_complet_finestra750_seguit_tar_l1 =
decisio(aux_lambda,inici,SNR_vector,f,tn_vector,reduit_azim_vector,red
uit_elev_vector,reduit_x_vector,lambda(Sats(i)),doy,tram,i,vector_5_12
_complet_finestra750_seguit_tar_l1);
                                    else

vector_5_12_complet_finestra750_seguit_tar_l2 =
decisio(aux_lambda,inici,SNR_vector,f,tn_vector,reduit_azim_vector,red
uit_elev_vector,reduit_x_vector,lambda(Sats(i)),doy,tram,i,vector_5_12
_complet_finestra750_seguit_tar_l2);
                                    end
                                end
                            end
                        elseif tram==length(vector) % last tram
                            x_vector= x(vector(tram) + 1:end);
                            y_vector= y(vector(tram) + 1:end);
                            elev_vector= elev(vector(tram) + 1:end);
                            azim_vector= azimuth(vector(tram) +
1:end);

                            %% FILTERING IN ELEVATION & AZIMUTH
                            [ SNR_vector, tn_vector, reduit_x_vector,
reduit_azim_vector, reduit_elev_vector ]=
filtre_menys(integer,inici,x_vector,y_vector,elev_vector,azim_vector,f
il_az_min,fil_az_max,fil_el_max,fil_el_min);%afageixo vector_dia_3_10
per a saber els index reals de al cap dun dia on esta el senyal
```

```
                            %% SPECTRAL ANALYSIS DECISION
                            if L1_activat==1
                                if length(tn_vector)> valor_finestra
                                    if aux_lambda ==1

vector_5_12_complet_finestra750_seguit_tar_l1 =
decisio(aux_lambda,inici,SNR_vector,f,tn_vector,reduit_azim_vector,red
uit_elev_vector,reduit_x_vector,lambda(Sats(i)),doy,tram,i,vector_5_12
_complet_finestra750_seguit_tar_l1);
                                    else

vector_5_12_complet_finestra750_seguit_tar_l2 =
decisio(aux_lambda,inici,SNR_vector,f,tn_vector,reduit_azim_vector,red
uit_elev_vector,reduit_x_vector,lambda(Sats(i)),doy,tram,i,vector_5_12
_complet_finestra750_seguit_tar_l2);
                                    end
                                end
                            end
                        else % TRAM OF THE MIDDLE
                            x_vector= x(vector(tram) +
1:vector(tram+1));
                            y_vector= y(vector(tram) +
1:vector(tram+1));
                            elev_vector= elev(vector(tram) +
1:vector(tram+1));
                            azim_vector= azimuth(vector(tram) +
1:vector(tram+1));
                            x_vector_aux= x_vector;
                            y_vector_aux= y_vector;
                            auxiliar= 0;

                            %% FILTERING IN ELEVATION & AZIMUTH
                            [ SNR_vector, tn_vector, reduit_x_vector,
reduit_azim_vector, reduit_elev_vector ]=
filtre_menys(integer,inici,x_vector,y_vector,elev_vector,azim_vector,f
il_az_min,fil_az_max,fil_el_max,fil_el_min);%afageixo vector_dia_3_10
per a saber els index reals de al cap dun dia on esta el senyal
                            %% SPECTRAL ANALYSIS DECISION
                            if L1_activat==1
                                if length(tn_vector)> valor_finestra
                                    if aux_lambda ==1

vector_5_12_complet_finestra750_seguit_tar_l1 =
decisio(aux_lambda,inici,SNR_vector,f,tn_vector,reduit_azim_vector,red
uit_elev_vector,reduit_x_vector,lambda(Sats(i)),doy,tram,i,vector_5_12
_complet_finestra750_seguit_tar_l1);
                                    else

vector_5_12_complet_finestra750_seguit_tar_l2 =
decisio(aux_lambda,inici,SNR_vector,f,tn_vector,reduit_azim_vector,red
uit_elev_vector,reduit_x_vector,lambda(Sats(i)),doy,tram,i,vector_5_12
_complet_finestra750_seguit_tar_l2);
                                    end
                                end
                            end

                        end
                    end
                end
            end
        end
```

```
    end
end
```

7.9.2. Filter in elevation and azimuth and detrending

```
function [ SNR_vector, tn_vector, reduit_x_vector, reduit_azim_vector,
reduit_elev_vector ] = filtre_menys(
integer,inici,x_vector,y_vector,elev_vector,azim_vector,fil_az_min,fil
_az_max,fil_el_max,fil_el_min )
%% ERASING NAN's VALUES FOR SNR
reduit_x_vector=  x_vector(isnan(y_vector) == 0);
reduit_y_vector= y_vector(isnan(y_vector) == 0);
reduit_elev_vector=  elev_vector(isnan(y_vector) == 0);
reduit_azim_vector= azim_vector(isnan(y_vector) == 0);
%% DETRENDING WITH A 6 DEGREE POLINOMIAL FUNCTION
r= polyfit(reduit_x_vector,reduit_y_vector,6);
f1 = polyval(r,reduit_x_vector);
reduit_y1= reduit_y_vector- f1;
SNR_vector= reduit_y1 - mean(reduit_y1);
tn_vector= sind(reduit_elev_vector);% change of variables x=
sin(elevation)

%% AZIMUTH FILTER
reduit_azim_vector= wrapTo360(reduit_azim_vector); %from rad to
degrees
SNR_vector(reduit_azim_vector <fil_az_min | reduit_azim_vector
>fil_az_max )=[];
tn_vector(reduit_azim_vector <fil_az_min | reduit_azim_vector
>fil_az_max )=[];
reduit_x_vector(reduit_azim_vector <fil_az_min | reduit_azim_vector
>fil_az_max )=[];
reduit_elev_vector(reduit_azim_vector <fil_az_min | reduit_azim_vector
>fil_az_max )=[];
reduit_azim_vector(reduit_azim_vector <fil_az_min | reduit_azim_vector
>fil_az_max )=[];
%% ELEVATION FILTER
SNR_vector( reduit_elev_vector > fil_el_max | reduit_elev_vector <
fil_el_min )=[];
tn_vector(reduit_elev_vector > fil_el_max | reduit_elev_vector <
fil_el_min )=[];
reduit_x_vector(reduit_elev_vector > fil_el_max | reduit_elev_vector <
fil_el_min )=[];
reduit_azim_vector(reduit_elev_vector > fil_el_max |
reduit_elev_vector < fil_el_min )=[];
reduit_elev_vector(reduit_elev_vector > fil_el_max |
reduit_elev_vector < fil_el_min )=[];
end
```

7.9.3. Spectral Analysis method and choosing right samples

```
function [confirmacio, vector_1_satelit_1setmana_gps_glonass] =
decisio(aux_lambda,inici,SNR_vector,f,tn_vector,reduit_azim_vector,red
uit_elev_vector,reduit_x_vector,lambda,doy,tram,satelit,vector_1_satel
it_1setmana_gps_glonass)

[~,ai,~]= unique(tn_vector); %only saving unique values
confirmacio = 0;% auxiliar variable
SNR_vector= SNR_vector(ai);
tn_vector= tn_vector(ai);
```

```
reduit_elev_vector= reduit_elev_vector(ai);
reduit_azim_vector= reduit_azim_vector(ai);
reduit_x_vector= reduit_x_vector(ai);
excepcio = 0;
contador=1;
auxiliar= 1;

%% POLINOMIAL APROXIMATION AGAIN
r= polyfit(tn_vector,SNR_vector,6);
f1 = polyval(r,tn_vector);
auxiliar= SNR_vector- f1;
SNR_vector= auxiliar - mean(auxiliar);
[Y,frequencia]= plomb(SNR_vector,tn_vector, f);% LOMB SCARGLE
PERIODOGRAM
temps= mean(reduit_x_vector); %saving average time of the tram
azimuth= mean(reduit_azim_vector); %saving average azimuth of the tram
elevacio= mean(reduit_elev_vector); %saving average elevation of the
tram

if Y ~=0 %if LOMB SCARGLE is not null
    [MaxValuex,MaxIdx] = max(Y); %find pic in LOMB SCARGLE
    if(f(MaxIdx)*lambda/(2) <XX & f(MaxIdx)*lambda/(2)>YY) %if maximum
represents a height inside [YY,XX] continue the process
        [MaxValue,MaxIdw] = findpeaks(Y); %find the rest of the pics
        if sum(MaxIdx==MaxIdw)>0 %confirm that the max pic is the
maximum of the Periodogram
            if (length(MaxIdw)==1) && (MaxIdw==MaxIdx) %if there is
only 1 pic
                if (Y(MaxIdx)>2*mean(Y)) %pick needs to be 2 times
bigger average Periodogram
                    vectt= repmat(str2num(doy)-inici+
temps,1,length(vector_1_satelit_1setmana_gps_glonass(3,:))); %assign
the height to the most adecuate time
                    [~,ind] = min(abs(vectt-
vector_1_satelit_1setmana_gps_glonass(3,:)));
                    vector_1_satelit_1setmana_gps_glonass (1,ind)=
f(MaxIdx); % put f in ind
                    vector_1_satelit_1setmana_gps_glonass (2,ind)=
azimuth; % put azim in ind
                    vector_1_satelit_1setmana_gps_glonass (4,ind)=
lambda;% put lambda in ind
                    if aux_lambda==1
                        vector_1_satelit_1setmana_gps_glonass (5,ind)=
0.127+0.1352; %bias terms of the antenna phase center for L1
                    else
                        vector_1_satelit_1setmana_gps_glonass (5,ind)=
0.135+0.1267; %bias terms of the antenna phase center for L2
                    end
                    confirmacio = 1;
                    vector_1_satelit_1setmana_gps_glonass (6,ind)=
satelit; %put satellite number in ind
                    vector_1_satelit_1setmana_gps_glonass (7,ind)=
elevacio;%put average elevation in ind
                end
            else
                MaxValue= MaxValue(MaxIdw ~= MaxIdx); %save the rest
of picks instead the max
                MaxIdw= MaxIdw(MaxIdw ~= MaxIdx);
                auxiliar= repmat(Y(MaxIdx),1,length(MaxIdw)); %do not
include the maximum pick
                auxiliar_reduit= repmat(Y(MaxIdx),1,length(MaxIdw)-1);
```

```
%the 1st and 2nd bigger picks not included
                quocient_auxiliar= auxiliar./((Y(MaxIdw))');
%normalizing the rest of picks with the maximum pick
                [MaxValueSort, SortIndex] = sort(MaxValue); % ordering
                MaxIdw_sorted = MaxIdw(SortIndex);
                if MaxIdx > MaxIdw_sorted(1) %if 1st bigger pick is
after the 2nd bigger
                    if (MaxIdw_sorted(1)+500 >
MaxIdx)&&((MaxValuex/MaxValueSort(1))>1.3)%if it is 1.3 times higher
than the 2nd higher pick save the sample
                        excepcio=1;
                    end
                else %if it is on the left
                    if (MaxIdw_sorted(1) <
MaxIdx+500)&&((MaxValuex/MaxValueSort(1))>1.3)
                        excepcio=1;
                    end
                end
                MaxIdw_sorted_new= MaxIdw_sorted(2:end);
                quocient_auxiliar_reduit =
auxiliar_reduit./((Y(MaxIdw_sorted_new))'); %normalizing the rest of
picks against the maximum
                if sum(quocient_auxiliar >
1.5)==length(quocient_auxiliar) || ((sum(quocient_auxiliar_reduit >
1.5)==length(quocient_auxiliar_reduit)) && (excepcio == 1))%maximum
pick needs to be 1.5 times bigger than the rest or fullfilling the
exception
                    if (Y(MaxIdx)>2.4*mean(Y)) %for this case maximum
pick needs to be 2.4 times bigger than the average
                        vectt= repmat(str2num(doy)-inici+
temps,1,length(vector_1_satelit_1setmana_gps_glonass(3,:)));
                        [~,ind] = min(abs(vectt-
vector_1_satelit_1setmana_gps_glonass(3,:)));
                        vector_1_satelit_1setmana_gps_glonass (1,ind)=
f(MaxIdx);
                        vector_1_satelit_1setmana_gps_glonass (2,ind)=
azimuth;
                        vector_1_satelit_1setmana_gps_glonass (4,ind)=
lambda;
                        if aux_lambda==1
                            vector_1_satelit_1setmana_gps_glonass
(5,ind)= 0.127+0.1352;
                        else
                            vector_1_satelit_1setmana_gps_glonass
(5,ind)= 0.135+0.1267;
                        end
                        confirmacio = 1;
                        vector_1_satelit_1setmana_gps_glonass (6,ind)=
satelit;
                        vector_1_satelit_1setmana_gps_glonass (7,ind)=
elevacio;
                    end
                end
            end
        end
    end
end
end
```

7.9.4. Basis B-Splines (Python)

```
def basis_factory(degree,t, i, knots): # Returns a basis_function for
the given degree
    if degree == 0:
        """ The basis function for degree = 0 as per eq. 7"""
        t_this = knots[i]
        t_next = knots[i + 1]
        out = 1. if (t >= t_this and t < t_next) else 0.

    else:
        out = 0.
        t_this = knots[i]
        t_next = knots[i + 1]
        t_precog = knots[i + degree]
        t_horizon = knots[i + degree + 1]

        top = (t - t_this)
        bottom = (t_precog - t_this)
        if bottom != 0:
            out = top / bottom * basis_factory(degree - 1,t, i, knots)

        top = (t_horizon - t)
        bottom = (t_horizon - t_next)
        if bottom != 0:
            out += top / bottom * basis_factory(degree - 1,t, i + 1,
knots)
    return out
```

7.9.5. Main Task and nonlinear squares B-Splines (Python)

```
mat_contents1 =
sio.loadmat('/Users/Hector/Documents/MATLAB/SNR_Analysis/Tecq_Europe/v
ector_gps_glo_tar_l1.mat')['vector_gps_glo_tar_l1']
mat_contents =
sio.loadmat('/Users/Hector/Documents/MATLAB/SNR_Analysis/Tecq_Europe/m
atriu_junt_gps_glo_l1.mat')['matriu_junt_gps_glo_l1']
ydefinitiu =
sio.loadmat('/Users/Hector/Documents/MATLAB/SNR_Analysis/Tecq_Europe/y
definitiu.mat')['ydefinitiu']

degree = 2

p0 = np.append([1,1] , 8.2*np.ones(24)) # C1 i C2 = 1 i els knots els
assigno igual a 8.2
tot_junt = np.loadtxt('results_nou_dia3_5.txt', delimiter=' ')
eix_x = np.loadtxt('eix_x_nou_3_5.txt', delimiter=' ')
ydata = np.loadtxt('y_data_nou_dia3_5.txt',delimiter=' ') #on vaig
obtenir els parametres individuals
bsplines_evaluades =
np.loadtxt('bsplines_evaluades_dia3_5.txt',delimiter=' ') #on vaig
obtenir els parametres individuals
tplFinal2 = np.loadtxt('parametres_nous1.txt',delimiter=' ')
polla = mat_contents1[2,:,0]
temporal_normal = np.array(polla)
resultats_1basis = np.loadtxt('totes_basis_3_5dia.txt',delimiter=' ')
#on vaig obtenir els parametres individuals
hsum_final = np.sum(np.transpose(resultats_1basis) *
```

```
np.transpose(tplFinal2),axis=1)  # weight each basis_bspline and add
them to obtain a temporal vector for 1 day
plt.plot(temporal_normal, hsum_final)
plt.show()


resultats_1basis = np.loadtxt('totes_basis_3_5dia.txt',delimiter=' ')
#on vaig obtenir els parametres individuals

lambda1 = 0.1903
k = 2*math.pi/lambda1
lambda_big = 0.002
def funcLine(tpl, eix_x):
    C1, C2, h = tpl[0], tpl[1], tpl[2:]
    hsum = np.sum(bsplines_evaluades * h, axis=1) #weight each
basis_bspline and add them to obtain a temporal vector for 1 day
    theta = 4 * np.pi * np.array(hsum) * np.array(eix_x) / lambda1
    return (C1 * np.sin(theta) + C2 * np.cos(theta))*np.exp(-4
*lambda_big *np.power(k, 2)*np.power(eix_x, 2)) #lambda_big = 2
if len(eix_x)!=0:
    ErrorFunc = lambda tpl, eix_x, ydata: funcLine(tpl, eix_x) -
ydata#np.power(func(tpl, eix_x) - ydata,2)
    param_values = p0
    tplFinal2, success = leastsq(ErrorFunc, param_values,args=(eix_x,
ydata))
    hsum_final = np.sum(np.transpose(resultats_1basis) *
np.transpose(tplFinal2[2:]), axis=1) #weight each basis_bspline and
add them to obtain a temporal vector for 1 day
    plt.plot(temporal_normal,hsum_final)
    plt.show()
    np.savetxt('parametres.txt', tplFinal2)
```

7.10. Gantt Diagram and Work Packages

<table>
<tr><td>Project:</td><td colspan="2">Mallorca Analysis</td></tr>
<tr><td>Major constituent: Software simulation</td><td colspan="2">Sheet 20 from 60 in my TFG</td></tr>
<tr><td rowspan="2">Short description: Develop an Spectral Analysis method to retrieve the Sea Height from the GNSS signal acquired. The algorithm was tested in a station located in Palma de Mallorca harbor. In order to asses the quality of the results, information about the Ground Truth level of the Sea was required. Puertos del Estado provided this information</td><td colspan="2">Planned start date: 01/02/2017
Planned end date: 01/03/2017</td></tr>
<tr><td colspan="2">Start event: 21/01/2017
End event: 14/01/2017</td></tr>
<tr><td>Internal task T1: Preprocessing Data (cleaning)

Internal task T2: Applying Spectral Analysis

Internal task T3: Conversion from frequency to Sea Height

Internal task T4: Comparison between Spectral Analysis results and Ground Truth</td><td>Deliverables:
All the tasks (T1-T4)</td><td>Dates:
24/01/2017</td></tr>
</table>

<table>
<tr><td>Project:</td><td colspan="2">Tarifa Analysis</td></tr>
<tr><td>Major constituent: Software simulation</td><td colspan="2">Sheet 30 from 60 in my TFG</td></tr>
<tr><td rowspan="2">Short description: Develop an Spectral Analysis method to retrieve the Sea Height from the GNSS signal acquired. The algorithm was tested in a station located in Tarifa harbor. In order to asses the quality of the results, information about the Ground Truth level of the Sea was required. Puertos del Estado provided this information. The analysis was similar to the one performed in Mallorca but due to differences in the Sea behavior between both stations, the preprocessing of the data was a bit different</td><td colspan="2">Planned start date: 25/02/2017
Planned end date: 15/03/2017</td></tr>
<tr><td colspan="2">Start event: 20/02/2017
End event: 04/03/2017</td></tr>
<tr><td>Internal task T1: Preprocessing Data (cleaning)

Internal task T2: Applying Spectral Analysis

Internal task T3: Conversion from frequency to Sea</td><td>Deliverables:
All the tasks (T1-T4)</td><td>Dates:
06/03/2017</td></tr>
</table>

Height Internal task T4: Comparison between Spectral Analysis results and Ground Truth		

Project:	B-Splines Analysis	
Major constituent: Software simulation	Sheet 50 from 60 in my TFG	
Short description: Develop a State of the Art algorithm to retrieve the Sea Height making use of B-Splines to define the tide´s behavior. A non linear mean square algorithm will be designed to obtain the correct parameters to represent the Sea Height along the time domain.	Planned start date: 20/03/2017 Planned end date: 15/05/2017 Start event: 15/03/2017 End event: 04/05/2017	
Internal task T1: Design of the B-Splines Internal task T2: Design of the minimization algorithm Internal task T3: Make it converge to a global minimum Internal task T4: Comparison between B-Splines results and Ground Truth	Deliverables: All the tasks (T1-T4)	Dates: 20/05/2017

Project:	Differences between L1 & L2 and GPS & GLONASS	
Major constituent: Software simulation	Sheet 60 from 60 in my TFG	
Short description: Asses the results obtained for the two stations analyzed in order to identify which is the frequency band (L1,L2) that results in less error between our analysis and Ground Truth as well as the most suitable Satellite System (GPS, GLONASS)	Planned start date: 15/02/2017 Planned end date: 01/06/2017 Start event: 15/02/2017 End event: 29/05/2017	
Internal task T1: Pull apart frequency band and Satellite system from the global results Internal task T2: Analyze each group separately Internal task T3: Obtain error results with respect the Ground Truth	Deliverables: All the tasks (T1-T3)	Dates: 12/06/2017

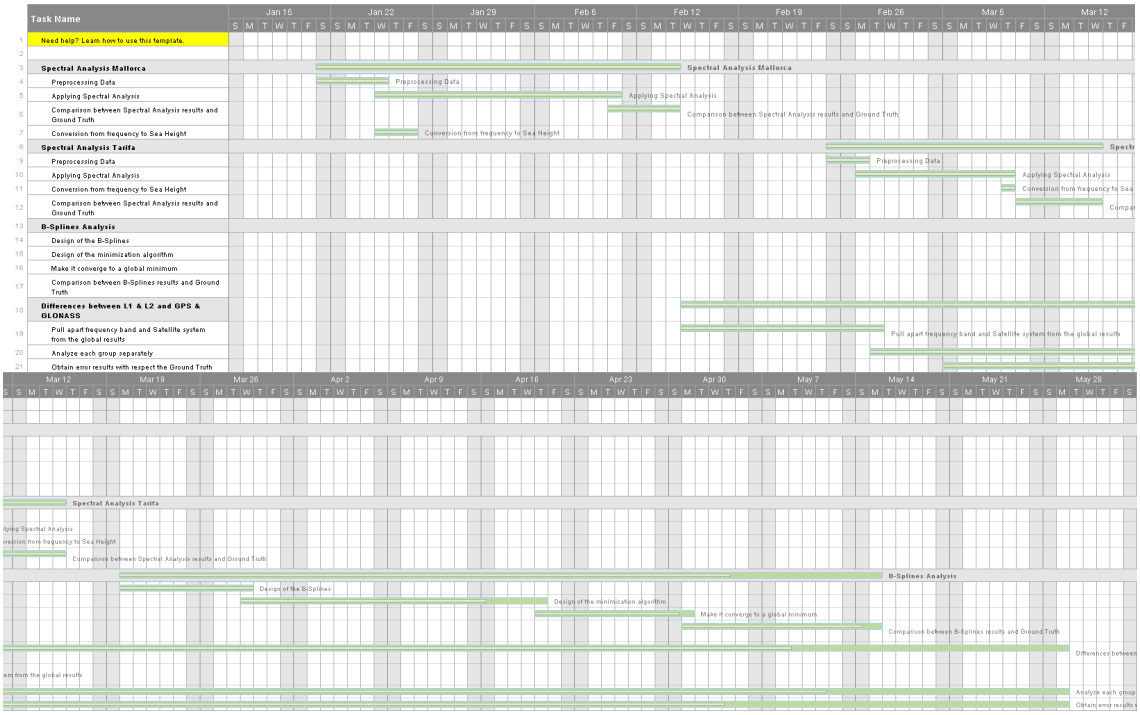

Figure 7.43: Time Plan

8. Bibliography

[1]: Pugh, D.T. (1996) Tides, surges and mean sea-level (reprinted with corrections), Chichester, UK, John Wiley & Sons Ltd, 486pp.

[2]: Garrett, C., and B. Toulany (1982), Sea level variability due to meteorological forcing in the northeast Gulf of St. Lawrence, J. Geophys. Res., 87(C3), 1968–1978, doi:10.1029/JC087iC03p01968.

[3]: Rovere, A., Stocchi, P. & Vacchi, M. Curr Clim Change Rep (2016) 2: 221. doi:10.1007/s40641-016-0045-7

[4]: R. Gehrels, "Rising Sea Levels as an Indicator of Global Change," in Clim. Chang. Obs. Impacts Planet Earth, 1st ed. Elsevier B.V., 2009, ch. 18, pp. 325–336. [Online]. Available: http://dx.doi.org/10.1016/B978-0-444-53301-2.00018-X

[5]: Tsang, L. and Li, Q. 1999. Microwave Remote Sensing Theory. Wiley Encyclopedia of Electrical and Electronics Engineering.

[6]: Millington, A. C., Walsh, S. J., & Osborne, P. E. (2001). GIS and Remote Sensing Applications in Biogeography and Ecology. Boston, MA: Springer US.

[7]: M. D. Steven and J. A. Clark, .Applications of Remote Sensing in Agricultures, Elesevier, 1990, ISBN: 978-0-408-04767-8

[8]: Watson, T.L., "Use of Remote Sensing Techniques for Military Terrain Analysis Applications", 1993, https://books.google.es/books?id=ymnkPgAACAAJ

[9]: Meier, R.R. Space Sci Rev (1991) 58: 1. doi:10.1007/BF01206000

[10]: "4 Active Earth Remote Sensing for Land Surface Applications." National Academies of Sciences, Engineering, and Medicine. 2015. *A Strategy for Active Remote Sensing Amid Increased Demand for Radio Spectrum*. Washington, DC: The National Academies Press. doi: 10.17226/21729.

[11]: Kristina B. Katsaros (University of Miami, Miami, FL, USA), "An Introduction to Ocean Remote Sensing", 2005, http://dx.doi.org/10.5670/oceanog.2005.36

[12]: Wahner, A., R. O. Jakoubek, G. H. Mount, A. R. Ravishankara, and A. L. Schmeltekopf (1989), Remote sensing observations of daytime column NO2 during the Airborne Antarctic Ozone Experiment, August 22 to October 2, 1987, J. Geophys. Res., 94(D14), 16619–16632, doi:10.1029/JD094iD14p16619.

[13]: Walker RS, Hamilton MJ, Groth AA. Remote sensing and conservation of isolated indigenous villages in Amazonia. *Royal Society Open Science*. 2014;1(3):140246. doi:10.1098/rsos.140246.

[14]: McGraw, G. A., & Braasch, M. S. (1999). GNSS multipath mitigation using gated and high resolution correlator concepts. In *Institute of Navigation, National Technical Meeting'Vision 2010: Present and Future', San Diego, CA* (pp. 333-342).

[15]: C. G. Hegarty y E. Chatre. “Evolution of The Global Navigation Satellite System (GNSS)”. In “Proceedings of the IEEE, Vol. 96, Nº 12, Dec.2008”, pp. 1902ss

[16]: Groves, P. D. (2013). *Principles of GNSS, inertial, and multisensor integrated navigation systems*. Artech house.

[17]: Alberto Alonso, “Contribution to Land, Sea and Sea-Ice Remote Sensing using GNSS-Reflectometry”, 2016, TDX (Tesis Doctorals en Xarxa)

[18]: F. Soulat, M. Caparrini, O. Germain, P. Lopez-Dekker, M. Taani, G. Ruffini, “Sea state monitoring using coastal GNSS-R”

[19]: Caparrini, M., L. Ruffini, and G. Ruffini (2003), PARFAIT: GNSS-R coastal altimetry, paper presented at 2003 Workshop on Oceanography with GNSS-R, Starlab, Barcelona, Spain, July, available at http://arxiv. org/abs/physics/0311052.

[20]: Larson, Kristine M.; Ray, Richard D.; Williams, Simon D.P.. 2017 A 10-Year Comparison of Water Levels Measured with a Geodetic GPS Receiver versus a Conventional Tide Gauge. *Journal of Atmospheric and Oceanic Technology*, 34 (2). 295-307.

[21]: Löfgren, J. S., R. Haas, and H-G. Scherneck (2014), Sea level time series and ocean tide analysis from multipath signals at five GPS sites in different parts of the world, Journal of Geodynamics, 80, 66-80

[22]: Alonso-Arroyo, A., A. Camps, P. Hyuk, D. Pascual, R., Onrubia, and F. Martin (2015), Retrieval of significant wave height and mean sea surface level using the GNSS-R interference pattern technique: results from a three-month field campaign, EEE Trans. Geosci. Remote Sens., 53 (6), 3198-3209.

[23]: Beckmann, P., and A. Spizzichino (1963), “The scattering of electromagnetic waves from rough surfaces”, Pergamon Press (Republished by Artech House 1987).

[24]: K. M. Larson, E. E. Small, "Normalized microwave reflection index: A vegetation measurement derived from GPS networks", *IEEE J. Sel. Topics Appl. Earth Observ. Remote Sens.*, 2014.

[25]: Masters, D., P. Axelrad, & S. Katzberg, (2004), “Initial results of land-reflected GPS bistatic radar measurements in SMEX02”, Rem. Sens. Env., 92(4), pp. 507–520.

[26]: Joakim Strandberg, Thomas Hobiger and Rüdiger Haas, “Improving GNSS-R sea level determination 1through inverse modeling of SNR data”, Radio Science, vol. 51, August 2016

[27]: Hobiger, T., R. Haas, and J. Löfgren (2014), “GLONASS-R: GNSS reflectometry with a Frequency Division Multiple Access-based satellite navigation system”, Radio Science, 49 (4), 271-282.

[28]: Nievinski, F. G., and K. M. Larson (2014c), Inverse modeling of GPS multipath for snow depth estimation- Part II: application and validation, IEEE Transactions on Geoscience and Remote Sensing, 52 (10), 6564-6573.

[29]: Nievinski, F. G., and K. M. Larson (2014a), Forward modeling of GPS multipath for near-

surface reflectometry and positioning applications, GPS solutions, 18 (2), 309-322.

[30]: Millman, K., and M. Aivazis (2011), "Python for scientists and engineers", Computing in Science & Engineering, 13 (2), 9-12.

[31]: http://www.7-zip.org

[32]: Löfgren, J.S. & Haas, "Sea level measurements using multi-frequency GPS and GLONASS observations" , J. Adv. Signal Process. (2014) 2014: 50. doi:10.1186/1687-6180-2014-50

[33]: Ali Ghavidel, Domenico Schiavulli, Adriano Camps, "Numerical Computation of the Electromagnetic Bias in GNSS-R Altimetry", IEEE Transactions on Geoscience and Remote Sensing (Volume: 54, Issue: 1 Publication Date, Jan. 2016)

[34]: Brown, Louis; *A Radar History of World War II*, Inst. of Physics Publishing, 1999

[35]: Scott, R. E. 1969. *Study and Evaluation of the Omega Navigation System for transoceanic navigation by civil aviation*. FAARD-69-39.

[36]: Gold, R., "Optimal binary sequences for spread spectrum multiplexing (Corresp.)". IEEE Transactions on Information Theory. 13 (4): 619–621. doi:10.1109/TIT.1967.1054048, October 1967

[37]: Betz J. The offset carrier modulation for GPS modernization. In Proceedings of ION Technical meeting, (Cambridge, Massachusetts) June 1999

[38]: J. S. Löfgren, R. Haas, H.-G. Scherneck, M. S. Bos, "Three months of local sea level derived from reflected GNSS signals", Radio Science, vol. 46, December 2011

[39]: [1] M. B. Priestley, *"Spectral Analysis and Time Series, Volume 1: Uni- variate Series"*. New York: Academic, 1981.

[40]: P. Stoica, "Spectral Analysis of Nonuniformly Sampled Data: A New Approach Versus the Periodogram ", IEEE Tansactions on Signal Processing, vol. 57, no. 3, March 2009

[41]: Petre Stoica, Niclas Sandgren, "Spectral analysis of irregularly-sampled data: Paralleling the regularly-sampled data approaches", Digital Signal Processing, Volume 16, Issue 6, 2006, Pages 712-734, ISSN 1051-2004.

[42]: Hatanaka, Y. (1996a): Compact RINEX Format and Tools (beta-test version), proceeding of 1996 Analysis Center. Workshop of IGS, March 19-21, 1996, 121-129.

[43]: Hatanaka, Y. (2008): A Compression Format and Tools for GNSS Observation Data Yuki Hatanaka. Abstract gsi.go.jp, April 2008.

[44]: Lou Estey, Stuart Wier. "Teqc Tutorial: Basics of Teqc Use and Teqc Products", June 2014

[45]: "GFZRNX 1.07 Users Guide", GFZ German Research Centre for Geosciences. May 30, 2017